Ferrites for Inductors and Transformers

E. C. Snelling
and
A. D. Giles

RESEARCH STUDIES PRESS LTD.
Letchworth, Hertfordshire, England
JOHN WILEY & SONS INC.
New York · Brisbane · Chichester · Toronto · Singapore

Ferrites for Inductors and Transformers

ELECTRONIC & ELECTRICAL ENGINEERING RESEARCH STUDIES

MAGNETIC MATERIALS AND THEIR APPLICATIONS

Series Editor: **Professor J. E. Thompson,** *University College, Cardiff, UK*

1. High Gradient Magnetic Separation
   Richard Gerber *and* **Robert R. Birss**

2. Ferrites for Inductors and Transformers
   E. C. Snelling *and* **A. D. Giles**

Ferrites for Inductors and Transformers

E. C. Snelling
Philips Research Laboratories, Redhill, Surrey, England
and
A. D. Giles
formerly with
Philips Research Laboratories, Redhill, Surrey, England

RESEARCH STUDIES PRESS LTD.
Letchworth, Hertfordshire, England
JOHN WILEY & SONS INC.
New York · Brisbane · Chichester · Toronto · Singapore

RESEARCH STUDIES PRESS LTD.
58B Station Road, Letchworth, Herts. SG6 3BE, England

Marketing and Distribution:

Australia, New Zealand, South-east Asia:
Jacaranda-Wiley Ltd., Jacaranda Press
JOHN WILEY & SONS INC.
GPO Box 859, Brisbane, Queensland 4001, Australia

Canada:
JOHN WILEY & SONS CANADA LIMITED
22 Worcester Road, Rexdale, Ontario, Canada

Europe, Africa:
JOHN WILEY & SONS LIMITED
Baffins Lane, Chichester, West Sussex, England

North and South America and the rest of the world:
JOHN WILEY & SONS INC.
605 Third Avenue, New York, NY 10158, USA

Library of Congress Cataloging in Publication Data:

Snelling, E. C. (Eric Charles), 1923–
Ferrites for inductors and transformers.
(Electronic & electrical engineering research studies.
Magnetic materials and their applications; 2)
1. Ferrites (Magnetic materials) I. Giles, A. D.
II. Title. III. Series.
TK7871.15.F4S527 1983 621.31'042'028 83-9595
ISBN 0 86380 003 3
ISBN 0 471 90208 X (Wiley)

British Library Cataloguing in Publication Data:

Snelling, E. C.
Ferrites for inductors and transformers.—(Magnetic materials and their applications; 2)
1. Magnetic cores 2. Ferrite cores
I. Giles, A. D. II. Series
621.34 TK7872.M25
ISBN 0 86380 003 3

Printed in Great Britain
Digitized and polished by PE1ABR

To our many colleagues
who shared our interest in ferrites

Preface

This book is one of a series devoted to Magnetic Materials and their Applications. It is concerned with ferrites that are intended for use as cores for inductors and transformers, that is, the magnetically soft ferrites. After a period of rapid development the rate of progress in this field has slowed somewhat in recent years and it is timely to review the current position. Clearly a book of monograph proportions cannot deal exhaustively with such a large subject. Instead, the object has been to present a concise text so that the reader can, in a short time, obtain an outline of the essential physics of magnetism as it relates to ferrites and their properties, and go on to the specific applications of ferrites as cores for inductors and transformers. Thus the treatment combines the electrical engineering aspects of wound component design with an outline description of the processes of magnetization necessary for a proper understanding of the properties of the core materials. Although the treatment is concise, it does not lack depth and detail where this is relevant. Sufficient design information and application data is given to enable practical designs to be made based on modern ferrite materials and core shapes.

The Authors acknowledge with sincere gratitude the valuable comments and discussion provided by their colleague John Knowles. They would also like to record their appreciation of the efforts of Pamela Martin who undertook the great task of typing and preparing the pages for copying, of Pat Tarrant who prepared the line drawings and of Norman Jackson who proof-read the text and checked some of the design data. Finally the Authors thank their respective spouses for their patient forebearance over many months.

A.D. Giles
E.C. Snelling

Table of Contents

List of Symbols

Following each symbol and definition there is, in general, a reference to the equation (in brackets), the figure or section in which the symbol is introduced or first used.

A	exchange coefficient	(2.12)
A	area	(3.4)
A	a const.	(3.51)
A_c	cooling area of a core plus winding	Table 5.3
A_{ck}	cooling area of a core	(5.49)
A_{cp}	cross-sectional area of transformer centre pole	Table 5.3
A_{cw}	cooling area of a winding	(5.61)
A_e	effective cross-sectional area of a magnetic circuit	(4.2)
A_g	effective cross-sectional area of an air gap	(4.6)
A_i	attenuation or insertion loss	(5.3)
A_L	inductance factor	(4.9)
A_w	cross-sectional area of a winding	(4.3)
b	conductor breadth	Fig. 5.24
b_w	winding breadth	(5.6)
B	magnetic flux density	(2.19)
B_e	effective flux density	(4.24)
B_r	remanent flux density	Fig. 2.13
B_{sat}	saturation flux density	Fig. 5.13

c	velocity of e.m. waves in vacuo	(5.20)
C	a const.	(3.50)
C_p	parallel capacitance	Fig. 3.1
C_{res}	resonating capacitance	(4.23)
C_s	total self-capacitance of a winding	(4.22)
C_1	core factor	(4.2)
d	diameter of bare conductor	(4.3)
d	diameter of a sphere which gives approximately the same rate of heat loss by convection as a given transformer	(5.24)
d_o	diameter of conductor over insulation	Section 5.2.5
d_{opt}	optimum diameter of conductor	(4.20), (5.57)
D	disaccommodation	(3.7)
D	least dimension of a core in a plane perp. to flux	(3.37)
D	a const.	(3.50)
D	pulse droop expressed in %	(5.4)
D_r	resonance dimension of a core cross-section	Fig. 5.12
e	charge on the electron	(2.1)
e	instaneous value of emf	(3.11)
e_w	a factor	(2.12)
E	emf	
E	energy/unit volume	(2.14)
E	emissivity of a surface	(5.25)
E_a	source voltage	Fig. 5.1
E_K	magnetocrystalline anisotropy energy	(2.5)
E_N	demagnetization energy	(2.8)
E_N'	demagnetization energy for multi-domain crystal	(2.14)
E_u	uniaxial anisotropy energy	(2.6)
E_w	wall energy/unit volume	(2.13)
E_ρ	activation energy of conduction process	(3.3)
E_λ	stress anisotropy energy	(2.10)
E_1	applied emf at fundamental frequency	(5.11)
E_3	third harmonic emf	(5.11)

f	frequency	
f_{res}	ferromagnetic resonance frequency	(3.47)
f_1, f_2	lower and upper limits of a transformer transmission band	Fig. 5.2
F	a function of R_p and Q	(5.16)
$F_{\cong}$	layer copper factor	(5.44)
F_p	packing factor of a winding	(4.4)
F_R	factor by which the a.c. resistance of a transformer winding exceeds the d.c. resistance	(5.43)
F_w	copper space factor of a winding	(4.3)
G	conductance	
G_r	factor expressing screening effect of eddy currents in a round conductor	(4.21)
G_s	conductance expressing the loss in the self-capacitance of a winding	(4.22)
h	Planck's constant	(2.1)
h	effective conductor height	Fig. 5.24
h_w	total height of transformer windings	(5.6)
H	magnetic field strength	
H_{cB}	coercivity on the B(H) curve	Fig. 2.13
H_f	friction field strength	(3.49)
H_A	anisotropy field	Section 2.3.1
I	current	
I_{dc}	d.c. polarizing current in a tranformer winding	Fig. 5.5
I_1	current in primary winding	Section 5.3.2.3
J	magnetic polarization	(2.19)
k	Boltzmann's constant	(3.3)
k	a constant of proportionality	
k_e	proximity effect constant	(4.17)
k_h	hysteresis power loss coefficient related to B_{p-p}	(5.39)
k_1, k_2, k_3	magnetic loss coefficients	(3.29)
k_1, k_2	constants of proportionality	Section 5.3.2.3

K_F	eddy current core loss coefficient	(5.47)
K_h	Hysteresis power loss coefficient related to $\hat{B}$	(5.46)
K_u	induced uniaxial anisotropy constant	(2.6)
K_1, K_2	magnetocrystalline anisotropy constants	(2.5)
ℓ	length	(2.7)
ℓ_e	effective length of a magnetic circuit	(4.2)
ℓ_g	length of air gap	(3.23)
ℓ_w	mean turn length of a winding	(4.3)
L	inductance	(3.14), (4.1)
L_ℓ	total leakage inductance of a transformer referred to the primary	Fig. 5.1
L_p	parallel inductance	(3.18)
L_s	series inductance	(3.16)
L_o	inductance for unity permeability	(3.15)
L	a linear dimension	(2.13)
m	mass of the electron	(2.1)
m	magnetic moment	(2.3)
m	exponent of frequency	(5.46)
M	magnetization	(2.8)
M_A	magnetization due to 'A' sublattice	(2.4)
M_B	magnetization due to 'B' sublattice	(2.4)
M_s	saturation magnetization	(2.3)
M_o	magnetisation at t = 0	(3.44)
M_∞	magnetization when $t \to \infty$	(3.44)
n	number of uncompensated spins	(2.2)
n	number of domains in a crystal	(2.13)
n	Steinmetz exponent	Section 5.3.2.3
N	demagnetization factor	(2.8)
N	number of turns on a winding	(3.11)
N_a	normalized number of primary turns on a transformer	(5.18)
N_ℓ	number of turns in a winding layer	(5.44)
N_1	number of turns on a primary winding of a transformer	(5.6)

p	number of layers per winding portion	Section 5.3.4
P	power loss	
P_c	total core loss	Section 5.3.2.3
P_{dc}	power loss due to d.c. winding resistance	(5.56)
P_{conv}	rate of heat transfer due to convection	(5.24)
P_{pe}	power loss due to the proximity effect in a winding	(5.42)
P_F	eddy current power loss (volume) density	(3.37)
P_h	hysteresis power loss (volume) density	(3.34)
P_m	total power loss (volume) density	(3.9)
P_{rad}	rate of heat transfer due to radiation	(5.25)
P_{tot}	total power dissipation of a transformer	(5.27)
P_w	total winding loss	Section 5.3.2.3
Q	quality (Q) factor	(4.14)
r	turns ratio	Fig. 5.1
R	resistance	
R	parallel combination of R_a and R_b'	(5.1)
R_a	source resistance	Fig. 5.1
R_{ac}	a.c. resistance of a winding	(4.18)
R_b'	load resistance of a transformer referred to primary	Fig. 5.1
R_{dc}	d.c. resistance of a winding	(4.3)
R_h	series resistance representing hysteresis loss	(3.35)
R_p	parallel resistance	(3.4) and (5.10)
R_{pe}	series loss resistance due to proximity effect	(4.17)
R_s	series loss resistance	(3.16)
R_s	total winding resistance of a transformer referred to the primary	Fig. 5.1
R_1	primary winding resistance	P.104
R_2'	secondary winding resistance of a transformer referred to the primary	P.104

s	number of strands in bunched conductor	(4.21)
S_ν	Néel constant	(3.49)
S_1, S_2'	primary and referred secondary self or stray capacitances respectively	Fig. 5.1
t	time	
t_d	pulse duration	Fig. 5.3
t_f	pulse fall time	Fig. 5.3
t_r	pulse rise time	Fig. 5.3
t_1, t_2	particular times	(3.7)
T	absolute temperature	(3.3)
T_s	surface temperature in K	(5.25)
T_o	temperature of surroundings in K	(5.25)
TC	temperature coefficient	Section 4.4.1
TF	temperature factor	(3.6)
U	voltage	
v	velocity of e.m. wave propagation	(5.20)
V	volume	
V_e	effective volume of a core = $\ell_e A_e$	Section 5.3.2.2
V_T	overall volume of a core	(4.5)
w_h	hysteresis energy loss (volume) density	(3.30)
x	distance	
X	reactance	
X_p	parallel reactance	Fig. 5.10 and (5.10)
Y	admittance	
Z	impedance	
$\alpha_1, \alpha_2, \alpha_3$	direction cosines	(2.5)
β	angle	(2.6)
β	eddy current shape factor	(3.37)
β	damping coefficient	(3.48)
γ	gyromagnetic ratio	(3.45)

δ	loss angle	
δ_{cp}	loss angle of an inductor due to the dielectric loss in its self capacitance	(4.23)
δ_d	dielectric loss angle	(3.5)
δ_{dc}	loss angle due to d.c. resistance of winding	(4.15)
δ_F	loss angle due to eddy current loss in a core	(3.28)
δ_h	hysteresis loss angle	(3.28)
δ_m	loss angle due to (any) magnetic loss	(3.17)
δ_{pe}	loss angle due to proximity effect in a winding	(4.17)
δ_r	residual loss angle	(3.28)
δ_{r+F}	loss angle due to residual plus eddy current loss in a core	(4.30)
δ_{tot}	total loss angle of an inductor	(4.14)
Δ	penetration depth	Fig. 4.6
ε	permittivity	(3.4)
$\varepsilon_p', \varepsilon_p''$	real and imaginary components respectively of the parallel complex permittivity	(3.5)
ε_w	domain wall energy/unit area	(2.12)
ε_o	electric constant = 8.854×10^{-12} F.m^{-1}	(3.4)
η_B	hysteresis loss coefficient	(3.31)
θ	temperature in ^oC	
θ	temperature difference between a transformer surface and the surroundings	(5.24)
θ_o	anisotropy compensation temperature	Section 3.4.1
κ	magnetic susceptability	(2.20)
λ	magnetostriction coefficient	(2.7)
λ	wavelength	(5.20)
λ_{100}	magnetostriction coeff. in <100> direction	(2.9)
λ_{111}	magnetostriction coeff. in <111> direction	(2.9)

μ	permeability	(3.1)
μ_a	amplitude permeability	Section 3.4
μ_B	Bohr magneton	(2.1)
μ_e	effective permeability	(4.6)
μ_i	initial permeability	Section 3.4
μ_p',μ_p''	real and imaginary parts of the parallel complex permeability	(3.18)
μ_r	relative permeability	(2.20)
μ_s',μ_s''	real and imaginary components of the series complex permeability	(3.1)
μ_Δ	incremental permeability	Section 3.4
μ_o	magnetic constant = $4\pi \times 10^{-7}$ H.m^{-1}	(2.19)
μ_1,μ_2	permeability at times t_1, t_2	(3.7)
ν	Rayleigh hysteresis coefficient	(3.32)
ρ	resistivity of core material	(3.3)
ρ_c	resistivity of copper	(4.3)
ρ_∞	resistivity of ferrite at $T \to \infty$	(3.3)
σ	stress	(2.10)
τ	relaxation time	(3.44)
ϕ	angle between stress direction and magnetization	(2.10)
ϕ	magnetic flux	(3.10)
ω	$2\pi \times$ frequency	
ω_r	angular frequency of gyromagnetic resonance	(3.45)

CHAPTER 1
Introduction

1.1. THE NATURE OF FERRITES

In the context of applied magnetism, ferrites can be defined as magnetic oxides formulated to obtain specific magnetic properties and used as core materials in a wide variety of applications. Long before the discovery of electromagnetism or magnetic alloys, the naturally occurring magnetic oxide, i.e. magnetite, Fe_3O_4, was virtually the only source of magnetism directly accessible to man. Initially it was used as loadstone in magnetic compasses and later the early iron magnets were magnetized by induction from magnetite[1].

After the discovery of electromagnetism had laid the foundations of the electrical industry, iron and its magnetic alloys dominated its growth. The development of magnetic materials was concentrated on producing alloys having properties specially matched to the various industrial applications. However, the possibility of magnetic oxides being reinstated as important magnetic materials was not entirely lost; there were various attempts from 1909 onwards to improve the properties of magnetite and to derive magnetic oxides of practical value[2-6].

The main motivation for the study of magnetic oxides was the need to have magnetic materials in which the occurrence of eddy currents would be greatly reduced. Eddy currents, induced in alloys by the time-varying magnetic fields encountered in most applications, give rise to substantial power loss and this can only be reduced to tolerable levels by sub-dividing the core into the form of laminations, wire or particles. The magnetic oxides, having electrical resistivities about a million times greater than those possessed by the alloys, would clearly meet this need provided the magnetic properties could be developed sufficiently. A systematic study by Snoek[7] culminated, in 1946, in the introduction of magnetic ferrites having technically and commercially viable properties and an important new class of magnetic material was established.

The first commercially-available ferrites had the cubic crystal structure of the mineral spinel. They are generally referred to as soft ferrites, a term indicating that they are relatively easy to

magnetize. This characteristic makes them particularly suitable as cores for inductors and transformers. The general formula for these ferrites is $MeFe_2O_4$ where Me is one or more of the divalent transition metals. The cubic ferrites of special interest in this book are those where Me is a combination of manganese and zinc, the MnZn ferrites, or nickel and zinc, the NiZn ferrites. The structure of these ferrites and the origin of their magnetic properties are considered in Chapter 2.

Ferrites may, in principle, be grown as single crystals but for most practical applications (an exception being very high quality recording heads) the product is polycrystalline. It is a ceramic, dark grey in appearance, very hard and brittle.

It is perhaps useful at this point to mention two other magnetic oxide structures which, although not relevant to the subject of this book, nevertheless are of great importance. Barium or strontium ferrite[8] having a hexagonal structure is extensively used as a ceramic permanent magnet material, and magnetic oxides based on yttrium iron garnet are used as gyromagnetic materials in non-reciprocal microwave devices[9]. Microwave ferrites are made on a small scale under laboratory conditions while the hexagonal ferrites are produced in large quantities in specially equipped factories.

The properties of cubic ferrites will be considered in detail in later Chapters, particularly Chapter 3. However it is appropriate in this introduction to outline briefly those properties which principally characterize these materials and to give an indication of the range of values that may be expected.

For reasons explained in Chapter 2, the saturation magnetization and (consequently) the saturation flux density, B_{sat}, of all ferrites is low compared with iron and this fact results in ferrites being inferior to iron alloys at low (mains power) frequencies. The relative permeabilities* can, however, be reasonably high and they are maintained virtually constant up to frequencies in the region of 100 kHz to 50 MHz depending on the composition. In contrast, eddy currents cause the permeability of magnetic alloys to fall rapidly as the frequency increases. The constancy of permeability with frequency exhibited by ferrites makes them suitable for a wide range of high frequency applications.

Finally the high resistivity, ρ, as already stated, is an essential property. Not only does it prevent, other than in exceptional circumstances, any dispersion of the permeability due to eddy current effects but in general it makes any power loss due to eddy currents very small and, in many applications, negligible.

---

* In this book the term permeability, μ, will be taken to mean the permeability relative to that of vacuum so that the absolute permeability is $\mu_o\mu$ where μ_o is the magnetic constant = $4\pi \times 10^{-7} H.m^{-1}$.

Table 1.1. shows the approximate compositions of two grades of cubic ferrite representing widely different types from the range that is commercially available, and it indicates the approximate range of values of the above properties that can be expected, depending on the grade. This table is intended only as an introduction; more comprehensive data is given towards the end of Chapter 3. For the purpose of comparison, the properties of a typical nickel iron alloy are included.

Approx. Composition in mol %				Typical Properties (at 25°C)		
MnO	NiO	ZnO	Fe_2O_3	B_{sat} mT	μ	ρ Ωm
27		20	53	350-500	1000-5000	0.3-10
	32	18	50	250-400	100	$> 10^3$
75% NiFe alloy				8000	10^5 (static value)	0.6×10^{-6}

TABLE 1.1. Indication of some salient characteristics

1.2. MANUFACTURE

It was indicated in the previous Section that, for certain special applications, single crystal ferrites are made. These are prepared in the form of cylindrical boules by the Bridgman process and the required piece parts are made by cutting from the solid.

Apart from this exceptional process, virtually all ferrites are manufactured as polycrystalline ceramics. The manufacturing stages vary a little from one plant to another but the following sequence is typical. For a more detailed description see reference 10.

- Starting materials. Finely divided oxides or carbonates of the constituent metals are used. Purity, particle size and cost are important parameters.

- Proportions. The starting materials are accurately weighed into the correct proportions. The ratio of zinc to the other non-ferrous metal has a controlling influence on many of the properties of the finished material and the proportion of iron is critical. Allowance has to be made for the anticipated losses or gains of the constituent metals during subsequent processing.

- Mixing. The constituent powders are thoroughly mixed to obtain a uniform composition. This may be a dry process but is more often carried out with the powder mixed with water to form a slurry. The mixture must then be formed into pellets or granules for ease of handling. The most common process is spray-drying, in which the slurry is sprayed down into a rising current of hot air, the droplets drying into granules during their descent.

- Pre-sintering. The granulate is calcined at a temperature of about 1000°C. Usually this is done in a rotary kiln. Pre-sintering is not essential but it gives certain advantages. It decomposes the carbonates and higher oxides thereby reducing the evolution of gases during the main sintering stage, it increases the homogeneity, and because a large proportion of the solid state reaction is completed at this stage the amount of shrinkage during the main sintering process is reduced and is therefore more easily controlled.

- Milling and granulation. The pre-sintered product is wet-milled to a specific particle size distribution and a small proportion of organic binder is added. The resultant slurry is spray-dried to form granules that give the product a good pouring consistency. A small amount of lubricant is added at this stage to improve the behaviour of the granules during forming.

- Forming. Most ferrite parts are formed by pressing. A suitably shaped die is filled with the granulated powder which is then compressed, usually from above and below simultaneously, using appropriately shaped upper and lower die punches. Typical pressures are between 1.6 and 16 $kg.mm^{-2}$ (1 and 10 ton. in^{-2}). The dimensions of the die cavity must be made larger, by a suitable factor, than the required finished piece-part dimensions to allow for the appreciable shrinkage that occurs during sintering.

  It is important to realize that the amount by which the powder can flow during pressing is very limited and this restricts the shapes that can be successfully pressed. In particular, any shape that would necessitate a feather edge on the die punches is impracticable. It is also important that the density of the pressed piece should be as uniform as possible since any inhomogeneity will cause the magnetic properties to vary from place to place within the piece and will also cause distortion of the piece during sintering. The former effect will degrade the overall performance of the product and the latter will make it difficult to hold acceptable dimensional tolerances.

  Other methods of forming can be used in appropriate circumstances. For making long rods, bars or tubes, the powder is mixed into a dough and extruded through a suitably shaped orifice. Where very high density is required, isostatic pressing is used. The powder is pressed into a simple shape, e.g. a bar, and this is placed in a soft envelope of rubber or plastic and compressed by the application of a large hydrostatic pressure. Usually the required piece-parts are cut from the resulting bar after sintering. These methods are not generally appropriate to cores for inductors and transformers.

Pressed cores are said to be in the 'green' state; they have mechanical characteristics similar to those of blackboard chalk.

- Sintering. The 'green' cores are loaded onto suitable trays or 'saggers' and heated to a temperature between 1150 and 1300°C following a precise temperature/time cycle. During this cycle the atmosphere is closely controlled, providing oxygen during the early stages to assist the burn-out of the binder but limiting the oxygen partial pressure to very low values after the maximum temperature has been reached. Sintering proceeds by the growing together of the partially reacted powder particles to form crystallites or grains, the residual space between the particles being preferably swept to the crystallite boundaries during the process[11,12]. Typically the resulting grains in the polycrystalline mass range in size from 5 to 40 μm and approximate to single crystals.

  During sintering the piece-part shrinks; typically the reduction of linear dimensions is between 10 and 25% depending on the process details.

  Most mass-produced ferrite cores are sintered in tunnel kilns[13]. These have a fixed temperature and atmosphere distribution along their length and the cores are transported slowly through the tunnel stacked on saggers which in turn are conveyed on ceramic tiles or trays. A typical transit time is 8 hours. An alternative is to use a box kiln[13] into which the cores are stacked. The box kiln is sealed and its temperature and atmosphere are controlled as functions of time. This type of kiln, which was used before the tunnel kiln came into general use, is now returning to favour as cores tend to become smaller and the required degree of control becomes more stringent.

- Finishing. After sintering, the dimensions of a core are typically within 2% of the nominal, except where a core is particularly subject to distortion such as an E core where the outer limbs are likely to splay. The ferrite is hard and its surface is somewhat rough. Normally certain dimensions are required to have tolerances of less than ± 2% and some surfaces need to have a smooth flat finish. These requirements are met by various types of grinding, using either silicon carbide or diamond-coated wheels.

  The mating surfaces of two-piece cores generally need to be particularly smooth and flat and this is achieved by fine grinding or by lapping. Any required air gap may also be provided by undercutting the appropriate pole face.

1.3. APPLICATIONS

As indicated in Section 1.1, the applications of cubic ferrites represent but one sector of the very wide range of applications of magnetic oxides in general. In order to place this sector in proper perspective it is useful to outline briefly the wider range. First the ferrites and applications that are outside the scope of this book will be summarized and then the survey will move on to the applications of the magnetically soft cubic ferrites.

Ferrites having hexagonal structure, i.e. barium or strontium ferrites, are widely used as permanent magnet materials[8] in applications where a very high resistance to demagnetization (high coercivity) is required and the flux density does not need to be as high as in the metal magnet materials. Other important advantages (compared with metal materials) are low cost, light weight and absence of eddy currents. There are many applications. Perhaps the most important is in d.c. motors where radially magnetized segments of ferrite have largely replaced the previous field coils and yoke. Although the automotive industry accounts for most of the segment production, they are used in the whole range of small d.c. motors. Another major application is ring magnets for loudspeakers. These ferrites are also used in magnetic holding systems, magnetic separators, toys, TV receivers, cycle dynamos, etc. In other applications, powdered ferrite is loaded into a plastic material which can then be formed by rolling or extrusion into flexible sheet or strip used, for example, for refrigerator door seals.

Moving now from magnetostatic applications to applications at microwave frequencies, most ferrite types will in principle exhibit the resonance phenomenon that is essential to such applications[9]. The resonance arises from the precession of the vector of the crystal magnetization at a frequency and in a direction that depends on the strength and direction of a saturating static magnetic field (see Section 3.5.3.2). An incident circularly polarized electromagnetic wave will only produce precessional resonance (and the accompanying absorption) if the rotation is in the right sense with respect to the direction of the steady field. This phenomenon is used to make a wide variety of microwave devices such as waveguide isolators which transmit in one direction but attenuate in the other. Types of magnetic oxide used for these applications include complex spinel ferrites based on nickel ferrite, hexagonal ferrites similar to the permanent magnet materials and, most important, materials based on the garnet structure, such as yttrium iron garnet.

Finally, the cubic ferrites based on the spinel structure find application wherever easy magnetization or a good coupling to a high frequency magnetic field is required[14]. In addition to their use as cores for inductors and transformers, the subjects of Chapters 4 and 5, their applications include antenna rods for radio receivers, deflection yokes for TV receivers, recording heads in tape recorders and interference suppression cores. Ring cores of less than 1 mm diameter and having specially developed magnetization characteristics have been used in vast quantities as data storage elements in computer memories and, at the other end of the scale, large numbers of rings, each weighing up to 19 kg, are used as coupling cores in particle accelerators such as proton-synchrotrons. Although the following Chapters are concerned with the properties and application of these cubic ferrites as cores for inductors and transformers, much of the treatment has some relevance to their wider field of application.

To meet the requirements of the inductor and transformer designers, many grades and types of cubic ferrites have been developed having specific properties, and many manufacturers offer comprehensive ranges. A survey of these ranges is given in Reference 15.

Research and development continues in order to improve the understanding of the factors that govern the properties of ferrites, and so improve the product performance. The papers in Reference 16 give a broad account of the current research and development activity.

Finally, to put the subject into an industrial perspective, it may be noted that the current total world production of soft ferrites is estimated[17] to be 100,000 tonnes per annum; this compares with an estimated figure of about 200,000 for permanent magnet ferrites.

CHAPTER 1. REFERENCES

1. Gilbert, W. De Magnete, (1600), translated by P. Fleury Mottelay, (1892). Dover Publications Inc., New York, (1958).
2. Hilpert, S. Genetische und Konstitutive Zusammenhänge in den magnetischen Eigenschaften bei Ferriten und Eisenoxyden. Ber. Dtsch. Chem. Ges., (1909), 42, p.2248.
3. Forestier, H. Transformations magnetiques du sesquioxide de fer, de ses solutions solides, et des ses combinaisons ferromagnétques. Ann. Chim. Xe Serie, IX, pp.316-401.
4. Kato, V. and Takei, T. Permanent oxide magnet and its characteristics. J. Instn. Elect. Engrs Japan, (1933), 53, p.408.
5. Kawai, N. Formation of a solid solution between some ferrites. J. Soc. Chem. Ind. Japan, (1934), 37, p.392.
6. Snoek, J.L. Magnetic and electrical properties of the binary systems $MO.Fe_2O_3$. Physica. Amsterdam, (1936), 3, p.463.
7. Snoek, J.L. New Developments in Ferromagnetic Materials. Elsevier Publishing Company, Inc., New York-Amsterdam, (1947).
8. van den Broek, C.A.M. and Stuijts, A.L. Ferroxdure. Philips Tech. Rev., (1977), 37, No.7, pp.157-175.
9. Lax, B. and Button, K.J. Microwave Ferrites and Ferrimagnetics. McGraw-Hill Book Co., (1962).
10. Swallow, D. and Jordan, A.K. The fabrication of ferrites. Proc. Br. Ceram. Soc., (1964), 2, pp.1-17.
11. Stuijts, A.L. Microstructural considerations in ferromagnetic ceramics. Proc. 3rd Int. Mater. Symp. on Ceramic Microstructures, Univ. Calif. Berkeley, (June, 1966).
12. Heck, C. and Weber, J. How firing atmospheres influence ferrite properties. Ceramic Ind., (1961), 77, Part 1, No.5, p.75; Part 2, No.6, p.66.
13. Jackson, H. Kilns for the manufacture of ferrites. Proc. Br. Ceram. Soc., (1964), 2, pp.43-53.
14. Owens, C.D. A survey of the properties and applications of ferrites below microwave frequencies. Proc. Inst. Radio Engrs. (1956), 44, pp.1234-1248.
15. Snelling, E.C. Ferrites for linear applications, Part 1, Properties. IEEE Spectrum, (1972), 9, No.1, pp.46-47.
16. Ferrites (Proceedings of ICF3). Edited by Watanabe, H., Iida, S. and Sugimoto, M. Centre for Academic Publications, Japan (1981).
17. Ruthner, M.J. The importance of hydrochloric acid regeneration processes for the industrial production of ferric oxides and ferrite powder. ibid., pp.64-67.

CHAPTER 2
Magnetization Processes in Ferrites

2.1. MAGNETIZATION

Magnetization is the result of movement of electric charge. An electric charge in rotary or circulatory motion constitutes a current loop and it has a magnetic moment, m, which in macroscopic terms is the product of the current and the area of the loop.

As the electron is the elementary particle of charge, the elementary quantity of magnetic moment is that due to the spin of the electron. This constant is called the Bohr magneton[1], μ_B.

$$\mu_B = eh/4\pi m = 9.2732 \times 10^{-24} \text{ J.T.}^{-1} \text{ or } \text{A.m}^{-2} \qquad (2.1)$$

where e = the charge on the electron, m = the mass of the electron and h = Planck's constant.

The transition metal elements, namely Mg, Ni, Co, Cu, Fe, Zn, Mn and Cd, form a group of materials important in the science of magnetism and, although there is no space here for a full quantum mechanical treatment of their atomic structure, some discussion of their electronic configuration is appropriate. According to the Pauli exclusion principle two electrons in the same system cannot be in the same energy state. The direction of electron spin constitutes an extra degree of freedom and each orbit can therefore be occupied by two electrons of opposite spin orientation. Thus most atoms will have no, or only one, uncompensated spin. The transition metal atoms, however, have five 3d orbitals of equal energy. Except in Zn, these orbitals are not fully populated so the 3d electrons may occupy the available orbitals in various ways. The lowest energy configuration is that for which the spins are parallel so the 3d electrons fill as many orbitals as possible with spins aligned, i.e. one electron per orbital up to five. This is known as Hund's first rule[2,3].

The total spin magnetic moment per ion is:-

$$m = n\mu_B \qquad (2.2)$$

where n = number of uncompensated spins.

In a magnetic oxide, divalent manganese, Mn^{2+}, and trivalent iron, Fe^{3+}, each having five 3d electrons, will both have the maximum magnetic moment per ion of $5\mu_B$. However, divalent iron, Fe^{2+}, with six 3d electrons has a moment of $4\mu_B$ because the sixth spin will occupy the same orbital as one of the other five electrons and compensate its spin in accordance with the Pauli principle. Divalent zinc, Zn^{2+}, with ten 3d electrons, has all its spins compensated and therefore has no resulting magnetic moment.

When the atoms of the transition metals are held together in a crystal, their moments interact and are held in spontaneous parallel alignment over regions of the crystal. These regions are called domains and may extend over many millions of lattice spacings. P. Weiss[4] first postulated the existence of a strong magnetic field, the Weiss molecular field, which below a certain critical temperature, the Curie temperature, is capable of overcoming the disordering effect of thermal agitation. The spontaneous magnetization thus produced decreases with increasing temperature, vanishing at the Curie temperature above which the magnetic order disappears and the material becomes paramagnetic.

The Weiss field, which causes the moments to be aligned, is attributed to an exchange interaction which is quantum mechanical in nature. The reader is referred to literature, e.g. Ref.5, for a detailed treatment.

This phenomenon of parallel alignment of moments in magnetic metals and alloys is known as ferromagnetism. At room temperature the only pure metals which exhibit ferromagnetism are iron, nickel and cobalt.

The magnetization, M_S, within a domain is defined as the total magnetic moment per unit volume:-

$$M_S = \Sigma m/V \qquad (2.3)$$

It has so far been assumed that the magnetic moment of the atoms is entirely due to the spins of the electrons and that any magnetic moment arising from the orbital motion of electrons can be ignored. For the transition metals in oxide compounds this is largely found to be the case. In a ferrite crystal the outer orbitals of the electrons, in this case the 3d orbitals, which would possess orbital angular momentum in free atoms, are perturbed considerably by the electrostatic field of the surrounding ions. This results, in most cases, in the disappearance of the orbital angular momentum, a phenomenon known as 'quenching'[6]. The quenching of the orbital moments is of particular significance when considering anisotropy, see Section 2.3.1.

2.2. FERRIMAGNETISM

Ferrites are oxides in which the transition metal ions (cations) are separated by oxygen ions (anions). In this book, only cubic ferrites are considered; these are a group of oxides which have the structure of the mineral spinel. This structure will now be described and the form of magnetism which results from it, namely ferrimagnetism, will be discussed.

Cubic ferrites have the general formula $Me^{2+}O.Fe_2^{3+}O_3$ where Me represents a combination of one or more of the divalent transition metal ions, Mg, Ni, Co, Cu, Fe, Zn, Mn or Cd.

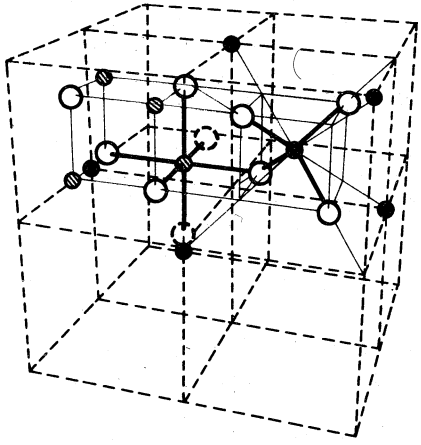

FIG. 2.1. Two octants of the unit cell of the spinel lattice showing the A ions (black circles) on the tetrahedral sites and the B ions (hatched circles) on the octahedral sites. The large open circles represent the oxygen ions.

The structure consists of eight unit cells of a close packed, face-centred, cubic lattice of oxygen ions, Fig. 2.1. The oxygen ions have a much larger radius (1.32Å) than the metal ions (0.6→0.8Å) which occupy some of the interstitial sites in the oxygen lattice. There are two types of interstitial site; the smaller, tetrahedral, site (A site) is surrounded by four oxygen ions placed at the vertices of a tetrahedron, whilst the larger, octahedral, site (B site) is surrounded by six oxygen atoms at the vertices of an octahedron. In a full unit cell there are 64 A sites, of which 8 are occupied, and 32 B sites, of which 16 are occupied. The A sites and B sites lie on interpenetrating cubic lattices or sub-lattices. If in the process of preparation the ratio of metal ions to oxygen ions is too small some of the B sites will be unoccupied. These sites are then referred to as vacancies.

Some simple ferrites, e.g. Zn and Cd ferrites, are called 'normal' ferrites. In these, the divalent ions have a strong preference for the A sites leaving the trivalent Fe^{3+} ions on the B sites:

$$(Zn^{2+})_A\ [Fe_2^{3+}]_B\ O_4^{2-}$$

Simple spinels also occur in which the eight divalent ions displace eight of the Fe^{3+} ions from B sites onto the A sites. Examples of these 'inverse' ferrites are Ni, Co, Cu ferrites and Fe_3O_4, e.g.

$$(Fe^{3+})_A\ [Ni^{2+}Fe^{3+}]_B\ O_4^{2-}$$

Completely normal or completely inverse spinels represent extreme cases; in general the structure is a mixed spinel having the

following general composition:

$$(Me_{\delta}^{2+} Fe_{1-\delta}^{3+})_A \, [Me_{1-\delta}^{2+} \, Fe_{1+\delta}^{3+}]_B \, O_4^{2-}$$

The factors which influence the distribution of the cations on A and B sites include the ionic radius, electronic configuration and electrostatic energies[7]. The nearest neighbour ions to those on the A sublattice are the ions on the B sublattice. Since these are separated by the oxygen ions the distance between them is such that direct exchange interaction of the type found in ferromagnetic materials is negligible. Instead, an exchange interaction operates via the anion and is known as indirect exchange interaction or super-exchange[8,9]. This interaction holds the atomic moments of the A sublattice antiparallel to those on the B sublattice, a phenomenon known as ferrimagnetism. The net magnetization is the difference in magnetization between the two sublattices:

$$M_S = M_B - M_A \qquad (2.4)$$

The cubic ferrites of practical interest are mixed spinel ferrites in which the 'normal' Zn ferrite is added to the 'inverse' Mn or Ni ferrite. The preference of Zn for the A site is strong and so some of the Fe^{3+} ions are displaced to the B sites:-

$$(Zn_{\delta}^{2+} Fe_{1-\delta}^{3+})_A \, [Me_{1-\delta}^{2+} \, Fe_{1+\delta}^{3+}]_B \, O_4^{2-}$$

M_S is actually increased by the introduction of non-magnetic zinc on the A sites. This is because it displaces Fe^{3+}, with its large magnetic moment, to the B sites while zinc contributes nothing to the magnetization on the A sites so the net magnetization increases according to Eqn. 2.4. If the proportion of zinc is progressively increased, the Fe^{3+} ions remaining on the A sites are eventually unable to maintain the antiparallel alignment with the ions on the B sites, the ferrimagnetic structure starts to break down and M_S decreases, (see Fig. 3.3).

2.3. MAGNETIC ANISOTROPIES

In a perfectly soft magnetic material, the orientation of the magnetization relative to the lattice would be arbitrary and it could be rotated by an indefinitely small applied magnetic field, i.e. the material would be magnetically isotropic. In practice, the magnetization on a microscopic scale is preferentially aligned along one of a number of possible minimum energy directions, and this imparts magnetic anisotropy to the material. Energy has to be put into the material, in the form of a magnetic field having a component perpendicular to the minimum energy direction before the magnetization can be rotated away from that direction.

There are several sources of anisotropy:

- Magnetocrystalline anisotropy. This arises from the fact that it is energetically favourable for the spins to align with certain crystallographic axes referred to as preferred (or easy) directions.

- Induced uniaxial anisotropy. This occurs in certain materials as a result of annealing. If this is done in a magnetic field, the preferred direction thus induced is related to the direction of this field.
- Magnetostriction and stress anisotropy. These are directional effects arising from elastic strain or deformation of the crystal.
- Shape anistropy. This is directionality imparted by the shape of a piece of magnetic material, e.g. a complete body or an individual grain, by the minimization of the energy of the free magnetic poles.

These forms of anisotropy will now be described in a little more detail.

2.3.1. MAGNETOCRYSTALLINE ANISOTROPY

Anisotropy energy in a single crystal is usually expressed as a free energy in terms of the direction cosines of the magnetization direction, α_i, with respect to the crystal axes. Symmetry considerations indicate that for a cubic material this energy, E_K, can be written as

$$E_K = K_1(\alpha_1^2\alpha_2^2 + \alpha_2^2\alpha_3^2 + \alpha_3^2\alpha_1^2) + K_2\alpha_1^2\alpha_2^2\alpha_3^2 + \ldots\ldots \qquad (2.5)$$

where K_1,K_2 are the magnetocrystalline anisotropy constants. In the absence of an external field the magnetization will lie along the direction for which E_K is minimal, i.e. the easy direction. When the external field is applied, the magnetization will rotate and E_K will increase, until the torque exerted by the external field just balances that originating from the increase in anisotropy energy. In other words it can be said that there is an effective field, the anisotropy field, H_A, acting on the magnetization.

Higher order terms in Eqn. 2.5 are negligible and to a first approximation the second order term $K_2\alpha_1^2\alpha_2^2\alpha_3^2$ can for practical purposes also be neglected (unless K_1 is very small). The sign and value of K_1 and K_2 determine which cube direction results in a minimal E_K as shown in Table 2.1.

Crystal Direction	[100]	[110]	[111]
Preferred direction if →	$K_1 > 0$ $K_2 > -9K_1$	$K_1 < 0$ $K_2 > -9K_1/4$	$K_1 < 0$ $K_2 < -9K_1/4$ or $K_1 > 0$ $K_2 < -9K_1$
E_K	0	$K_1/4$	$K_1/3 + K_2/27$
H_A	$2K_1/M_s$	(100) plane: $-2K_1/M_s$ (110) plane: $(K_1+K_2/2)/M_s$	$\frac{-4(K_1 + K_2/3)}{3M_s}$

TABLE 2.1. Preferred directions, magnetization energies and anisotropy fields in cubic ferrite crystals. (After Brailsford, Ref.10)

The values of K_1 and K_2 depend on the material composition and are temperature dependent. They are usually determined directly by measurements of mechanical torque on a single spherical crystal as a function of the direction of a large applied magnetic field[11]. Fig. 2.2. shows the anisotropy energy surface for a MnZn ferrite having a [100] easy direction. The length of the radius vector from the origin to the surface represents the anisotropy energy when the magnetization lies along that direction.

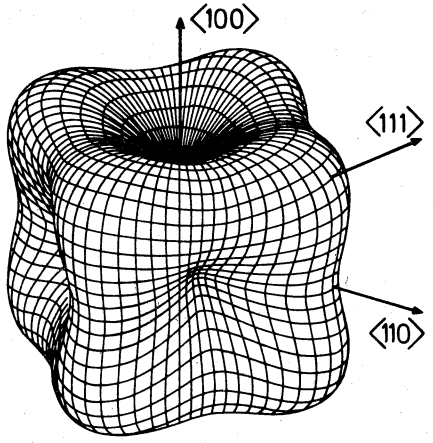

FIG. 2.2. Magnetocrystalline anisotropy energy surface for a MnZn ferrite having K_1 positive and $K_2 = 0$. (After Pearson, Ref.11)

The origin of the magnetocrystalline anisotropy lies in the incomplete quenching of the orbital angular momentum of the ions in the crystal lattice. Detailed discussion of this subject is beyond the scope of the present treatment and the reader is referred to other texts[12,13]. Briefly, the electron is in orbit around the nucleus. Referred to the electron the nucleus is travelling around the electron, which is consequently influenced by the magnetic field caused by the circulating nuclear charge. This results in an interaction between the spin and orbit of the same electron called the spin-orbit interaction. In other words, the energy of the electron is minimised when its spin moment is aligned with its orbital moment. Because of the electrostatic field of the surrounding ions, the electron orbits are fixed with respect to the lattice and so via the spin-orbit interaction the electron spin itself can interact with the lattice. It is this interaction which results in magnetic anisotropy. It can only happen if there is some orbital angular momentum; if not, the spin-orbit coupling is zero.

Fe^{2+} and Co^{2+} on B sites possess a non-zero orbital angular momentum, the spin-orbit coupling is large and a large anisotropy results. Other ions, e.g. Mn^{2+} and Fe^{3+}, have no orbital momentum even as free ions, while others again, e.g. Ni^{2+} on B sites, have their orbital momentum quenched by the electrostatic field. These ions can recover a little orbital momentum as a result of pertubations, for example, in the electrostatic field and some anisotropy results. A review of the contributions to magnetocrystalline anisotropy of individual ions in spinel ferrites is given in Ref. 14.

2.3.2. INDUCED UNIAXIAL ANISOTROPY

Anisotropy can be induced in ferrites, in particular those containing Co^{2+}, as a result of annealing. This is called induced uniaxial anisotropy and is the result of ion diffusion processes. The diffusing ion is influenced by the local magnetization; in the absence of an applied field this is the spontaneous domain magnetization but where a particular directionality is required the annealing is carried out in an applied saturating magnetic field. The resulting anisotropy energy, E_u, for a polycrystalline material is:

$$E_u = -K_u \cos^2\beta \qquad (2.6)$$

where K_u is the induced uniaxial anisotropy constant and β is the angle between the direction of magnetization during the measurement and that during the annealing treatment.

The method of annealing usually employed is to hold the specimen at a suitably elevated temperature, below the Curie temperature, for a time long enough for the diffusion processes to go to completion. The specimen is then cooled slowly to room temperature. If the material is susceptible to induced uniaxial anisotropy then its magnetization will exhibit an enhanced crystallographic anisotropy or, in the case of field annealing, the preferred direction will coincide with the direction of the saturating field. The magnitude of the anisotropy depends on the Co^{2+} content and the rate of diffusion depends on the number of cation vacancies. The vacancies provide a means of achieving the necessary diffusion of the Co^{2+} ions during annealing.

Induced uniaxial anisotropy is an important phenomenon in relation to magnetic losses and domain wall stabilization (see Section 3.5.3.1). However, most MnZn ferrites intended for inductors and transformers contain no cobalt and do not exhibit this anisotropy. A notable exception is cobalt-substituted NiZn ferrite where cobalt is added specifically to stabilize the domain structure and consequently reduce hysteresis effects.

2.3.3. MAGNETOSTRICTION AND STRESS ANISOTROPY

When a magnetic crystal is magnetized or when the direction of its magnetization is changed, a small deformation occurs which depends on the magnitude but not the sense of the magnetization; the deformation is anisotropic. This phenomenon is known as linear magnetostriction. The magnetostriction is said to be positive if the dimensions increase in the direction of magnetization and negative if they decrease. The magnetostriction coefficient λ is expressed as a strain:

$$\lambda = \Delta\ell/\ell \qquad (2.7)$$

which varies with the applied field strength and crystallographic direction (λ_{111} is the magnetostriction coefficient for the <111> direction, etc.).

The theory of magnetostriction is complex and models are generally related to those of magnetocrystalline anisotropy since both of these phenomena depend on the coupling of electron spin orientation to the lattice symmetry. The ions which show the largest magnetocrystalline anisotropy, i.e. Co^{2+} and Fe^{2+}, also show the largest magnetostriction. A review of measurements of magnetostriction in spinel ferrites is given in[15].

If a crystal is subjected to an external tensile stress, the magnetization will tend to align itself either parallel to the direction of the applied stress, if λ is positive, or orthogonally, if λ is negative. A stress can thus induce a preferred direction of magnetization and the resultant stress-induced anisotropy can be of great importance in practical ferrites.

2.3.4. SHAPE ANISOTROPY

When a body of finite size is magnetized, free magnetic poles form at the ends of the body as shown in Fig. 2.3a).

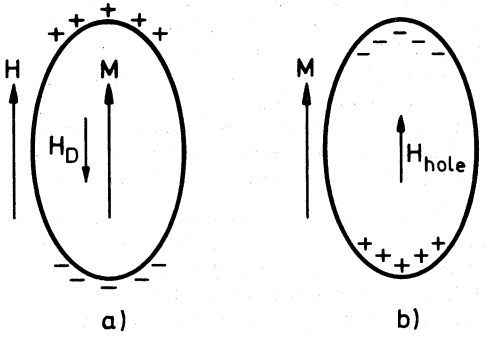

FIG. 2.3. Demagnetization fields and free pole distribution for a) a finite magnetic body b) a pore inside a magnetic body

These give rise to a magnetic field, H_D, within the body which is in opposition to the magnetization; this is called the demagnetization field.

The associated field outside the material is usually referred to as the stray field. H_D is proportional to the pole strength and therefore to the magnetization; for regularly shaped specimens $H_D = -NM$, where N is the demagnetization factor which is a function of the shape of the specimen. N only has exact meaning for general ellipsoids; for other shapes N and thus H_D vary throughout the body and an effective value of N is difficult to define[16].

It is easier to magnetize a body along its major axis than along its minor axis, since on the major axis the free poles are further apart. In general, the shape factor gives a non-spherical body easy and hard directions of magnetization referred to as shape or magnetostatic anisotropy. The energy per unit volume, E_N, required to establish the magnetization against the demagnetizing field is called the

demagnetization, magnetostatic or free-pole energy; it is given by

$$E_N = NM^2/2\mu_o \qquad (2.8)$$

A similar effect occurs at a pore or crack inside a magnetic material except that here the field induced is parallel to the magnetization. This is shown in Fig. 2.3b) for an ellipsoidal hole in a magnetic body. Here free poles form on the surface of the pore, the pole density being proportional to the magnetization of the body. $H_{hole} = +NM$, where N is the demagnetization factor for a magnetic body of the same shape as the hole.

2.3.5. ANISOTROPY IN POLYCRYSTALLINE MATERIALS

Some of the foregoing discussion relates to polycrystalline materials as well as to simple crystals. However, this Section will summarize the relevance of the various anisotropies specifically to polycrystalline ferrites. Ferrites for inductors and transformers are ceramics which consist of an array of randomly oriented crystallites or grains. The easy axes or preferred directions of magnetization of these grains will also be randomly oriented and so the material will have no overall easy axis of magnetization. The magnetocrystalline anisotropy will still be of importance in determining the ease with which the material can be magnetized; the higher the magnetocrystalline anisotropy the more difficult it will be for the magnetization to be influenced by an external field.

The linear magnetostriction of a polycrystalline material will be a combination of the magnetostrictions along the principal axes of the randomly orientated grains. This has been shown to be[17], for cubic ferrites:

$$\lambda = \frac{2}{5}\lambda_{100} + \frac{3}{5}\lambda_{111} \qquad (2.9)$$

A grain in a polycrystalline material is constrained by the surrounding grains and so is not free to deform. If the material has a non-zero magnetostriction coefficient this physical constraint will result in stress, and stress anisotropy will occur. Stress anisotropy may also occur as a result of stresses in the material introduced in manufacture due to inhomogeneity, surface grinding, etc. Under the influence of an externally applied stress, the stress anisotropy energy, E_λ, for a polycrystalline material under conditions of magnetic saturation, is given by

$$E_\lambda = -\frac{3}{2}\sigma\lambda\cos^2\phi \qquad (2.10)$$

where σ = the applied stress
λ = the linear magnetostriction (see Eqn. 2.9)
and ϕ = the angle between the stress direction and the magnetization.

2.4. MAGNETIZATION PROCESSES

The contributions to the energy associated with a magnetic crystal resulting from magnetocrystalline anisotropy, E_K, magnetostriction or stress anisotropy E_λ, and shape or magnetostatic anisotropy E_N, have been discussed in the previous Section. The total anisotropy energy per unit volume, E, is the sum of these contributions:

$$E = E_K + E_\lambda + E_N \qquad (2.11)$$

In the absence of an applied field the magnetization configuration, i.e. the domain structure, must be such as to minimize the total anisotropy energy. The configuration will in principle depend on the type and strength of the anisotropies present but in fact many different configurations can each result in a stable minimum.

2.4.1. DOMAIN STRUCTURE

Various idealized domain configurations that might be supported in a uniform single crystal are shown in Fig. 2.4. If, as in a), the crystal were composed of a single domain with the magnetization pointing in an easy direction, then E_K would be minimized but the magnetic poles appearing at the surface would give rise to a large value for E_N. In the absence of any magnetocrystalline anisotropy the magnetization would be free to assume a circular configuration inside the crystal as in b). This would reduce E_N by bringing the magnetic poles of opposite sign closer together. Since the spins would no longer be parallel, this configuration would be achieved at the expense of an increase in exchange interaction energy.

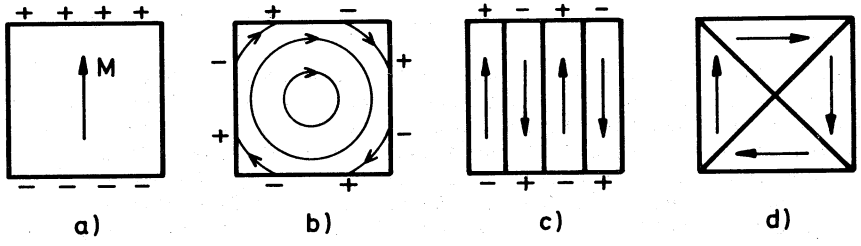

FIG. 2.4. Some idealized domain configurations.

In most magnetic materials, magnetocrystalline anisotropy results in one or more easy directions of magnetization. A material with a strong uniaxial anisotropy might show the configuration of c) with the magnetization pointing either parallel or antiparallel to the easy direction. E_N is then small compared to its value in a) since the magnetic poles of opposite sign are closer together. E_N is reduced to approximately 1/n of its single domain value if the crystal is divided into n domains. Since there is a domain wall energy which

is proportional to the wall area (see Section 2.4.2.) this will increase in proportion to n and the number of domains formed in practice will reflect a balance between the magnetostatic energy and the domain wall energy.

For a cubic crystal with <100> easy axes, the configuration of Fig. 2.4d) is possible, this reduces E_N to zero whilst minimizing E_K, at the expense of domain wall energy. However, for materials exhibiting magnetostriction this configuration results in a high stress anisotropy energy, E_λ. If a material having positive magnetostriction were to be cut along the domain boundaries and allowed to deform as a result of magnetostriction this unconstrained deformation would be as shown in Fig. 2.5.

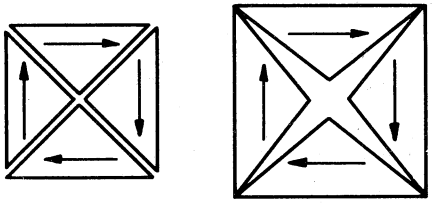

FIG. 2.5. Illustration of the strain in domains resulting from positive magnetostriction in the easy direction (arrows).

a) zero magnetostrictive strain
b) large magnetostrictive strain in the easy direction, the domains being free to deform.

Obviously in a solid material such a deformation is constrained and if λ is not zero a large value for E_λ can result. E_λ can be considerably reduced by restricting the volume under strain to small closure domains, e.g. the small triangular regions as shown in Fig. 2.6. The resulting domain configuration minimizes the sum of the domain wall energy and stress anisotropy energy, E_λ.

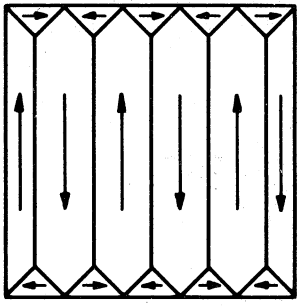

FIG. 2.6. Domain configuration with closure domains.

The internal shape anisotropy energy due to pores, non-magnetic inclusions and other imperfections within a crystal can be reduced as shown in Fig. 2.7.

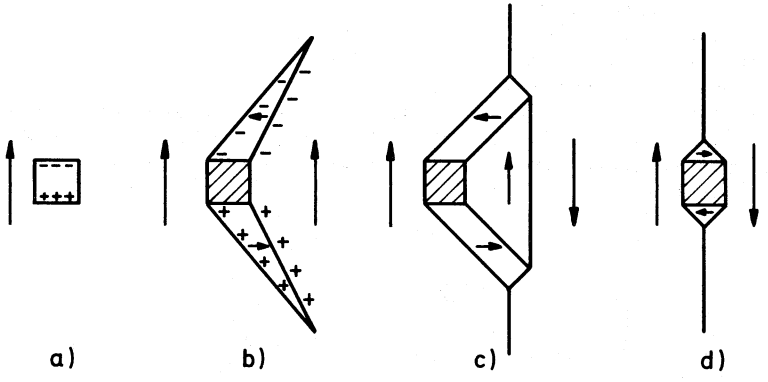

FIG. 2.7. Domain boundary formation around a pore or inclusion.

The high magnetostatic energy associated with a pore or inclusion, a), can be reduced by redistribution of the magnetic poles over the wider surface of spike domains[18] shown in b). If a domain wall approaches the pore or inclusion, the spike domains are attracted to the domain wall so as to reduce the magnetostatic energy still further as in c) and d).

2.4.2. BLOCH WALLS

Domains are separated by zones of finite thickness called Bloch walls. Within a Bloch wall there is a gradual transition of the direction of magnetization from that on one side of the wall to that on the other, (see Fig. 2.8). In cubic ferrites the angle between these directions may be 180° or 90° for $K_1 > 0$ and 180°, 109.5° or 70.5° for $K_1 < 0$.

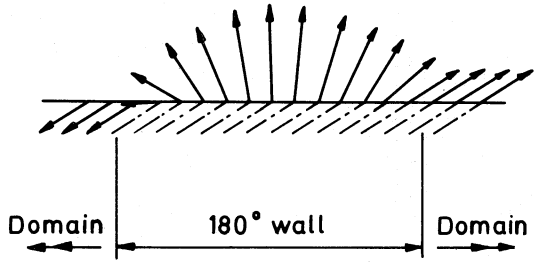

FIG. 2.8. Transition of spin direction at a 180° Bloch wall (domain boundary)

The thickness of the Bloch wall is governed by the balance between exchange energy and magnetocrystalline anisotropy energy. The exchange energy between adjacent spins within the wall will increase with increasing angle between them. The exchange energy considerations will thus favour a gradual rotation of the spins within a wall, i.e. an increase in thickness of the Bloch wall. On the other hand any rotation of spins out of the easy directions of magnetization causes an increase in magnetocrystalline anisotropy energy. This consideration thus tends to favour a reduction in wall thickness.

The domain wall energy per unit area, is given by[19]:

$$\varepsilon_w = e_w \left(A|K_1|\right)^{\frac{1}{2}} \tag{2.12}$$

where e_w = a factor which depends on the direction of the normal to the wall with respect to the crystal axes
A = the exchange coefficient
$|K_1|$ = the absolute value of the anisotropy constant.

In a crystal divided into n parallel domains the wall energy per unit volume is

$$E_w = \varepsilon_w (n-1) L^2/L^3 \tag{2.13}$$

where L = the linear dimension of the crystal.

The plane of the Bloch wall should ideally be parallel to the difference vector of the magnetizations on either side of the wall. If this is the case, the component of magnetization normal to the plane of the wall will be equal on either side of the wall and no magnetic poles will form. This is not always possible; see, for example, the spike domains of Fig. 2.7b).

The number and configuration of domains which will form in a magnetic crystal will be such as to minimize the total energy of the system. For example, in the simple case of Fig. 2.4c), where it is assumed that E_K and E_λ are both zero, the free pole energy, E_N, that would correspond to the single domain case is reduced to $E_N' = E_N/n$ when the crystal is divided into n domains. The total energy per unit volume is then given by:

$$E = E_N' + E_w \tag{2.14}$$

Differentiating Eqn. 2.14 with respect to n gives

$$n^2 = E_N L/\varepsilon_w \tag{2.15}$$

for minimum energy. Small particles having high shape anisotropy, e.g. acicular particles, may support a single domain as the minimum energy state.

In general, the domain configurations will change with temperature because the anisotropies and the exchange energy are both temperature dependent. Imperfections within a crystal will cause local variations in the anisotropy and these will have a strong effect on domain structure.

In polycrystalline materials the grain boundaries act as sources of magnetic poles as they separate grains having differing directions of magnetization. Here also the magnetostatic energy is reduced by the introduction of domains as shown in Fig. 2.9.

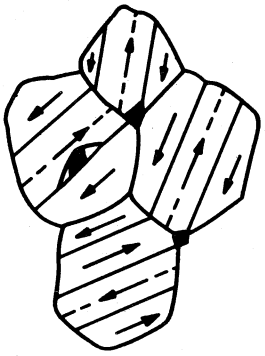

FIG. 2.9. Domains in polycrystalline material; the broken lines show the easy direction within each grain.

In practice the domain configuration will be complex. It will be influenced by second phases and pores which are common at the grain boundaries and which may also occur within the grains, local variations of composition across the grains and the stresses in the material due to magnetostriction. These stresses are intrinsic because as the material is cooled from the Curie Point, where there is no magnetization and therefore no magnetostriction, the spontaneous magnetization is established and so in general the grains are stressed. In order to minimize this stress the magnetostriction in the easy directions has to be made as near zero as possible.

2.4.3. MAGNETIZATION DUE TO WALL MOVEMENT

When an external magnetic field, H, is applied to a perfect magnetic crystal in which domains exist, the domains having a component of their orientation in the direction of the applied field will grow at the expense of those that have a component opposed to that direction, see Fig. 2.10a) and b).

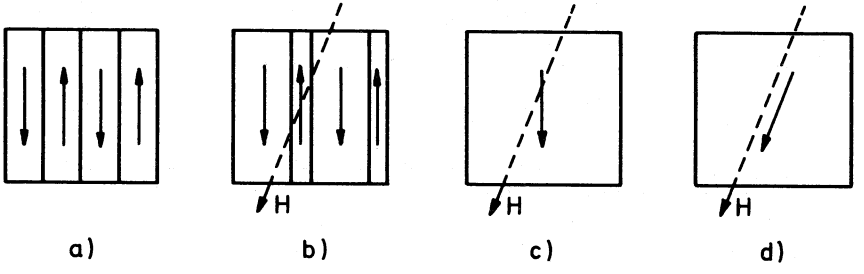

FIG. 2.10. Diagrammatic representation of the effect of an applied field on domain configuration: a) H zero, b) H small, c) H large, d) saturation.

Favourably oriented domains will coelesce and others will be annihilated. At this stage, c), the material will consist of crystallites each composed of a single domain magnetized along a preferred direction, having a component in the direction of the applied field. Further increase in H will begin to rotate the magnetization vectors towards the direction of the applied field, d), (see next Section).

This simple picture is complicated in both single crystals and polycrystalline materials by imperfections which tend to pin the domain walls and prevent them from moving freely in response to the applied field. For example, if a domain wall has to move away from a pore, see Fig. 2.7, the wall area must increase in order to minimize magnetostatic effects. Energy is required for this to happen and so the pore effectively pins the domain wall, thus restricting the magnetization resulting from a given applied field strength.

Even if the imperfection is so small that no closure domains would form around it, it will still tend to pin the wall; this is because the disturbance of the uniform magnetization and the associated exchange and magnetocrystalline energy will be smaller when the imperfection is within the wall. Wall mobility is most seriously impaired by inclusions and pores having dimensions commensurate with the wall thickness.

Where the movement of the wall is impeded by imperfections or grain boundaries, the magnetization can respond to the applied field by bulging the walls, see Fig. 2.11.

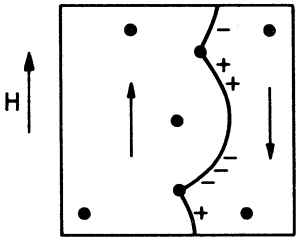

FIG. 2.11. An applied field, H, causes domain walls to bulge when they are pinned at imperfections.

If, during bulging, the surface of the wall cannot remain parallel to the difference vector of the magnetization on either side of the wall, free poles will form which will hinder wall movement. Even if the surface of the wall can remain parallel to the difference vector, the increase of the domain wall length during bulging will oppose movement, that is, the wall exhibits a type of surface tension.

In polycrystalline materials domain wall bulging is usually described in terms of spherical or cylindrical bulging[20,21]. The wall is assumed to be pinned at the grain boundary either along its circumference, Fig. 2.12a) (spherical bulging) or along two edges, Fig. 2.12b) (cylindrical bulging). In the first case magnetic poles will form on the wall and when bulging occurs both magnetostatic energy and the increase in domain wall energy must be overcome.

In the second case the surface of the domain wall remains parallel to the difference vector of the magnetization and when a magnetic field is applied the gain in field energy is set against only the increase in domain wall energy.

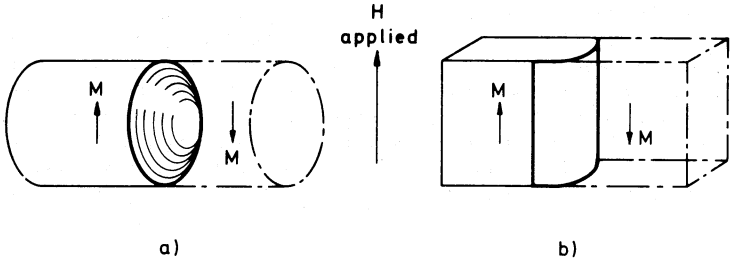

FIG. 2.12. Domain wall bulging: a) spherical, b) cylindrical.

Hysteresis occurs as a result of irreversible domain wall movements (and irreversible domain rotations). Various models to describe the movement of a domain wall through inhomogeneous materials have been suggested to explain magnetic hysteresis and to provide a theory of coercive force[22,23,24]. A segment of a domain wall moves reversibly through a grain in response to an applied field until it impinges on a defect and is locally pinned. The rest of the wall continues to move forward by bulging and the defect exerts a retarding force on the wall movement. Energy increases due to the increase in wall area and to magnetostatic effects until, at some critical point, the wall breaks away from the defect and relaxes towards its planar state (minimum local energy). In this process, the energy stored due to the deformation of the domain wall is dissipated. It is this irreversible "snapping free" of the flexible domain wall from its pinning points that is the origin of magnetic hysteresis; it is also the reason for the rapid increase in magnetization with applied field that occurs in the centre region of the magnetization curve (see Fig. 2.13).

Pinning defects in polycrystalline ferrites may, for example, arise from pores within grains, stress-induced variations in magnetic anisotropy and magnetic poles on the grain boundaries.

2.4.4. MAGNETIZATION DUE TO ROTATION

In a perfectly homogeneous material, magnetization due to rotation of the spins will only occur after magnetization due to wall displacement has been completed. Saturation is then reached by the reversible rotation of all the domain magnetization vectors towards the direction of the applied field. The field strength required for near-complete saturation depends on the strength of the magnetic anisotropy energy,

against which the field exerts a torque given by

$$M_s H \sin\beta = -\partial E_a / \partial \beta \qquad (2.16)$$

where β is the angle between the magnetization and the applied field. Normally β is small ($<90°$) and the rotation is reversible.

If reverse magnetized domains exist, ($\beta > 90°$), for whatever reason, then at some critical field strength the magnetization will switch, i.e. rotate irreversibly[25,26]. Such a reverse domain may arise from a domain wall which has become too strongly pinned to be moved or from a grain which is too small to support a Bloch wall.

2.4.5. STATIC HYSTERESIS LOOPS

In the previous two Sections the way in which the magnetization increases in response to a magnetic field has been described. Magnetic materials may be characterized by a graph of the magnetization as a function of the field strength; this is called the magnetization curve. It is of more practical use, when describing materials for use in transformer and inductor applications, to use the B(H) curve rather than the M(H) curve.

The magnetic field strength H inside a very long uniform solenoid or radially thin toroid with N turns of conductor wound evenly over the length ℓ and carrying a current of I Amps is:-

$$H = NI/\ell \qquad A.m^{-1} \qquad (2.17)$$

When the solenoid or toroid is filled with the magnetic material the internal field H_i is augmented by the magnetic moments of the material characterized by the magnetization M

$$H_i = NI/\ell + M \qquad A.m^{-1} \qquad (2.18)$$

The field H_i (or H in the absence of the magnetic material) produces a magnetic induction or magnetic flux density, B, the unit of which is the Tesla (or Weber/m^2).

$$B = \mu_o H_i = \mu_o (H + M) = \mu_o H + J \qquad T \qquad (2.19)$$

where μ_o is the permeability of free space ($= 4\pi \times 10^{-7}$) and J is the magnetic polarization or intrinsic flux density.

A material in the virgin state, i.e. having no magnetic history, is said to be magnetically neutral and its magnetic state is represented by the origin, O, of the curve in Fig. 2.13. For small applied fields, Oa, reversible domain wall movements predominate. As the field strength increases, irreversible domain wall movements occur as the domains break away from their pinning points and the curve rises steeply to 'b'. At higher fields, irreversible and reversible spin rotations occur, as described in Section 2.4.4, and the material approaches saturation at 'c'. Further increases in field will merely improve the alignment of the magnetization against the forces of anisotropy.

In magnetically soft materials, inhomogeneities result in a statistical distribution of the magnetization processes i.e. the reversible and irreversible wall movements and rotations merge so that there is a gradual transition from 'a' to 'c'. The curve Oabc is called the initial magnetization or commutation curve.

When the applied field is decreased from its saturation value at 'c', the decrease in flux density lags behind the decrease of H, due to the irreversible processes of magnetization, and the upper limb of the loop is traced. As the field is reduced the domain magnetizations will rotate reversibly back to their nearest easy direction. When the applied field has been reduced to zero the flux density will be left at B_r; this point is called the remanence. If H is then reversed, irreversible domain wall movements and domain rotations magnetize the material in the reverse direction, reaching saturation at 'd'. On increasing the field from 'd' the lower limb of the loop is traced to form, after a few cycles, the closed loop shown. The field at which the loop crosses the B=0 axis is called the coercivity $H_{c(B)}$. (This differs from the field required to reduce the magnetization to zero H_{cM}, according to Eqn. 2.19), but this distinction is of little significance in the characterization of soft ferrites).

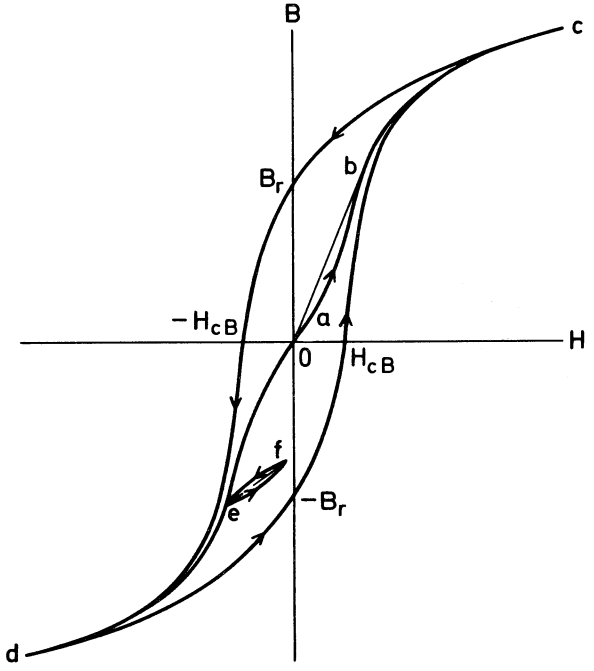

FIG. 2.13. The B(H) hysteresis loop.

Since B is a two-valued function of H, the quotient of flux density and applied field strength will depend not only on the field strength but also on the immediate magnetic history, i.e. the way in which the magnetic field reached its given value. At any point on the commutation curve,

$$B/H = \mu_o (1 + M/H) = \mu_o (1 + \kappa) = \mu_o\mu_r \qquad (2.20)$$

where κ is the susceptibility
μ_r is the relative permeability
and the product $\mu_o\mu_r$ is the absolute permeability.

In applied magnetism it is the relative permeability that is most widely used and it is this permeability that is implied in the present text when the term permeability, or μ, is used. Specific permeabilities relating to particular conditions of magnetization will be defined in Chapter 3.

CHAPTER 2. REFERENCES

1. Smit, J. and Wijn, H.P.J. Ferrites. pp.6-9. Philips Technical Library, Eindhoven, (1959).
2. Hund, F. Linienspektren und Periodisches System der Elemente. Julius Springer, Berlin, (1927).
3. Chikazumi, S. Physics of Magnetism. pp.52-59. John Wiley and Sons, Inc., New York, (1964).
4. Weiss, P. L'hypothèse du champ moleculaire et la proprieté ferromagnétique. J. Phys., (1907), 6, p.661.
5. Chikazumi, S. Physics of Magnetism. pp.60-77. John Wiley and Sons, Inc., New York, (1964).
6. Smit, J. and Wijn, H.P.J. Ferrites. pp.9-11. Philips Technical Library, Eindhoven, (1959).
7. Smit, J. and Wijn, H.P.J. ibid. pp.140-145.
8. Anderson, P.W. Molecular field theory of antiferromagnetism. Phys. Rev., (1950), 79, p.350.
9. Broese van Groenou, A., Bongers, P.F. and Stuijts, A.L. Magnetism, microstructure and crystal chemistry of spinel ferrites. Mater. Sci. Eng., (1968/9), 3, pp.325-331.
10. Brailsford, F. Physical Principles of Magnetism. p.124, D. Van Nostrand Co. Ltd., London, (1966).
11. Pearson, R.F. Magnetic anistropy, Experimental Magnetism. (Edited by G.M. Kalvius and R.S. Tebble), 1, pp.138-223, John Wiley and Sons, Chichester, (1979).
12. Yosida, K. and Tachiki, M. On the origin of magnetic anisotropy energy in ferrites. Prog. Th. Phys., (1957), 17, No.3, pp.331-359.
13. Chikazumi, S. Physics of Magnetism. pp.153-159. John Wiley and Sons, Inc., New York, (1964).
14. Broese van Groenou, A., Bongers, P.F. and Stuijts, A.L. Magnetism, microstructure and crystal chemistry of spinel ferrites. Mater. Sci. Eng., (1968/9), 3, pp.331-341.

15. Birss, R.R. and Isaac, E.D. Magnetostriction, Magnetic Oxides. (Edited by D.J. Craik). pp.289-346, John Wiley and Sons, London, (1975).
16. Chikazumi, S. Physics of Magnetism. pp.19-24. John Wiley and Sons, Inc., New York, (1964).
17. Brailsford, F. Physical Principles of Magnetism. pp.143-159. D. Van Nostrand Co. Ltd., London, (1966).
18. Néel, L. Effet des cavités et des inclusions sur le champ coercitif. Cah. Phys., (1944), No.25, pp.20-44.
19. Chikazumi, S. Physics of Magnetism. pp.186-192. John Wiley and Sons, Inc., New York, (1964).
20. Chikazumi, S. ibid. pp.260-280..
21. Hoekstra, B. et al. Initial permeability and intrinsic magnetic properties of polycrystalline MnZn-ferrites. J. Appl. Phys., (1978), 49, No.9, pp.4902-4907.
22. Baldwin, J.A. Jr. Nature of the material perturbations responsible for hysteresis in magnetic domain-wall motion. J. Appl. Phys., (1968), 39, No.13, pp.5982-5986.
23. Baldwin, J.A. Jr. and Culler, G.J. Wall pinning model of magnetic hysteresis. J. Appl. Phys., (1969), 40, No.7, pp.2828-2835.
24. Knowles, J.E. The simulation of domain wall motion in square loop ferrites, and other aspects of wall behaviour. Brit. J. Appl. Phys. (J.Phys.D), (1968), ser.2, 1, pp.821-830. (Based on Mullard Res. Labs. Report No.2625, (Aug. 1967).
25. Chikazumi, S. Physics of Magnetism. pp.281-285. John Wiley and Sons, Inc., New York, (1964).
26. Smit, J. and Wijn, H.P.J. Ferrites, pp.75-77, Philips Technical Library, Eindhoven, (1959).

CHAPTER 3
Properties of Ferrites

3.1. INTRODUCTION

In the previous Chapter magnetization processes have been examined from what is essentially a static viewpoint. After a brief résumé of the mechanical and thermal properties, this Chapter examines the way in which ferrites behave under more practical conditions, that is, the dynamic situation when they are subjected to a time-varying magnetic field.

Soft ferrites are used over a wide range of frequencies and generally it is desirable to have high permeability and low magnetic losses up to the highest possible frequency. The magnetic losses are the various energy losses observed as the difference between the energy stored during the application of a magnetic field and the energy recovered when the field is returned to its initial value. If the applied field is alternating, the loss is basically expressed in Joules/cycle.

The various loss mechanisms cause the flux density, B, to lag behind the applied alternating field, H, by a phase angle δ_m. The permeability is complex and must be expressed in terms of its real (inductive) component, μ', and its imaginary (loss) component, μ'':-

$$\mu = \mu_s' - j\mu_s'' \qquad (3.1)$$

The losses are often expressed as the tangent of the loss angle:-

$$\tan\delta_m = \mu_s''/\mu_s' \qquad (3.2)$$

$\tan\delta_m$ is called the magnetic loss tangent. Where permeability or μ is used without further specification the real component μ_s' is implied.

The structure of this Chapter is as follows. After a brief indication of the mechanical and thermal properties in Section 3.2, Section 3.3 describes the electrical properties of ferrites, in Section 3.4 the real part of the permeability and its dependence on composition, temperature, time and stress are discussed while Section 3.5 will

describe the various loss mechanisms present in ferrites and their dependence on the operating conditions. Finally some of the important properties of ferrites typical of those commercially available are tabulated in Section 3.6.

3.2. MECHANICAL AND THERMAL PROPERTIES

Table 3.1 gives values for the mechanical properties of some pressed ferrites measured on one manufacturer's range of materials. Care should be taken in interpreting these values, particularly those for tensile strength, since the tensile fracture of the material is often initiated by a firing crack or other imperfection, and the larger the piece the more chance there will be of such an imperfection being present. The value obtained may thus depend on the size of the specimen measured. Typical thermal properties of ferrites are given in Table 3.2.

	Density ($kg.m^{-3}$)	Ultimate tensile strength ($kgf.mm^{-2}$)	Ultimate compressive strength ($kgf.mm^{-2}$)	Young's modulus ($kgf.mm^{-2}$)
MnZn ferrite	4500-4900	3.5 - 6.5	20 - 60	$(9\text{-}15) \times 10^3$
NiZn ferrite	4000-5000	3 - 6	18 - 70	$(8\text{-}15) \times 10^3$

TABLE 3.1. Mechanical properties of ferrites

Property	Conditions	Value	Units
Coeff. of linear expansion			
MnZn ferrites	0 - 50°C	10×10^{-6}	$°C^{-1}$
	0 - 200°C	11×10^{-6}	$°C^{-1}$
NiZn ferrites	0 - 50°C	7×10^{-6}	$°C^{-1}$
	0 - 200°C	8×10^{-6}	$°C^{-1}$
Specific heat			
MnZn ferrites	25°C	1100	$J.kg^{-1}.°C^{-1}$
		0.26	$cal.g^{-1}.°C^{-1}$
NiZn ferrites	25°C	750	$J.kg^{-1}.°C^{-1}$
		0.18	$cal.g^{-1}.°C^{-1}$
Thermal conductivity			
MnZn ferrites)	25 - 85°C	3500 - 4300	$\mu W.mm^{-1}.°C^{-1}$
		35 - 43	$mW.cm^{-1}.°C^{-1}$
NiZn ferrites)		0.0083 - 0.010	$cal.s^{-1}.cm^{-1}.°C^{-1}$

TABLE 3.2. Typical thermal properties of ferrites

3.3. ELECTRICAL PROPERTIES

Ferrites are semiconductors having resistivities that are generally more than a million times greater than those of the magnetic alloys. At room temperature, most MnZn ferrites have resistivities between 0.01 and 10 Ωm while NiZn ferrites normally have values > 10^3Ωm (values as high as 10^8 Ωm have been reported). Although ferrite resistivities are high, eddy currents in MnZn ferrites are not entirely negligible and they can result in significant energy losses particularly at high frequencies.

The mechanism of conduction in MnZn ferrites is thought to be electron hopping[1,2]. The presence of both Fe^{2+} and Fe^{3+} ions on octahedral sites results in an n-type conductivity arising from the interchange of electrons between the two ions. NiZn ferrites do not contain Fe^{2+} ions and their resistivities are consequently very much higher. The temperature dependence of the resistivity can usually be described by:-

$$\rho = \rho_\infty \exp\left(E_\rho/kT\right) \qquad (3.3)$$

where ρ_∞ is the resistivity extrapolated to $T \to \infty$

T is the absolute temperature

k = Boltzmann's constant = 8.62×10^{-5} eV.K^{-1}

and E_ρ is the activation energy for the conduction process expressed in electron volts.

In MnZn ferrites the substitution of some Fe^{3+} ions by, for example, a combination of Fe^{2+} plus the tetra-valent titanium ion Ti^{4+}, significantly increases the resistivity over a wide frequency range. The Ti^{4+} ion represents local excess of positive charge in the lattice which is offset by one of the neighbouring iron ions tending to remain in the divalent state. Thus, in effect, E_ρ is raised above the value observed when only Fe^{2+} ions are present[3].

Polycrystalline ferrites are usually regarded, as far as the low frequency resistivity is concerned, as being homogeneous. The main eddy currents circulate in the bulk of the material, crossing the grain boundaries. In fact, on a microscopic scale the resistivity is not homogeneous; the resistivity of the grain boundaries in MnZn ferrites is typically a million times that of the ferrite within the grains. The consequence of this granular structure is that the low frequency bulk resistivity is determined by the grain boundary resistivity and has a high value, but at high frequencies the grain boundary resistance is to some extent shunted by the capacitance of the boundary and so the observed bulk resistivity tends to decrease with increasing frequency. This effect is much smaller in NiZn ferrites. Any micro eddy currents that may circulate within the grains would contribute a small additional loss but this is generally indistinguishable from and incorporated with the residual loss considered in Section 3.5.3.

The same granular structure has, in MnZn ferrites, a dominant influence on the effective permittivity. Such ferrites are, in effect, compound dielectrics composed of very thin high resistivity grain boundaries separating semiconducting grains of low resistivity. The result is that effective permittivities as high as 100,000 are commonly observed.

A ferrite block of length ℓ, cross-sectional area, A, may be represented by the equivalent circuit of a dielectric shown in Fig. 3.1.

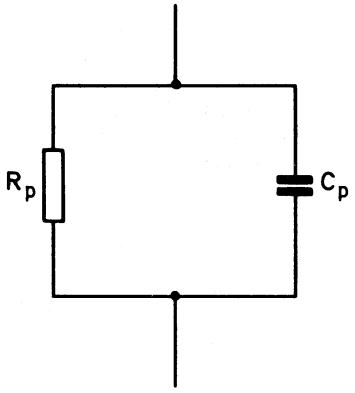

FIG. 3.1. The equivalent circuit of a dielectric

C_p is an ideal capacitor and R_p represents the parallel combination of the d.c. resistance and the dielectric loss of the ferrite.

$$\left.\begin{aligned} C_p &= \varepsilon_o \varepsilon\, A/\ell \quad & F \\ R_p &= \rho\ell/A \quad & \Omega \\ Y &= j\omega C_p + 1/R_p \end{aligned}\right\} \qquad (3.4)$$

where ε_o is the electric constant = 8.854×10^{-12} $F.m^{-1}$

Since the equivalent dielectric is not loss free, the permittivity may alternatively be regarded as complex; $\varepsilon = \varepsilon_p' - j\varepsilon_p''$ and the dielectric loss tangent is then given by:-

$$\tan\delta_d = \frac{1}{\omega C_p R_p} = \frac{\varepsilon_p''}{\varepsilon_p'} = \frac{1}{\omega \varepsilon_o \varepsilon_p' \rho} \qquad (3.5)$$

ε_p' and ε_p'' are the parallel components of the real and imaginary permittivity respectively.

As explained above, the grain boundary resistivity has a dominant effect on the dielectric properties of ferrites. It was formerly thought that the high grain boundary resistivity was due to the presence of a natural or artificially induced insulating second phase occurring at the grain boundary as a result of the sintering reaction.

Calcium and silicon oxides are often added to ferrites in small quantities since these segregate to the grain boundaries and increase its resistivity. Ti^{4+} substitutions are observed to increase the bulk resistivity across the frequency spectrum. The increase in granular and thus high frequency resistivity has already been explained as being due to the localization of the Fe^{2+} ions; the increase in low frequency resistivity suggests an enrichment of Ti^{4+} at the grain boundaries. Recent work[4] using Transmission Electron Spectroscopy (TEM), Auger Electron Spectroscopy (AES) and Photo-Electron Spectroscopy (ESCA) has shown that the grain boundary region occurs not as a segregation of a second phase as was previously thought, but rather as an enrichment of Ca, Si and Ti ions in the crystallite lattice to a depth of about 10Å from the grain boundary. The titanium ions, while enriched at the boundary are also distributed throughout the grains as shown in Fig. 3.2.

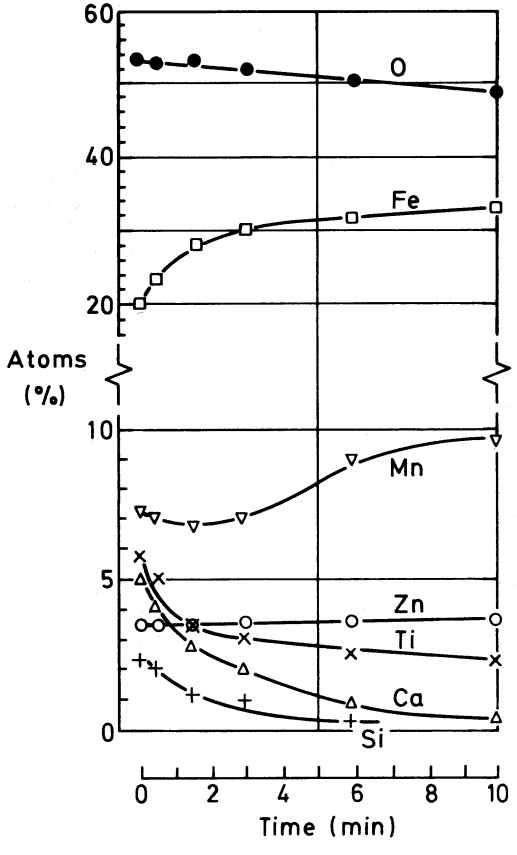

FIG. 3.2. The concentration of elements in an inter-granular fracture surface of low-loss MnZn ferrite with Ca, Si and Ti additions, as a function of argon-ion etching time, measured by AES (after Bongers et al.[4])

3.4. PERMEABILITY

Equation 2.20 defines the relative permeability in relation to the instantaneous ratio of B/H.

$$B/H = \mu_o(1 + M/H) = \mu_o\mu_r$$

In the case of alternating magnetization it is usually relevant to consider only the peak amplitudes of B and H i.e. the tips of the B(H) loops (see Fig. 2.13). If the material is in the symmetrical cyclic state about the origin, O, and $\hat{H}$ is vanishingly small, then the permeability is referred to as the initial permeability, μ_i; this is $1/\mu_o$ times the slope at the origin. For larger cyclic fields the amplitude permeability, μ_a, is the relevant parameter; it is defined as $1/\mu_o$ times the slope from the origin to the tip of the loop, i.e. $\mu_a = \hat{B}/\mu_o\hat{H}$. If a d.c. field is applied to a previously demagnetized material and a small alternating field is superimposed, a minor non-symmetric loop, ef, is traced, $1/\mu_o$ times the slope of which is referred to as the incremental permeability μ_Δ. Finally, $1/\mu_o$ times the slope at any point on the hysteresis loop is called the differential permeability.

High permeabilies are achieved by control of the composition and the microstructure. The permeability itself is made up of contributions from both the rotation of the magnetization and from domain wall movement. The rotational permeability is found[5] to be proportional to $M_s/|K_1|$, where M_s is the saturation magnetization; the permeability due to spherical bulging of domain walls is also proportional to this expression[6] (see Section 2.4.3). However, cylindrical bulging of domain walls results in a permeability proportional to $M_s/\sqrt{|K_1|}$, Ref.7. This cylindrical bulging of domain walls is thought to be the major contribution to the permeability in MnZn ferrites.

These proportionalities suggest that μ_i would tend to infinity if $|K_1| = 0$. In practice this is not the case since when K_1 is very small, second order magnetocrystalline anisotropy terms and also the anisotropy resulting from stresses and inhomogeneities become significant and must be taken into account.

The ratio of the permeability due to wall movement, μ_W, to the rotational permeability, μ_R, has been measured for a high permeability MnZn ferrite[8] and found to be approximately 1.7 over a wide temperature range. The ratio for a medium permeability, low-loss material, was seen to be similar except at temperatures in the region of low anisotropy (anisotropy compensation, see below) where it drops to approximately 1.2.

3.4.1. EFFECT OF COMPOSITION ON PERMEABILITY

The permeability is strongly dependent on the composition because this affects the intrinsic parameters (M_s, K_1 and λ) and the composition may in addition affect the microstructure. A composition chosen for a particular application is therefore usually a compromise taking all effects into account.

In Section 2.2 it was shown how M_s may be maximized by the correct choice of zinc content in MnZn and NiZn ferrites (Fig. 3.3).

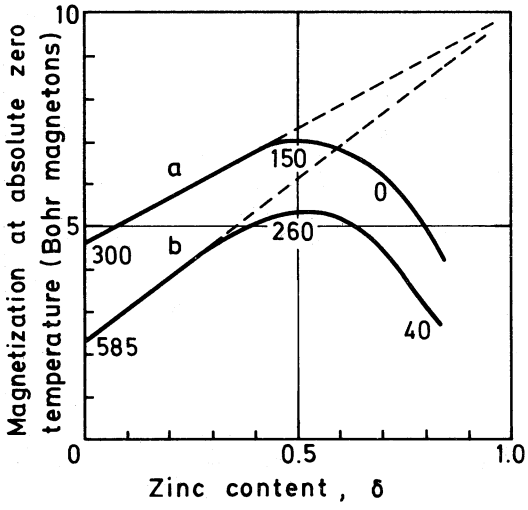

FIG. 3.3. Variation of magnetization with zinc content for $Me_{1-\delta}Zn_{\delta}Fe_2O_4$; a) Me=Mn and b) Me=Ni. The numbers on the graph give an indication of the Curie point in that region.

The Curie point is lowered by increasing the zinc content since the sublattice interactions are weakened by the introduction of the non-magnetic ions. The variation of μ_i with temperature is shown in Fig. 3.4 for ferrites with various Mn/Zn and Ni/Zn ratios.

The principle of anisotropy compensation is well known[9]. K_1 is made up of contributions from the various cations present in the material, the value and temperature dependence of these contributions depend on the cation species and the anisotropy mechanism. Both positive and negative contributions are found and so it is possible to obtain some cancellation of K_1 by the addition of certain cations in the appropriate proportions. In particular the introduction of Fe^{2+} in MnZn ferrites or Co^{2+} in NiZn ferrites has been very effective in reducing $|K_1|$ over a wide temperature range.

The presence of Fe^{3+} ions on octahedral sites contributes a negative K_1 and this may be compensated by the large positive and highly temperature-dependent contribution of the octahedral site Co^{2+} ions as shown in Fig. 3.5a) or by the less temperature-dependent contribution of the Fe^{2+} as in Fig. 3.5b). In the two cases illustrated, complete compensation of K_1 occurs at one temperature, θ_o, the compensation temperature. The aim is to keep K_1 as small as possible over a wide temperature range and to this end combinations of cations have been suggested to obtain compensation at two or more temperatures[3].

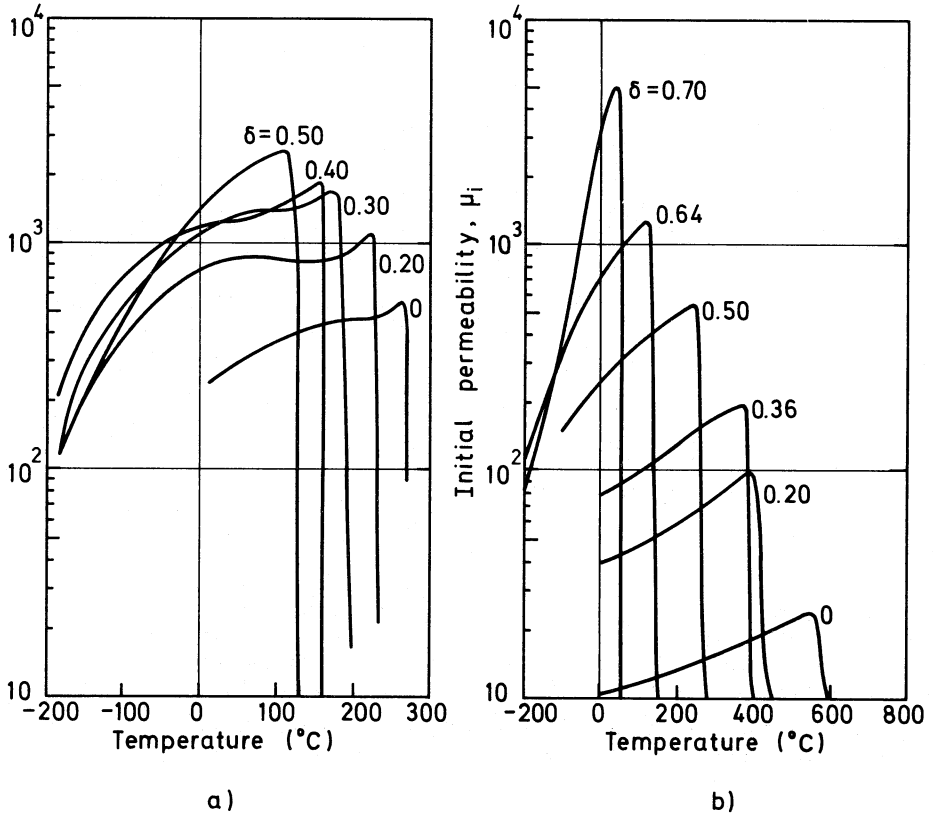

FIG. 3.4. Initial permeability as a function of temperature and zinc content for $Me_{(1-\delta)}Zn_{\delta}Fe_2O_4$; a) Me=Mn and b) Me=Ni

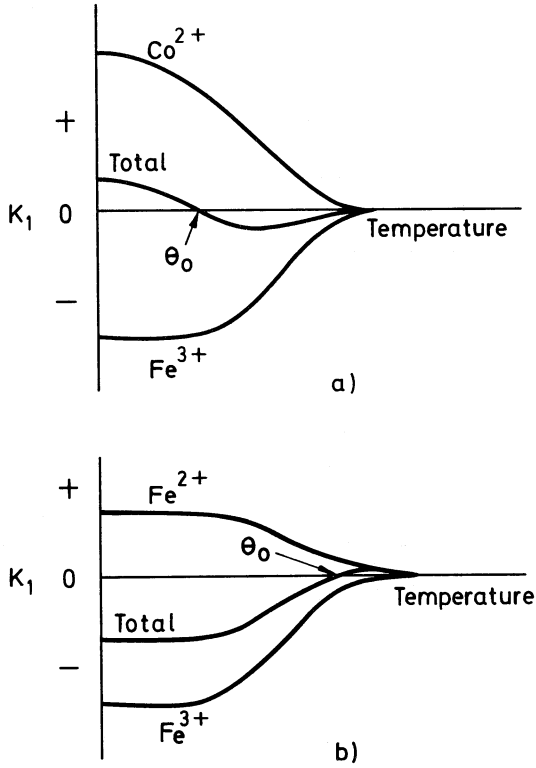

FIG. 3.5. Illustration of anisotropy compensation

Similarly magnetostriction is also a function of the contributing cations, and very small values of λ are observed in some MnZn ferrous ferrites. The magnetostriction constants λ_{100} and λ_{111} depend in value and sign on the cation species and their relative importance will depend on the crystalline anisotropy. For example, the overall magnetostriction has been found to change sign at the compensation temperature where a change of easy direction occurs and where λ_{100} and λ_{111} are of opposite signs. The magnitude of the magnetostriction is especially important when K_1 is small, since it controls the stress anisotropy which in polycrystalline materials limits the permeability in the region of θ_o, (see Section 2.3.3).

Magnetostriction in NiZn ferrites is found to be much larger than that in MnZn ferrites and it is always negative.

3.4.2. EFFECT OF MICROSTRUCTURE ON PERMEABILITY

A polycrystalline ferrite intended for high permeability applications should show the following features in its microstructure:

a) Large, homogeneous grains that are relatively free from imperfections such as pores, inclusions and dislocations.

b) Little or no second phase, non-magnetic segregations or pores at the grain boundaries.

c) Chemical homogeneity both within individual grains and across the whole component.

A linear relationship between permeability and grain size has been found[10] in both MnZn and NiZn ferrites provided the grains are pore-free (Fig. 3.6).

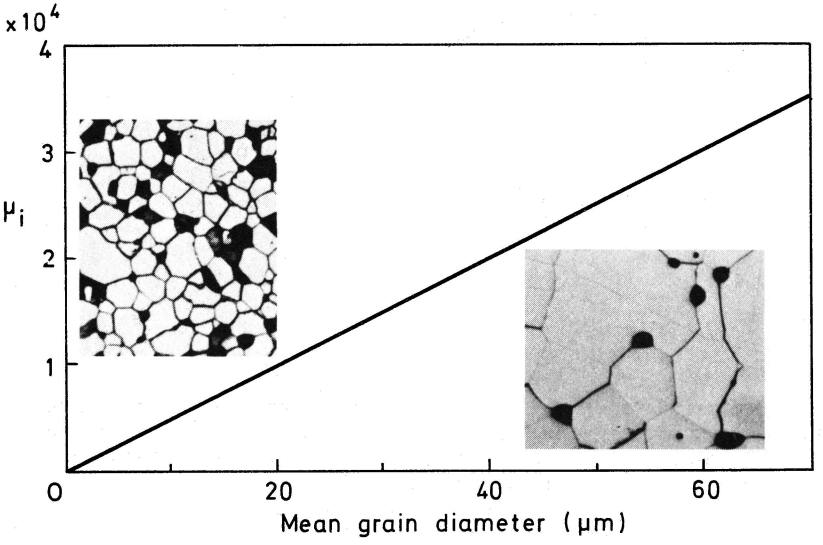

FIG. 3.6. Initial permeabiity as a function of grain size for a MnZn ferro-ferrite.

Pores within grains act as pinning points for domain walls and effectively reduce the grain size to the pore spacing. However, near $K_1 = 0$ the walls become wider and are less effectively pinned by the pores; this contributes to the secondary peak which occurs in the $\mu(\theta)$ characteristic at the compensation temperature. Large grain size and low porosity are achieved by control of the sintering conditions. In general, high permeability materials are made from pure, highly reactive, powders sintered at relatively high temperatures. Additives to accelerate sintering cannot be used because the presence of impurities may lead to stresses or may impede domain wall movement both of which would limit the permeability. Therefore long sintering times are usually required. This combination of long sintering time and high temperatures results in zinc evaporation from the outer surfaces of ferrite pieces and this reduces the permeability by the introduction of chemical inhomogeneity (and therefore stress) in the surface region. Prevention of zinc evaporation entails either the use of a static atmosphere at the top sintering temperature (so that evaporated zinc is not swept away) or by the sintering of the ferrite pieces under granules of a similar composition.

3.4.3. TEMPERATURE DEPENDENCE OF INITIAL PERMEABILITY

Fig. 3.7 shows curves of $\mu_i(\theta)$ for two polycrystalline MnZn ferro-ferrites and one polycrystalline NiZn ferrite.

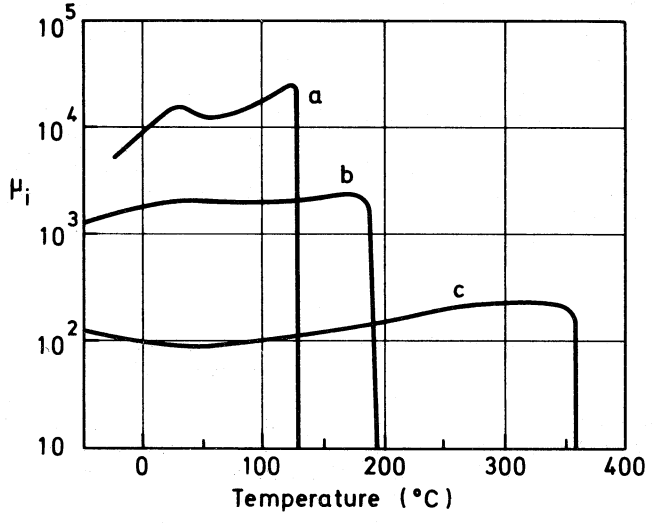

FIG. 3.7. Initial permeability as a function of temperature for a) a high permeability MnZn ferro-ferrite b) a low-loss, Ti-substituted linear MnZn ferro-ferrite and c) a low-loss NiZn ferrite

Curve 3.7a) is typical of a high permeability material sintered under optimum conditions to obtain a large average grain size of approximately 30 μm. K_1 for this material is low over a wide temperature range and is zero in the region of compensation temperature (about 25°C) resulting in a secondary peak at that temperature. That this peak is of finite height is an indication of the presence of second order anisotropy effects and stresses. Detailed analysis of the $\mu_i(\theta)$ curve is difficult in the case of a polycrystalline material because of its inherent inhomogeneity. Some years ago single crystals were produced by the seeded Bridgman technique; they had compositions comparable with practical polycrystalline materials and a detailed analysis of the $\mu_i(\theta)$ curve with respect to M_s, K_1 and K_2 became possible[11]. Further work by Brough[12] on the same material has extended the analysis to include the intrinsic stress effects arising from rotation of the magnetization within a domain wall. It has been shown that the secondary peak in the $\mu_i(\theta)$ curve occurs at a temperature which is determined not only by $K_1=0$ but by the other contributions to the anisotropy as well. Indeed, for a single crystal measurement of $\mu_i(\theta)$, a change in slope is observed just below the secondary peak; this occurs at the temperature at which $K_1=0$ and the easy direction changes from <100>. The curve for a polycrystalline material shows a wider peak than that for a single crystal and there is a shift in the position of the secondary peak. This shift is attributed to the stresses within the grains which modify the anisotropies present. The increase in peak width is thought to be due to a small distribution in K_1 values, at a given temperature, caused by compositional non-uniformity; for example, a 2% variation in ferrous ion content is enough to shift the peak by 10°C.

Curve 3.7b) shows the $\mu_i(\theta)$ characteristic of a medium permeability, low loss material. In this case the secondary peak is suppressed and is merely an undulation in a gently rising curve. Such materials are used for inductors where the positive temperature factor, TF, has to be controlled over a certain range of temperatures so that it can be matched to the negative temperature characteristics of a resonating capacitor.

$$TF = \frac{\mu_2 - \mu_1}{\mu_1 \mu_2 (\theta_2 - \theta_1)} \qquad {}^{o}C^{-1} \tag{3.6}$$

where μ_1 and μ_2 are the initial permeabilities measured at temperatures θ_1 and θ_2 respectively. See also Eqn. 4.12.

Clearly a non-linear characteristic such as that shown in curve a) would be most unsuitable for this application. Curve b) is much nearer to the requirement: generally the approximately linear region around the point of inflection in the curve (to the right of the compensation temperature θ_o) would be used. The magnetic losses are at a minimum at the compensation temperature (see Section 3.5.3) so that it is advantageous to have the operating temperature range as close as possible to θ_o). To be able to do this, the secondary peak must be sufficiently suppressed so that the slope of the curve near θ_o corre-

sponds with the required TF. This is achieved by control of both the microstructure and composition. The average grain size is restricted to about 10 μm and there is a fairly high intergranular porosity.

Additions, such as TiO_2, in MnZn ferro-ferrites are very effective in producing a small, approximately constant TF as well as improving other properties of the ferrite[3]. Ti^{4+} ions in combination with Fe^{2+} ions make a large, strongly temperature-dependent contribution to K_1, rather similar to that of Co^{2+}, and it has been suggested that this leads to a double compensation of K_1 thus spreading the region of low K_1 over a wide temperature range[13]. The Fe^{2+} ions are tied to the Ti^{4+} ions due to charge compensation and so the observed gradient of Ti^{4+} ions towards the outer surface of the grains[4] (see Section 3.3) is likely to cause a similar gradient of Fe^{2+} ions. It seems likely therefore that the suppression of the secondary peak occurs as a result of a spread in K_1 values at a given temperature due to the variation in density of these ions across the grain.

Small amounts of Co^{2+} added to MnZn ferro-ferrites can produce a very flat linear $\mu_i(T)$ curve over a wide temperature range[14]. The shape of the curve is, however, very dependent on the thermal history of the sample and the material is rather sensitive to magnetic and mechanical shock which can make it unreliable in applications requiring high stability.

NiZn-Co ferrites[15] with a deficiency of iron show good high frequency properties. The introduction of Co^{2+} ions results in some compensation of K_1 and a secondary peak may occur in the $\mu_i(\theta)$ characteristic. However, the permeability is generally depressed over the whole temperature range since the cobalt has the effect of stabilizing the domain walls and the contribution of domain wall movements to the permeability is considerably reduced.

3.4.4. TIME DEPENDENCE OF INITIAL PERMEABILITY

Inductors used in high quality telephony filters are required to have a sufficiently stable inductance such that the characteristic of the filter remains within specification for the duration of its service life, e.g. 20 years. The permeability of ferrite materials used for such applications must be correspondingly stable with time.

If a magnetic material is subjected to a disturbance, which may be magnetic, thermal or mechanical, the permeability immediately after removal of the disturbing influence is observed to have an increased value. The permeability then shows a gradual decrease over a period of time, returning asymptotically towards its undisturbed or stable value. This phenomenon is known as disaccommodation. The reduction in permeability is usually taken to be proportional to the logarithm of time and the I.E.C. recommendation for expression of the disaccommodation, D, is:

$$D = (\mu_1 - \mu_2)/\mu_1 \log_{10}(t_2/t_1) \qquad (3.7)$$

where μ_1 and μ_2 are the permeabilities measured at times t_1 and t_2 respectively after a specified test disturbance.

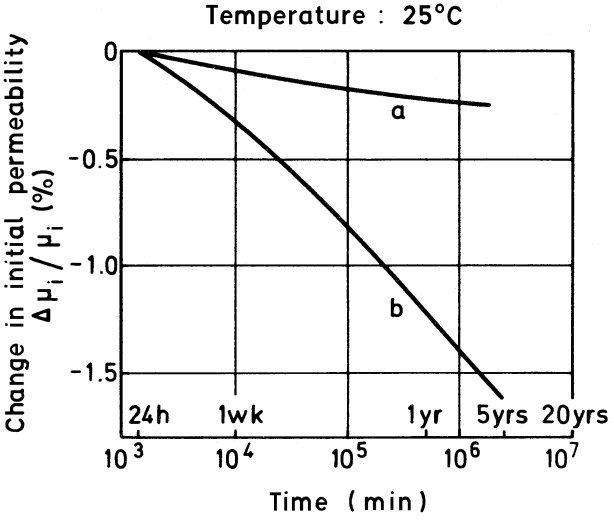

FIG. 3.8.
Time change of initial permeability relative to the value at 24 hr after a standard test disturbance of
a) a high quality Ti-substituted MnZn ferrite &
b) a more typical MnZn inductor ferrite

Fig. 3.8 shows initial permeability as a function of time following such a disturbance. It is clear from this Figure that the graphs are not straight lines and that some errors will occur if short term observations are used to predict long term behaviour using Eqn. 3.7.

The most fundamental disturbance for a magnetic material is to raise its temperature above its Curie point and then return it at a controlled rate back to the measuring (room) temperature. This procedure is usually not very practical as a quantitative method for obtaining a measure of the disaccommodation and in general a.c. demagnetization is preferred. The usual standard test disturbance is to subject the material to a saturating a.c. field for a few cycles and then reduce the amplitude of the field steadily to zero over a number of cycles. This method of disturbance is less extreme in that the domain magnetizations are left oriented around the direction of the demagnetizing field and not isotropically oriented as they are after Curie point demagnetizing. It should be remembered that both methods of magnetic disturbance are artificial and are unlikely to occur during the life of a filter inductor. However, the amount of disaccommodation is strongly correlated to the magnitude of the disturbance, so that the disaccommodation parameter, D, obtained following the test disturbance is a measure of the time dependence of permeability. Smaller disturbances occurring during the service life of an inductor, e.g. a relatively small step in temperature, will result in a correspondingly smaller change of permeability with time.

There are a number of possible mechanisms for disaccommodation in ferrites all of which involve the migration of magnetically active cations to positions that are energetically more favourable. The preference, on energy considerations, for a particular lattice site depends on the local direction of the magnetization. As a result of the cation migration, the domain wall becomes stabilized in position, i.e. it "sinks into an energy well" and loses some of its mobility; it is thus less able to contribute to the permeability. Hence the permeability progressively decreases towards its stable value until a further disturbance results in the domain wall being moved from the relatively stabilized position, and the disaccommodation cycle is re-started. The rate at which stabilization occurs is very temperature-dependent, shorter time constants occurring at higher temperatures. The measurement of μ_i during the disaccommodation must not itself disturb the material and vanishingly small measuring amplitudes are used.

A convenient way of distinguishing different diffusion processes that contribute to the disaccommodation is to express the disaccommodation as a function of temperature, referred to as a disaccommodation spectrum[17]. The disaccommodation spectra for two MnZn ferrites are shown in Fig. 3.9.

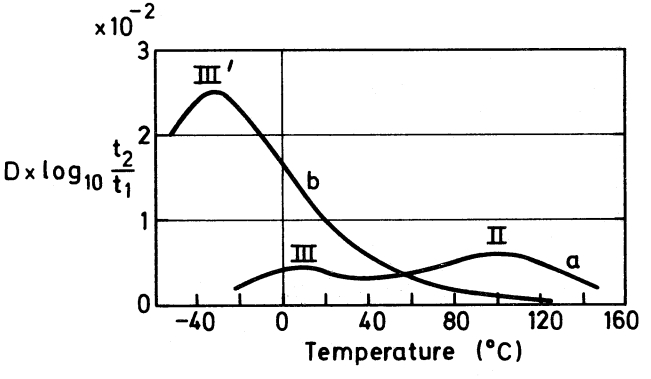

FIG. 3.9. Disaccommodation between 5 sec and 5 min after demagnetization as a function of temperature for two MnZn materials: a) typical MnZn ferrite and b) a Ti-substituted ferrite.

The position of the peaks is not very dependent on the observation intervals t_1 and t_2 (5 and 300 secs respectively in the Figure) and each peak represents a process having a different relaxation time. It is the higher temperature process (peak II), having a time constant of the order of minutes at about 100°C, that is the cause of long term disaccommodation in MnZn ferro-ferrites. At room temperature this process has a time constant of the order of years. Process II[16,17] is thought to arise primarily from the orientation of Fe^{2+}-Fe^{2+} pairs through the agency of the diffusion of vacancies although it is observed that the vacancy concentration does not affect the amplitude of the peak. Simple statistical theory shows

that the number of ferrous ion pairs per formula unit is $3y^2(1-y/2)$[8] where y is the Fe^{2+} content per formula unit. For the small Fe^{2+} contents found in practice the amplitude of the process II peak shows an approximate square law dependence as indicated by the above expression. The addition of Ti^{4+} to MnZn ferro-ferrites results in a strong suppression of the process II peak and the long term stability of such a material is very good. The Fe^{2+} ion binds itself strongly to a Ti^{4+} ion, thus reducing the number of Fe^{2+} ions free to participate in process II.

For an unsubstituted ferrite, as stated above, the amplitude of peak II is proportional to (Fe^{2+} concentration)^2. For a similar ferrite substituted with Ti^{4+}, the amplitude of peak II becomes proportional to (the unbound Fe^{2+} concentration)^2. In practice, and particularly where the vacancy concentration is low, the peak virtually disappears (see curve b) of Fig. 3.9). Here two effects are at work, first the amplitude of the peak is reduced as just described and secondly the decrease of the vacancy concentration increases the relaxation time so much that any residual peak is shifted to a temperature above the Curie point.

The lower temperature peak, process III, has a relaxation time of the order of minutes at room temperature. The amplitude of the peak is proportional to both the Fe^{2+} ion and the vacancy concentrations while the relaxation time is independent of the Fe^{2+} content. Process III is associated with Fe^{2+}-vacancy pairs and is thought to arise from the migration of vacancies in the presence of Fe^{2+} ions[17]. In the Ti^{4+} substituted material, the process III peak is shifted to lower temperatures. The shifted peak is labelled III'. It is thought that the large electrostatic charge of the Ti^{4+} ions distorts the lattice sufficiently to facilitate the diffusion of the neighbouring iron ions in the presence of cation vacancies, the activation energy is lowered and the peak is shifted to a lower temperature. Any excess Fe^{2+} ions in addition to those bound to the Ti^{4+} contribute to the normal process III and two separate peaks have been observed[18].

3.4.5. STRESS DEPENDENCE OF INITIAL PERMEABILITY

Components made from ferrite materials may be subjected to stresses in various ways. In many cases surface grinding is necessary to bring certain dimensions within limits or to provide a required surface finish. Such grinding leaves the surface in a state of stress that approximates to the ultimate compressive stress (see also Section 4.7). This stress drastically reduces the surface permeability and causes the bulk of the material below the surface to be subjected to a tensile stress. Other causes of stress are the clamping of core parts for the purpose of assembly and the application of materials such as epoxy resins as adhesives or protective coatings.

In ferrites where the magnetocrystalline anisotropy has been minimised, the anisotropy due to stress (see Section 2.3.3) may have the dominant role. At high stress levels the permeability is always decreased due to stress anisotropy operating through the magnetostriction. Fig. 3.10 shows the initial permeability as a function of both compressive and tensile stress for some MnZn and NiZn ferrites.

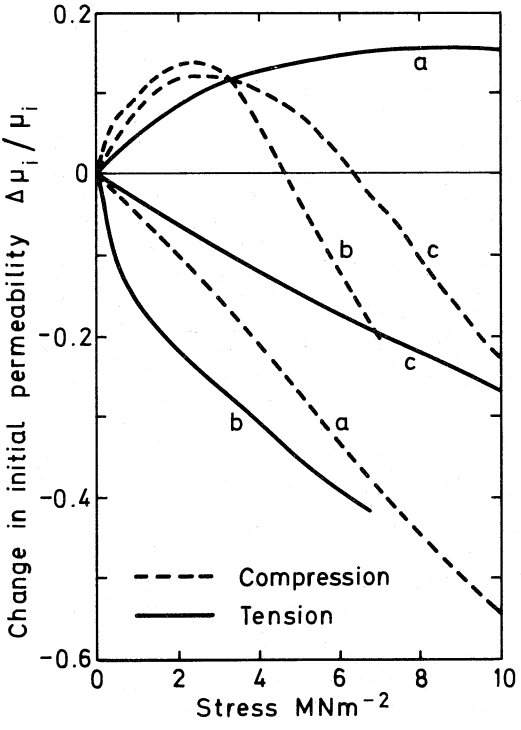

FIG. 3.10. Changes in initial permeability as a function of applied longitudinal stress:
a) NiZn ferrite; μ_i = 100
b) MnZn ferrite; μ_i = 4850
c) MnZn ferrite; μ_i = 1650

It is observed that for small applied stresses, ferrites having negative bulk magnetostriction will have the permeability raised by compression and lowered by tension. For positive magnetostriction the reverse applies.

Fig. 3.11 shows two $\mu_i(\theta)$ curves for a toroidal specimen consisting of monocrystalline, high permeability, MnZn ferro-ferrite. The core is relatively thin in the axial direction so that the surface to volume ratio is large. The curve having the solid points is for the toroid as cut from the bulk material. The cutting operation leaves the surface with a large compression stress which induces a relatively small tensile stress through the bulk of the material. The compressed surface layer is very thin and, being of low permeability, it has negligible contribution. The resultant tensile stress in the bulk of the ferrite is directed circumferentially and dominates the shape of the curve. When the surface layer is etched away, the tensile stress is relieved and the resultant curve is indicated by open circles.

It is seen that the effect of the tensile stress is to lower the peak that occurs at the anisotropy compensation point and to cant the curve around a point near the compensation temperature. The lowering of the peak is consistent with the stress anisotropy having a dominant role when the magnetocrystalline anisotropy is near zero.

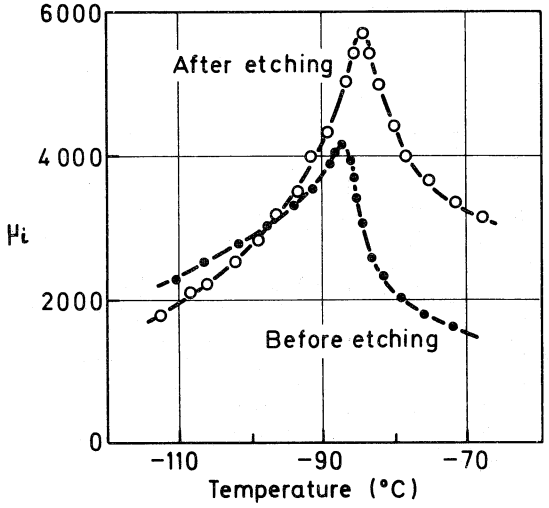

FIG. 3.11. Initial permeability as a function of temperature for a toroid of MnZn ferrite cut from the bulk and ground (closed circles), and after etching to remove a surface layer of 10μm (open circles). After Stopples et al[19].

The canting of the curve is usually ascribed to a change[19] in the preferred direction of magnetization at the compensation point, θ_o. At temperatures below θ_o the preferred direction is <111> and the magnetostriction λ_{111} is positive; above θ_o the preferred direction is <100> and λ_{100} is negative. Thus the presence of a small tensile stress when $\theta < \theta_o$ will raise the permeability whereas when $\theta > \theta_o$ tension will lower the permeability. The two curves demonstrate this effect, although imperfectly. However, this explanation assumes that the permeability is predominantly the result of domain rotation, but at low stress values this assumption is not valid. Further, this model does not account for the reduction of permeability at high stress levels.

Brough[12] has recently studied the effect of stress on permeability in some detail. He notes that at low field strength in high permeability materials, the permeability is dominated by movement of 180° domain walls, therefore he analyzed the effect of stress on the wall permeability. It is clear that when the rotation of the magnetization within the domain walls under the influence of stress is considered, both magnetostriction constants are of importance at any given temperature. He showed that the stress dependence of permeability could be evaluated only for compressive stress after a.c. demagnetization. For high stress levels the calculated slope of the μ(stress) curves was negative and consistent with measured values. For small values of stress the permeability measured in a polycrystalline sample rises to a peak before decreasing asymptotically to the calculated negative slope. He attributes this initial rise in permeability to a distribution of preferred directions over a much larger solid angle than is generally assumed, the initial rotation of the magnetization from these wider angles under the influence of small stresses giving rise to an increase in permeability.

3.5. MAGNETIC LOSSES

The nature of the magnetic losses has been described in Section 3.1. In this Section the commonly used loss expressions will be derived, the various contributions to the magnetic losses will then be defined and this will be followed by a brief account of the dependence of the losses on frequency, temperature and stress.

The way in which the loss in a material is expressed will depend on the situation in which the component, made from that material, is used. Very often components are made in two halves which are then butted together, resulting in an air-gap, either deliberate or residual, within the magnetic flux path, so that the effective permeability of the core is less than that of the material. In this situation it is advantageous to express the losses as a material parameter which is independent of the permeability of the core. For materials used in low-loss, low-amplitude applications, e.g. for inductors, the material parameter used is the loss factor, $(\tan\delta_m)/\mu_i$ and for materials used in high power applications the parameter used is the power loss (volume) density, P_m. P_m has the units $W.m^{-3}$ while $(\tan\delta_m)/\mu_i$ is dimensionless.

For the following derivations an 'ideal' core shape is defined as an infinitely long cylinder or a radially thin toroid having cross-sectional area A (in m^2) and length ℓ (in m), and a loss-free winding of N turns.

If an alternating voltage, U volts, is applied:

$$P_m = U^2G/A\ell \qquad W.m^{-2} \qquad (3.9)$$

where G is the conductance in Ω^{-1} appearing across the winding due to the magnetic loss in the core.

The area integral of the flux density is the magnetic flux ϕ. For the 'ideal' core shape

$$\phi = BA \qquad Wb \qquad (3.10)$$

The measurement of B depends on the law of induction, i.e. the emf., e, induced by a change in magnetic flux is given by

$$e = -Nd\phi/dt = -NA\, dB/dt \qquad V \qquad (3.11)$$

where N is the number of turns in the winding which senses e. The negative sign indicates that the emf induced opposes the change in flux. If the flux density is sinusoidal i.e. $B = \hat{B}\sin\omega t$, then by differentiation the induced emf is:

$$\hat{E} = \omega\hat{B}AN \qquad \text{or} \qquad E = \omega\hat{B}AN/\sqrt{2} \qquad (3.12)$$

If the loss tangent is small the applied voltage, U, will approximately equal the induced emf so:

$$U = \omega\hat{B}AN/\sqrt{2} \qquad V \qquad (3.13)$$

Thus for a given core and number of turns the flux density is determined by the frequency and applied voltage.

The inductance of a circuit may be defined as the flux linkage per unit current:

$$L = N\hat{\phi}/\hat{I} \qquad H \tag{3.14}$$

where $\hat{I}$ is the peak amplitude of the alternating current.

For the 'ideal' core shape (from Eqns. 2.17 and 2.20):

$$L = N\hat{B}A/\hat{I} = \frac{NA}{\hat{I}}\,\mu_o\mu\,\frac{N\hat{I}}{\ell}$$

$$L = \mu_o\mu\, N^2A/\ell = L_o\mu \qquad H \tag{3.15}$$

where $L_o = \mu_o N^2 A/\ell$ is the inductance of a core having unity permeability, the flux distribution remaining unaltered.

The permeability is a complex quantity expressing the loss of energy which occurs as the magnetization alternates, so that the impedance of the winding is not purely reactive but has also a resistive component.

$$\left.\begin{aligned} Z &= j\omega L_s + R_s \\ &= j\omega L_o(\mu_s' - j\mu_s'') \end{aligned}\right\} \tag{3.16}$$

where R_s is the series loss resistance and L_s the series inductance. μ_s' and μ_s'' are the real and imaginary parts of the series complex permeability.

$$\left.\begin{aligned} &\text{Then} \quad \omega L_s = \omega L_o\mu_s', \quad R_s = \omega L_o\mu_s'' \\ &\text{and} \quad \tan\delta_m = R_s/\omega L_s = \mu_s''/\mu_s' \end{aligned}\right\} \tag{3.17}$$

where δ_m is the loss angle.

The equivalence of series and parallel inductive circuits is shown in Fig. 3.12.

Fig. 3.12a) shows the vector diagram corresponding to the series circuit and the equivalent diagram in terms of parallel components is given in Fig. 3.12b). The applied voltage, U, and current, I, in each case corresponds exactly in magnitude and phase.

For the parallel case, the admittance:

$$Y = 1/j\omega L_p + 1/R_p = (1/\mu_p' - 1/j\mu_p'')/j\omega L_o \qquad \Omega^{-1} \tag{3.18}$$

Then $\omega L_p = \omega L_o\mu_p', \quad R_p = \omega L_o\mu_p''$

where μ_p' and μ_p'' are the components of the parallel permeability

$$\therefore \quad \tan\delta_m = \omega L_p/R_p = \omega L_p G = \mu_p'/\mu_p'' \tag{3.19}$$

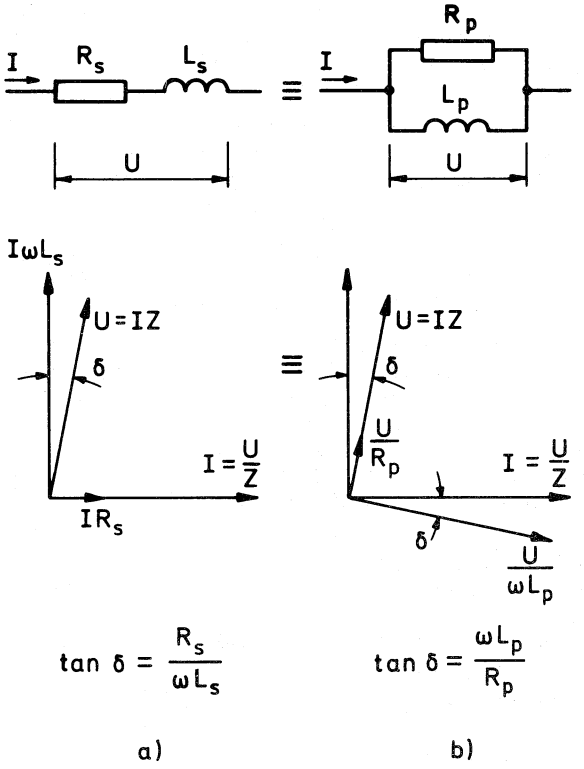

FIG. 3.12. Equivalence of series and parallel inductive circuits; $L_p = L_s\ (1 + \tan^2\delta)$, $R_p = R_s\ (1 + 1/\tan^2\delta)$

By analogy with the conversion of series to parallel impedances in Fig. 3.12, the following relations exist between the series and parallel components of the complex permeability:

$$\begin{aligned} \mu_p' &= \mu_s'(1 + \tan^2\delta_m) \\ \mu_p'' &= \mu_s''(1 + 1/\tan^2\delta_m) \end{aligned} \qquad (3.20)$$

For $\tan\delta_m << 1$ the distinction between series and parallel inductance can be dropped and from Eqns. 3.15 ad 3.19:

$$\tan\delta_m = \omega\mu_o\mu\, N^2AG/\ell \qquad (3.21)$$

From Eqn. 3.9

$$G = P_m A\ell/U^2$$

thus

$$(\tan\delta_m)/\mu = \mu_o P_m/\pi f\hat{B}^2 \qquad (3.22)$$

The loss factor, $(\tan\delta_m)/\mu$, is thus a material property which depends only on the power loss density, P_m, the frequency and the flux flux density; if eddy current loss is negligible (see Section 3.5.2) it is independent of core shape and size.

In the foregoing, an 'ideal' core of uniform cross-section and having no air-gaps in the magnetic length has been assumed. Transformer and inductor cores, in general, have magnetic circuits where the magnetic path is substantially closed, but the cross-section is generally not uniform along the magnetic path length. Such cores are conveniently characterized by effective dimensions, ℓ_e, A_e and V_e which are calculated from the actual dimensions in such a way that the core may be regarded as an ideal toroid having these dimensions[20].

Once the effective dimensions have been obtained it is possible to calculate the performance of a non-uniform core by substituting these dimensions into the equations derived for the ideal core shape. Such calculations, using the effective dimensions of a non-uniform core, yield an effective flux density $\hat{B}_e$ which will in turn yield the correct core loss provided the core is operating in the low flux density region where the Rayleigh relations (Eqns. 3.32 and 3.33) are obeyed.

The effect of the introduction of an air gap, of length ℓ_g, into a core of effective magnetic length ℓ_e, is to reduce the volume by a factor $(1-\ell_g/\ell_e)$ and to reduce the inductance so that the core behaves as though it had a reduced permeability, referred to as the effective permeability, μ_e.

It can be shown that[21]:

$$1 - \ell_g/\ell_e = \mu(\mu_e-1)/\mu_e(\mu-1) \qquad (3.23)$$

If the frequency and flux density remain unchanged, then the power loss (volume) density, P_m, is unchanged and the total power loss will be reduced by the same ratio as the volume. Therefore the conductance due to the gapped core:

$$= \text{power loss}/U^2 = P_m(1-\ell_g/\ell_e)/U^2$$

$$= G\,\mu(\mu_e-1)/\mu_e(\mu-1) \qquad \Omega^{-1} \qquad (3.24)$$

Thus the conductance is reduced from its ungapped value by the ratio of the gapped to ungapped volumes. The new loss tangent:

$$(\tan\delta_m)_{gapped} = (\omega L\mu_e/\mu) \times G\mu(\mu_e - 1)/\mu_e(\mu-1)$$

$$= \omega LG(\mu_e-1)/(\mu-1) \qquad (3.25)$$

or

$$\frac{(\tan\delta_m)_{gapped}}{\mu_e - 1} = \frac{\tan\delta_m}{\mu-1} \qquad (3.26)$$

and since μ_e and μ are in general >> 1, Eqn. 3.26 approximates to

$$\frac{(\tan\delta)_{gapped}}{\mu_e} = \frac{\tan\delta}{\mu} \qquad (3.27)$$

The subscript m is dropped since the loss tangent may be due to any specific form of loss and need not be due to the total loss.

Various contributions to the losses are identified and listed below:

(i) Hysteresis loss
(ii) Eddy current loss and dimensional resonance
(iii) Residual losses
  a) relaxation losses
  b) ferromagnetic resonance loss
  c) domain wall resonance loss
  d) thermal after-effect loss

The loss factor is usually written in terms of the three main components

$$(\tan\delta_m)/\mu = (\tan\delta_h)/\mu + (\tan\delta_F)/\mu + (\tan\delta_r)/\mu \qquad (3.28)$$

where $(\tan\delta_h)/\mu$ = hysteresis loss factor
$(\tan\delta_F)/\mu$ = eddy current loss factor
and $(\tan\delta_r)/\mu$ = residual loss factor

It is shown in the following Sections that, within the Rayleigh region, the first term is proportional to $\hat{B}$, the second to f while the residual loss factor is independent of both provided the residual loss factor of the material is constant. Thus

$$\tan\delta_m/\mu = k_1\hat{B} + k_2 f + k_3 \qquad (3.29)$$

k_1 and k_3 characterize the material only, while k_2 depends on the material and the core size and shape[22].

3.5.1. HYSTERESIS LOSS

Hysteresis loss arises from the irreversible movement of domain walls and irreversible domain rotations. The energy lost during each cycle in a unit volume of material due to hysteresis is equal to the hysteresis loop area and is called the hysteresis energy loss (volume) density, w_h.

$$w_h = \oint B.dH \qquad J.m^{-3}.cycle^{-1} \qquad (3.30)$$

The coefficient k_1 (Eqn. 3.29) is more usually called η_B the hysteresis loss coefficient, (unit: T^{-1})

$$(\tan\delta_h)/\mu = \eta_B \hat{B} \qquad (3.31)$$

At low and decreasing values of applied field, resulting in $\hat{B}$ values in the region of 0-1 mT, the amplitude permeability (of iron) was observed, by Rayleigh[23], to linearly approach the initial permeability:

$$\mu_a = \mu_i + \nu\hat{H} \tag{3.32}$$

where ν is the Rayleigh coefficient. He also observed that under these conditions the sides of the hysteresis loop could be represented by parabolic curves. The vertical width of the loop at any given field strength, H, is then $\mu_o\nu(\hat{H}^2-H^2)$. By integration, the loop area is $4\mu_o\nu\hat{H}^3/3$ so from Eqn. 3.30:

$$w_h = 4\mu_o\nu\hat{H}^3/3 = 4\nu\hat{B}^3/3\mu_o{}^2\mu_a{}^3 \quad J.m^{-3}.cycle^{-1} \tag{3.33}$$

It should be pointed out that with alternating magnetization the non-hysteresis losses will also cause a phase angle between B and H. This will result in an elliptical B(H) relation which will be superimposed on the hysteresis loop, i.e. will change the shape of the loop. However the parabolic component will still be present and the associated non-linear hysteresis phenomena will still occur.

The hysteresis power loss, P_h, associated with an alternating field $\hat{H}$ and frequency f is:

$$P_h = w_h f \qquad W.m^{-3} \tag{3.34}$$

which is proportional to $\hat{B}^3$ from Eqn. 3.33. The hysteresis loss may also be expressed in terms of a series loss resistance, R_h.

$$P_h = I^2R_h/A_e\ell_e \qquad W.m^{-3} \tag{3.35}$$

where I is the RMS current = $\hat{H}\ell/\sqrt{2}.N$ and therefore

$$R_h = \frac{P_h A_e \ell_e}{I^2} = \frac{4\nu\hat{B}}{3\pi\mu_o\mu_a{}^2}\, 2\pi f\, \frac{N^2A_e\mu_o\mu_a}{\ell_e}$$

$$\therefore \quad R_h = \frac{4\nu\hat{B}}{3\pi\mu_o\mu_a{}^2} \cdot \omega L \qquad \Omega \tag{3.36}$$

and $\tan\delta_h = R_h/\omega L = 4\nu\hat{B}/3\pi\mu_o\mu_a{}^2$. At low amplitudes where $\mu_a \approx \mu_i$, the hysteresis loss factor, $\tan\delta_h/\mu$, is thus proportional to $\hat{B}$ and, by comparison with Eqn. 3.31, η_B is expected to be a constant.

At higher amplitudes the B-H relation becomes increasingly non-linear and there will be appreciable waveform distortion. It therefore becomes difficult to express the hysteresis loss in terms of coefficients and a.c. theory. Instead it is usual to express the high amplitude loss in terms of the power dissipated per unit volume as measured by a wattmeter or calorimeter. Corrections for other losses, in particular eddy current losses, must be made. It is observed that the corrected high-amplitude loss per cycle increases with frequency due to loss contributions that do not have their origins in the irreversible processes that are described as hysteresis. For this reason,

true hysteresis loss is sometimes defined to be the loss measured at frequencies that are low enough for the loss to be independent of frequency, i.e. hysteresis is essentially a static phenomenon. However, it is also common usage to apply the term hysteresis to the field dependent loss at any frequency provided it does not include eddy current loss.

3.5.2. EDDY CURRENT LOSS

An alternating magnetic flux in a conductive medium will induce eddy currents in that medium and the resulting loss of energy is called the eddy current loss. At low frequencies where the inductive effect of the eddy currents may be neglected, the eddy current power loss (volume) density, P_F, is given by:

$$P_F = \dot{B}^2_{rms} D^2/2\rho\beta \qquad W.m^{-3} \qquad (3.37)$$

where $\dot{B}_{rms}$ = the rms rate of change of flux density, dB/dt, in the medium, assumed perpendicular to the plane containing the dimension, D, and uniform across it at any instant.

D = the least dimension of the medium in a plane perpendicular to B.

ρ = resistivity of the medium

β = 6 for laminations of thickness D
16 for a cylinder of diameter D
20 for a sphere of diameter D

For sine wave excitation $B = \hat{B}\sin\omega t$ and therefore $\dot{B}_{rms} = \omega\hat{B}/\sqrt{2}$

Thus $$P_F = (\omega\hat{B}D)^2/4\rho\beta \qquad W.m^{-3} \qquad (3.38)$$

For a symmetrical square wave excitation having frequency f, the flux density will rise linearly from zero to $\hat{B}$ in time 1/4f so that at time t the instantaneous flux density $B = \hat{B}4ft$. Therefore $\dot{B} = 4f\hat{B}$ = constant during the half cycle, so $\dot{B}_{rms} = \dot{B} = 4f\hat{B} = 2\omega\hat{B}/\pi$.

Therefore

$$P_F = 2(\omega\hat{B}D)^2/\pi^2\rho\beta \qquad W.m^{-3} \qquad (3.39)$$

i.e. P_F(sine wave) = P_F(square wave) x $\pi^2/8$

$$= 1.23P_F(\text{square wave}) \qquad (3.40)$$

For sinusoidal excitation the eddy current series loss resistance R_F is given by:

$$R_F = P_F A_e \ell_e / I^2 = \frac{\mu_o \mu D^2 \omega}{2\rho\beta} . \omega L \qquad (3.41)$$

(from Eqns. 2.17, 2.20 and 3.15)

$$\therefore \quad \tan\delta_F = R_F/\omega L = \mu_o\mu\, D^2\omega/2\rho\beta \qquad (3.42)$$

and $$(\tan\delta_F)/\mu = \mu_o D^2\omega/2\rho\beta \qquad (3.43)$$

Thus the eddy current loss depends on the size and shape of the conductive region and it may be reduced by the subdivision of the medium into electrically insulated laminations or grains. When this is done, e.g. in metal magnetic cores, it is the size and shape of the subdivisions, not the overall dimensions of the core that determine P_F. However, in ferrite cores it is, of course, the overall dimensions of the core cross-section that determine P_F.

3.5.2.1. Dimensional Resonance Loss

In the foregoing it has been assumed that the flux is distributed evenly across the cross-section of the magnetic core. At high frequencies in some magnetic materials this may not be the case.

Due to the high values of μ and ε in the MnZn ferrites the electromagnetic wave velocity within the material is very low and this can give rise to standing waves of magnetization across the cross-section of the core. This phenomenon is called dimensional resonance. If the smallest cross-sectional dimension of the core, perpendicular to the magnetic field, is half a wavelength, then a fundamental standing wave pattern will be set up across that section. The flux in the sample is cancelled and the apparent permeability drops to zero. A peak is observed in the magnetic loss at resonance.

If the material has high losses it will not support standing waves but in such cases only limited penetration of the flux into the material occurs. This loss can in principle be avoided if the relevant cross-sectional dimensions are kept smaller than half a wavelength in the operating frequency range. This subject is covered in more detail in Section 5.2.4.

3.5.3. RESIDUAL LOSS

The losses which remain after extrapolation to zero flux density, and after eddy current loss has been eliminated, are known as residual losses (see Eqn. 3.28). These have their origins in various loss contributions, each of which depends on the frequency and not all of which are clearly defined. Some of these will now be described.

3.5.3.1. Relaxation Losses[24,25,26]

After a change in the applied magnetic field the magnetization does not immediately reach its final equilibrium value. If the change of field is initiated at time t = o, when the magnetization is M_o, then after an elapsed time t the magnetization, M, is given by:

$$M = M_\infty - (M_\infty - M_o)e^{-t/\tau} \qquad (3.44)$$

where M_∞ is the magnetization at $t \to \infty$ and τ is the relaxation time, i.e. the time taken for the magnetization to reach 63.2% of the total change $(M_\infty - M_o)$.

When an alternating field is applied, this relaxation of the magnetization causes a phase lag between M (or B) and H which can lie between 0 and $\pi/2$, this results in a dispersion of the permeability and a corresponding energy loss. Energy losses of this type are called relaxation or magnetic after-effect losses. Depending on the cause of the relaxation, the values of τ may be in the region of microseconds or years. Relaxation time constants of the order of years have already been encountered in connection with disaccommodation (see Section 3.4.4). If the frequency of the applied field is such that $\omega = 1/\tau$, the energy loss is at a maximum and so is the rate of decrease of permeability (see Fig. 3.13).

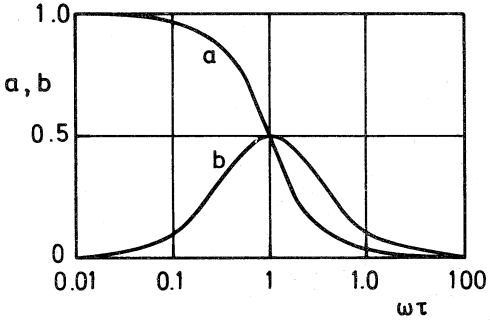

FIG. 3.13. Normalized curves of a) = $1/[1+(\omega\tau)^2] \propto \mu'-1$ and b) = $\omega\tau/[1+(\omega\tau)^2] \propto \mu''$ as a function of frequency for a single relaxation process of time constant τ.

The relaxation time decreases with increasing temperature so that if a relaxation phenomenon is present it can be observed as a maximum in the energy loss either at constant temperature by varying the frequency, or at constant frequency by varying the temperature and, thereby, τ.

The nature of this phenomenon may be illustrated by adapting Snoek's analogy[27]. A ball is imagined to be placed on a concave rigid surface e.g. a smooth plate, covered with a smooth layer of viscous material, e.g. grease. In the quasistatic situation, if the ball is displaced by a force from the lowest point to a new position, it will gradually sink into the grease finally reaching its new equilibrium position on the surface of the plate above the lowest point. Alternating magnetization is analagous to the ball oscillating about the lowest point on the surface. At low temperatures (τ long) the viscosity of the grease is high and the ball will move on the surface of the hardened grease with very low loss of energy. At high temperature (τ short) the viscosity of the grease is greatly decreased and the ball will roll on the surface of the plate virtually unimpeded by the grease, again with very little loss of energy. At an intermediate temperature the motion of the ball is severely damped as it tries to move in the viscous layer; the mobility of the ball (analogous to permeability) has an intermediate value and there is a large energy loss. The magnetic relaxation process has similar characteristics and there is a maximum in the energy loss at an intermediate temperature.

The causes of the time lag in the magnetization process are attributed to three types of relaxation process.

a) Electron diffusion between cations of differing valency. In MnZn and NiZn ferrites relaxation losses are found which appear to be closely related to ferrous content.

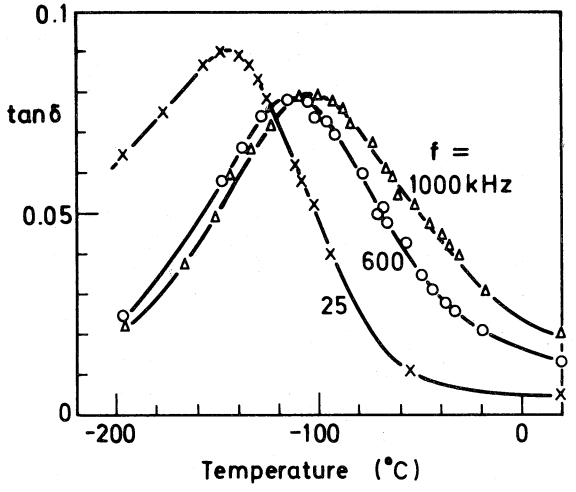

FIG. 3.14. The loss tangent of $Mn_{0.66}Zn_{0.28}Fe^{2+}_{0.06}Fe^{3+}_{2}O_4$ as a function of temperature measured at various frequencies and at a field strength of about 0.4 Am^{-1} (after Smit and Wijn).

Fig. 3.14 shows relaxation in a MnZn ferro-ferrite. The small activation energy, of the order of 0.1 eV, associated with this relaxation suggests that the cause is diffusion of electrons between Fe^{2+} and Fe^{3+}. At room temperature, these relaxations would be expected to give a maximum in the loss tangent, i.e. when $\omega\tau = 1$, at frequencies in the region of hundreds of megahertz where it is difficult to observe due to the onset of ferromagnetic resonance (see Section 3.5.3.2).

A similar relaxation can be observed in NiZn ferrites (see Fig. 3.15). Here the ferrous content is very small and the activation energy is 0.4 eV. Relaxations having activation energies of the region of 0.1 to 0.4 eV are characteristic of materials in which an element such as iron occurs with different valencies, giving rise to an electron diffusion process.

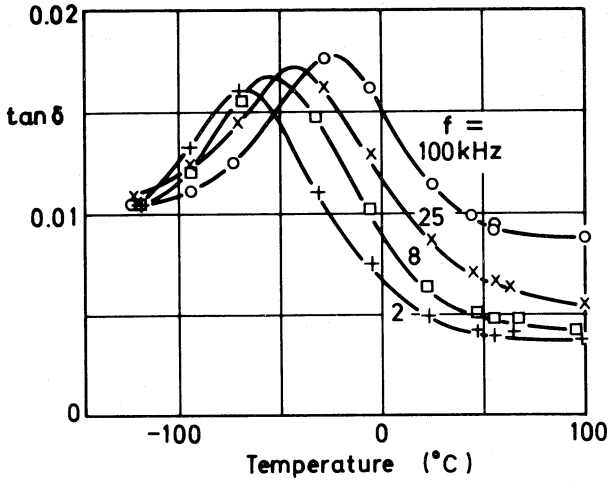

FIG. 3.15. The loss tangent of $Ni_{0.5}Zn_{0.5}Fe_2O_4$ as a function of temperature measured at a field strength of about 0.2 Am^{-1} (after Smit and Wijn).

b) Diffusion of cations in the presence of cation vacancies. In some materials, e.g. MnZn ferro-ferrites, Fe^{2+} diffuses in the lattice by interchanging position with cation vacancies; this leads to the preferential occupation of certain classes of site in the lattice. The activation energy of such cation diffusion processes is higher, in the region of 0.9 to 1.0 eV, and relaxation times are longer so that the maximum in the losses occurs at very low frequencies at room temperature. This relaxation thus gives rise to a negligibly low loss at the frequencies of interest but is the main cause of the time change in permeability, i.e. disaccommodation (see Section 3.4.4).

c) Single ion relaxations involving the diffusion of cobalt in both MnZn and NiZn ferrites have τ values of the order of minutes at temperatures just below the Curie Point. This effect is used in the heat treatment of cobalt-containing ferrites (see Section 2.3.2). A uniaxial anisotropy is induced when the material is annealed just below the Curie Point and it is retained when the material is cooled. The result is that the domain walls are trapped in relatively deep energy wells in which they can only move reversibly. This gives the advantage of low loss but it is inevitably accompanied by a rather low permeability[28,14]. If the material is subsequently subjected to a large magnetic field, the walls are ejected from the energy wells and the material then exhibits normal hysteresis behaviour, i.e. as though there were no induced uniaxial anisotropy.

A review of various relaxations in ferrites is given in Ref. 26.

3.5.3.2. Ferromagnetic Resonance Loss

The high frequency application of ferrites is limited by the onset of ferromagnetic resonance, FMR. This arises from the fact that the spinning electron behaves like a gyroscope. If an electron is in a static magnetic field, H, the direction of which is at some arbitrary angle to the magnetic moment of the electron, a couple is exerted on the magnetic moment of the electron causing it to precess about the direction of H. The angular frequency, ω_r of this precession is independent of the inclination of the moment to the applied field and is given by:

$$\omega_r = \gamma\mu_o H \tag{3.45}$$

where γ is the gyromagnetic ratio $\approx 176 \times 10^9$ C.kg^{-1}.

In a magnetic material the precession frequency of the spins is determined by the local value of the magnetic field. Where there is no external static field and no demagnetizing fields present precession will still occur, the precession frequency being determined by the anisotropy field, H_A[29].

$$\omega_r = \gamma\mu_o H_A \tag{3.46}$$

In practical materials, losses occur which damp the precessional motion and cause the moment to spiral towards the direction of the static field. The precession can be excited by an a.c. field and resonance occurs when the frequency of the a.c. field coincides with the natural frequency of the precession. This causes a dispersion of the permeability and an increase in the losses at frequencies in the vicinity of the resonance. In ferrimagnetic materials, the magnetic moments of the electrons on the two sublattices have antiparallel alignment and dissimilar values. However, the strong mutual coupling between spins on the two sublattices causes them to resonate together in the same sense and with the same value of γ as for the ferromagnetic case[30].

If demagnetizing fields are present these will add to the anisotropy field and raise the resonant frequency[31]. Local variations in static field values result in the broadening of the line width of the resonance. In unsaturated polycrystalline materials in general, the a.c. field will be at an arbitrary angle to the easy directions and the resulting demagnetizing fields formed on domain walls will raise the resonant frequency and broaden the line width. Imperfections such as second phase on grain boundaries, pores and inclusions will also induce local demagnetizing fields. The angular frequency of the resonance can be shown[31] to lie between:

$$\omega_r(\text{min}) = \gamma\mu_o H_A \text{ and } \omega_r(\text{max}) = \gamma\mu_o(H_A + M_s)$$

where M_s is the saturation magnetization in A.m^{-1}.

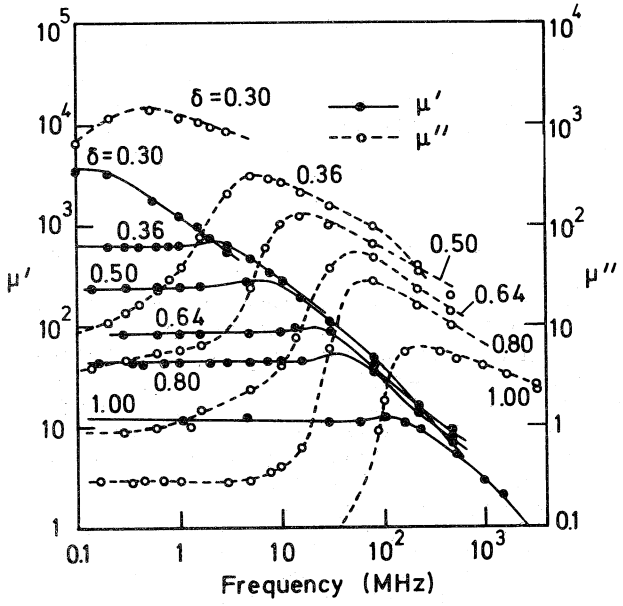

FIG. 3.16. The magnetic spectrum of the real and imaginary parts of the initial permeability for polycrystalline specimens of the NiZn ferrites $Ni_{\delta}Zn_{1-\delta}Fe_2O_4$.

Fig. 3.16 shows the real and imaginary components (μ' and μ'') of the permeability of a range of polycrystalline NiZn ferrites; there is no applied static field. The curves exhibit the ferromagnetic resonance characteristic with broad line widths. The smaller the value of H_A the higher the permeability at low frequency and the lower the frequency of resonance. Materials with higher anisotropy will have a higher resonant frequency and a wider frequency range of operation but with a lower permeability at low frequency.

The line width and, in particular, the low frequency tail of the resonance is of importance in determining the losses at practical operating frequencies. In polycrystalline materials the complexity of domain configurations will result in the whole range of resonant frequencies from $\omega_r(\text{min})$ to $\omega_r(\text{max})$ being present; in addition the line width may be further broadened by inhomogeneities in the material which will cause local variations in the anisotropy field itself.

The following formula derived from an expression given by Snoek[29] indicates the approximate value of the frequency of maximum μ'' for a polycrystalline ferrite

$$f_{res} = 23.4\ M_s/(\mu_i - 1) \qquad \text{kHz} \tag{3.47}$$

where M_s is in $A.m^{-1}$ ($M_s \approx B_{sat}/\mu_o$ in practice).

3.5.3.3. Domain Wall Resonance Loss

Domain wall resonance (or relaxation) losses arise from the damped motion of a domain wall as it responds to an alternating field[32]. If an a.c. field, $\hat{H}\sin\omega t$, is applied parallel to the direction of magnetization, M_s, in the domains, the domain wall moves as a result of the rotation of spins within the wall in response to the applied field. The wall exhibits inertia and a frictional resistance to movement. The equation of motion for a 180° wall of unit area can be expressed as:

$$m\ddot{x} + \beta\dot{x} + ax = 2JH \qquad (3.48)$$

where m is the virtual mass of the wall and is inversely proportional to the wall thickness. β is a damping coefficient related to the damping of the precessional motion of the spins and is also inversely proportional to wall thickness. The stiffness constant, a, is inversely proportional to the domain wall permeability, μ_w-1. J is the magnetic polarization = $\mu_o M$. For high wall-permeability materials, $\beta^2 >> ma$, and the wall motion has the character of a relaxation while for low wall-permeability materials with low wall damping, $\beta^2 << ma$ and the motion has the character of a resonance.

The domain wall losses associated with the relaxation or resonance are not usually distinguishable from the ferromagnetic resonance losses in ferrites (see Fig.3.16) and are not very significant in ferrites having low wall-permeability. However, for high wall-permeability ferrites, domain wall losses result in a broadening of the line width of the loss maximum with an extension towards low frequencies. The frequency of the loss maximum also deviates from that expected for FMR, the deviation increasing with the wall-permeability.

3.5.3.4. Thermal After-effect Loss

The principle contribution to the low frequency residual losses in MnZn and NiZn ferrites arises from what is essentially a thermal activated hysteresis loss. Néel first postulated a mechanism for a frequency-independent contribution to the residual loss[33]. At an absolute temperature T, any magnetic material will possess an amount of thermal disorder proportional to kT where k is Boltzmann's constant. Magnetization changes due to wall movement are hindered by energy barriers caused by random inhomogeneities in the material while domain rotations are hindered by the constraint of the various anisotropies present. Thermal disorder provides an extra driving force which may overcome these barriers and may be considered as equivalent to a fluctuating field within the material. This fluctuating field, $\pm H_f$, is known by various names; the friction field, thermal after-effect field or viscosity field.

Néel predicted the contribution to the residual loss due to the thermal after-effect field would be:-

$$(\tan\delta)_{H_f} = \pi\nu S_v/\mu \qquad (3.49)$$

where ν is the Rayleigh coefficient in $m.A^{-1}$. S_ν is the Néel constant estimated by Néel to be in the region of 0.04 to 0.07 $A.m^{-1}$ for a soft magnetic material. This constant depends on temperature and the volume of the material involved in magnetization changes (Barkhausen volume), which he assumed to be independent of temperature. Other authors[34,35] have approached the subject in a different way and assumed that thermal agitation acts to alter the height of the energy barriers themselves. The basis of these theories is that, after a change in applied magnetic field, some domain walls are in positions of metastable equilibrium. Thermal agitation has the effect of altering the height of the energy barriers and allowing irreversible transitions to more stable orientations, causing a hysteresis loss.

Recent work[36] has confirmed the presence of significant thermal after-effect losses in low-loss MnZn ferrites although the temperature dependence of the effect predicted by Néel was not confirmed. This may be due to the low, temperature-dependent nature of the crystalline anisotropy of these materials which may result in a variation of the Barkhausen volume with temperature.

3.5.4. FREQUENCY DEPENDENCE OF RESIDUAL LOSS

The residual loss factor expressed as a function of frequency is an important ferrite material parameter (Fig. 3.17)

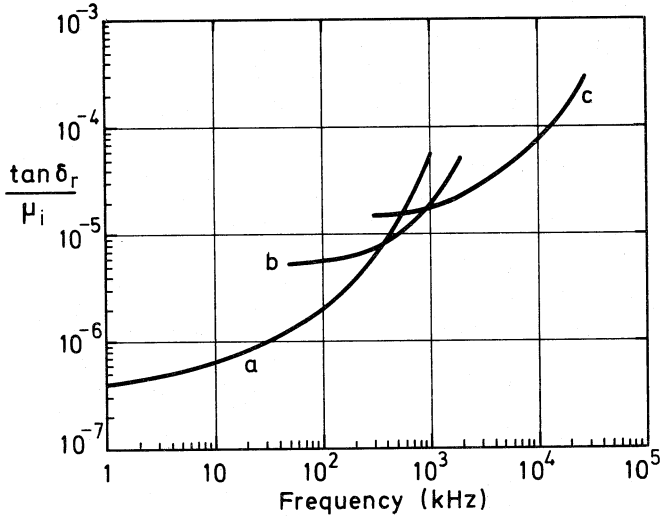

FIG. 3.17. $\tan\delta_r/\mu$ versus frequency for various low-loss grades of MnZn and NiZn ferrites.

Within the low-loss grades of material, those having higher permeabilities tend to have lower values of $(\tan\delta_r)/\mu$ at low frequencies. Conversely, at higher frequencies, the higher permeabilities are associated with the earlier onset of ferromagnetic resonance[29] and therefore higher values of $(\tan\delta_r)/\mu$. As Fig. 3.17 shows, this leads to a frequency region for each material where its residual loss is lower than that for materials having either higher or lower permeabilities.

At high frequencies the main contributions to the residual loss factor arise from ferromagnetic resonance and domain wall resonance (or for high μ_w materials, from domain wall relaxations). At the lower frequencies, the main contribution to the residual loss is the thermal after-effect loss. Relaxation losses and micro-eddy current loss also contribute. Calculations of micro-eddy current loss based on bulk resistivity data usually under-estimate this contribution because the behaviour of the grain boundaries, the effect of impurities and the presence of domain walls complicate the model.

3.5.5. RELATION BETWEEN HYSTERESIS AND RESIDUAL LOSSES

During the manufacture of ferrites, despite careful control of the composition and firing conditions, a certain spread in the material properties inevitably occurs. In particular, in MnZn ferro-ferrites very small variations in Fe^{2+} content can cause relatively large variations in properties because of the strong dependence of the position of the anisotropy minimum on the Fe^{2+} level.

If the hysteresis coefficient η_B is plotted as a function of $(\tan\delta_r)/\mu$ or $[(\tan\delta)/\mu]_{\hat{B}=0}$ for materials having the same basic composition but showing typical production spreads in Fe^{2+} content, a linear relationship is apparent as shown in Fig. 3.18. The higher the Mn/Zn ratio the weaker the dependence of $[(\tan\delta)/\mu]_{\hat{B}=0}$ on η_B, (Ref.36).

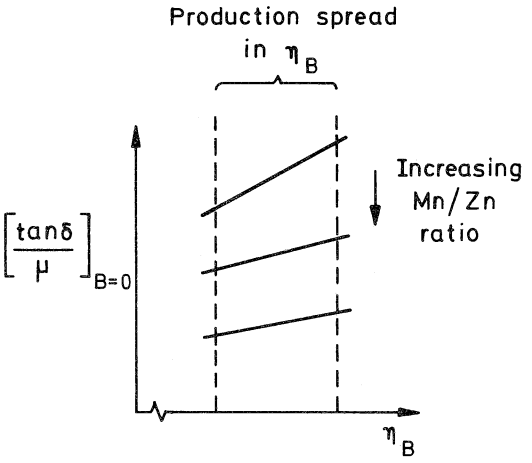

FIG. 3.18. Qualitative illustration of the observed dependence of $(\tan\delta)/\mu$ on the variation in η_B found in normal production.

Fig. 3.18 implies that for a group of materials having the same basic composition (i.e. same Mn/Zn ratio) but varying Fe^{2+} content, the following relation applies

$$[(\tan\delta)/\mu]_{\hat{B}=0} = C\eta_B + D \qquad (3.50)$$

while for any one material, at the low $\hat{B}$ levels of interest, it has been seen that

$$(\tan\delta)/\mu = \eta_B \hat{B} + A \qquad (3.51)$$

From Eqn. 3.50,

$$[(\tan\delta)/\mu]_{\hat{B}=0} = A = C\eta_B + D$$

Thus the residual loss factor, (which is defined as the loss factor, excluding bulk eddy current losses, extrapolated the zero flux density) contains an element of hysteresis loss $C\eta_B$. This is the contribution of the thermal after-effect losses discussed in Section 3.5.3.4. and it forms a significant part of the residual loss[36].

It is clear that measures which reduce the hysteresis losses and thus η_B will also reduce the hysteresis element of the residual loss. Substitutions of large tetravalent ions such as titanium and tin in MnZn ferro-ferrites have been observed to reduce both the hysteresis and residual losses. This is in addition to their beneficial effect on the $\mu(\theta)$ curve, the resistivity[3] and the disaccommodation noted in earlier Sections of this Chapter.

Very low losses have also been achieved by the addition of cobalt to MnZn ferrous ferrites, especially after heat treatment. These materials tend, however, to be unstable and sensitive to stress which makes them difficult to use in practice (see Section 3.5.3.1). Cobalt substitutions in NiZn ferrites are also very successful in reducing losses. Here the practical materials are iron deficient (no Fe^{2+}) and stability is not a problem[15].

3.5.6. POWER LOSSES

The power loss (volume) density, P_m, is the relevant material loss parameter for ferrites operating at high amplitudes (e.g. > 10 mT). The operating frequencies are usually low, approximately 15-100 kHz. P_m is primarily due to hysteresis loss although eddy current loss may also contribute. In power applications of ferrites, it is advantageous to operate the core at the highest temperature consistent with retaining acceptable material properties (see Section 5.3.2). Typical operating temperatures are 70-100°C so the composition of the ferrite is chosen so that the power loss density is minimum in this range.

Power losses in commercial materials have been significantly improved in recent years and losses of < 50 $\mu W.mm^{-3}$ at 200 mT, 16 kHz and 100°C have been achieved in materials, although this level is not generally realized in production transformer cores.

The ferrite material composition that is optimum for low hysteresis loss together with high permeability is generally not compatible with the composition requirements for a high saturation flux density. Thus substitutions which might be used to reduce the hysteresis loss are usually detrimental to the values of saturation flux density obtainable. The ferrous iron content is important to control the compensation temperature and so achieve maximum μa and minimum P_m at the operating temperature. The compensation temperature is usually controlled by firing conditions, although the addition of tri- and tetra-valent metal oxides to increase the Fe^{2+} content has been investigated[37].

3.5.7. TEMPERATURE DEPENDENCE OF THE LOSSES

The residual loss, the low amplitude hysteresis loss and high amplitude power loss all show a dependence on temperature which is linked to the magnetocrystalline anisotropy

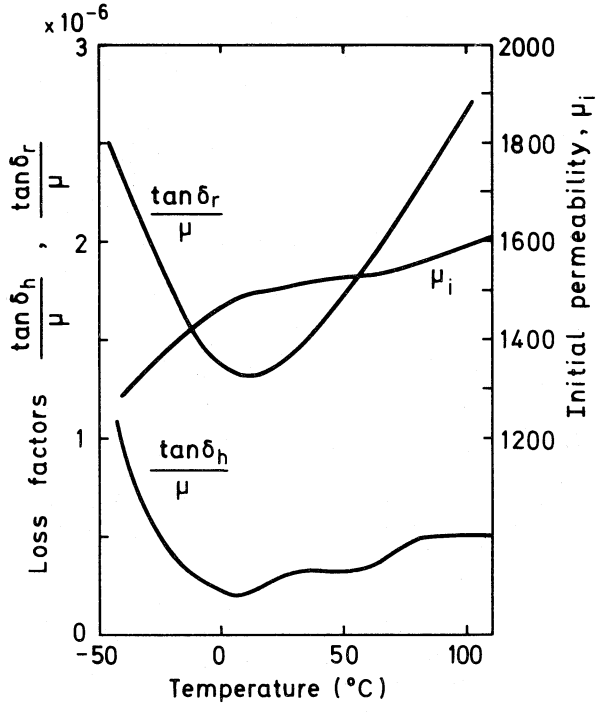

FIG. 3.19. Temperature dependence of the losses (measured at f = 100 kHz) and the permeability for a high quality Ti-substituted inductor MnZn ferrite.

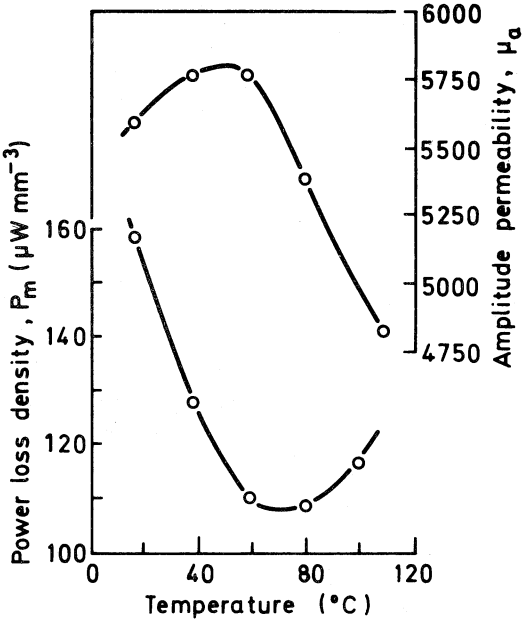

FIG. 3.20. Temperature dependence of the losses and permeability for a MnZn power ferrite. (Losses measured at f = 25 kHz, B = 200 mT).

Figs. 3.19 and 3.20 show the temperature dependence of such parameters for a low loss MnZn ferrite and a MnZn power ferrite respectively. The anisotropy compensation temperature ($K_1 \to 0$) is indicated by the secondary maximum (suppressed in Fig.3.19) of the permeability. It is seen that the low and high amplitude losses are all at a minimum in the vicinity of this temperature. This reduction of loss is believed to arise mainly from the increase in thickness of the domain walls as $K_1 \to 0$. As explained in Section 2.4.3, a domain wall that is thick compared to the dimensions of the pinning centres is less impeded by such centres and so the hysteresis loss is reduced. If the hysteresis loss is reduced then, via the thermal after-effect loss (see Section 3.5.3.4), the low frequency residual loss is reduced.

It is evident from Fig. 3.19 that as the minimum in the residual loss occurs near the temperature of the secondary maximum of the $\mu(\theta)$ curve it cannot coincide with the linear, low TC region, which would be desirable in practice.

3.5.8. STRESS DEPENDENCE OF THE LOSSES

Residual loss, low amplitude hysteresis loss and high amplitude power loss are all, in general, increased by both compressive and tensile stresses. Perhaps the most significant stress-induced increase in losses arises from the grinding of ferrite surfaces which are perpendicular to the flux path (transverse surfaces), e.g. the pole-face grinding of mating surfaces. Here the compressive stress approaches the ultimate compressive stress of the ferrite[38], typically 600 MNm^{-2}, at the surface and decreases to zero at a depth of about 5 μm. The

permeability in this layer is drastically decreased and thus the loss factor $(\tan\delta)/\mu = \mu''/(\mu')^2$ is increased accordingly. Knowles[38] has shown that the mean value of the residual loss factor (at 100 kHz) in a ground surface layer is approximately 600 x 10^{-6} compared with about 1.5 x 10^{-6} in the unstressed ferrite.

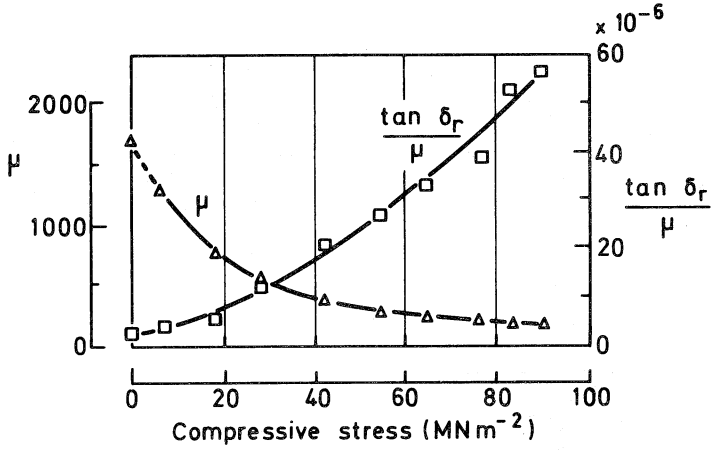

FIG. 3.21. Measured values of permeability and residual loss factor for a MnZn ferrite as a function of compressive stress applied perpendicular to the direction of the flux (transverse stress), measured at a frequency of 100 kHz. (After Knowles[38]).

Fig. 3.21 shows the effect of compressive stresses, applied perpendicular to the flux path and extending up to about 15% of the ultimate compressive stress, on the residual loss factor and the initial permeability.

Grinding a transverse surface also introduces surface roughness into the magnetic circuit. It has been shown, by comparison of ground, etched and stress-free polished surfaces, that surface roughness contributes perhaps 25% to the increase of residual loss factor induced in an inductor core by grinding. This contrasts strongly with the effect on hysteresis loss. The hysteresis loss coefficient, η_B, for an inductor core with ground transverse surfaces is twice that for a core with polished surfaces. Etching the ground surfaces, which removes the stresses but not the roughness, produces no improvement. Knowles (unpublished) has demonstrated that this effect arises not from surface stress or from flux concentrations at the points of contact of the rough surfaces but from the surface layers having a very high coercivity e.g. 155 $A.m^{-1}$ compared to 30 $A.m^{-1}$ in an unstressed ferrite. He deduces that these high coercivities probably arise from large local demagnetizing fields associated with a rough surface.

Turning finally to the effect of stress applied externally in the direction of the flux path, Fig. 3.22 shows how low levels of compressive and tensile stress influence the residual loss factor and the power loss. It can be seen that, in general, at these low stress levels, the losses increase significantly with stress even if the permeability is increased. This can be of importance in practical inductor and transformer cores which are generally subjected to some stress on assembly.

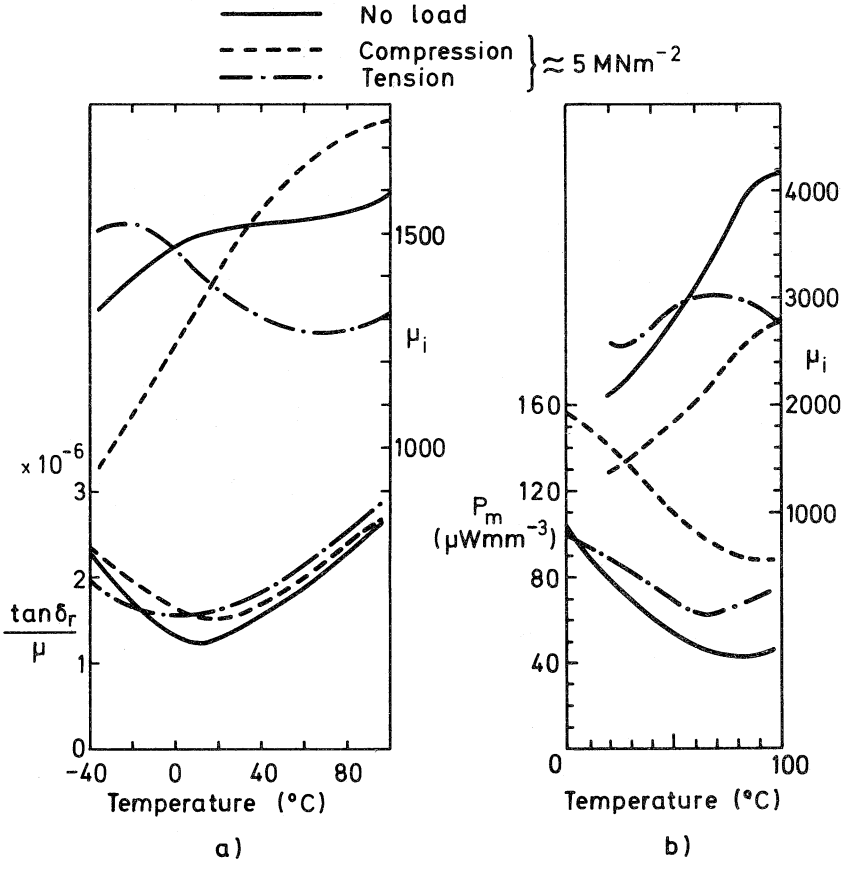

FIG. 3.22. The effect of a low level of compressive and tensile (longitudinal) stress on a) the 100 kHz residual loss factor and permeability of a high quality Ti-substituted MnZn inductor ferrite and b) the power loss density (at f = 16 kHz, B = 200 mT) and permeability of a MnZn power ferrite.

3.6. TYPICAL PROPERTIES OF FERRITES

The foregoing Sections have defined the main parameters used to express the electrical and magnetic properties of ferrites, and they have outlined the physical processes on which these properties depend. To conclude this Chapter, typical values of the main parameters are presented in Tables 3.3 and 3.4. The values quoted are representative of those to be found in manufacturers' current catalogues.

Table 3.3 contains data on four categories of manganese zinc ferrites corresponding to four application categories recognised by most manufacturers. Not all the parameters are relevant to all of the categories, e.g. for inductor materials the loss factor is given while for power ferrites the loss is expressed as power loss density.

Table 3.4 similarly presents typical properties of nickel zinc ferrites. Here three categories are distinguished; since all three are used for inductors and transformers (in ascending order of frequency) the classification has been made in terms of the typical permeability ranges.

For typical mechanical and thermal properties, see Tables 3.1 and 3.2 in Section 3.2.

Property	Symbol or expression	Measuring conditions			Principal applications				Units
		f kHz	$\hat{B}$ mT	Misc.	L.F. inductors	M.F. inductors	W.B. and pulse transformers	Power transformers	
Initial permeability	μ_i	< 10	< 0.1		1200 - 2500	500 - 1000	3800 - 10000	1000 - 3000	
Saturation flux density	B_{sat}	< 50		$H = 800\ A.m^{-1}$ $\theta = 85^oC$				300 - 350	mT
Coercivity	H_c			from sat. $\theta = 85^oC$				10 - 20	$A.m^{-1}$
Residual loss factor	$(\tan\delta_r)/\mu$	30 100 1000	< 0.1		0.8 - 2.0 1.5 - 3.0	 3 - 8 10 - 30	5 - 10 20 - 70		10^{-6} 10^{-6} 10^{-6}
Hysteresis coefficient	η_B	4 100	{ 1.5 to 3 }		0.5 0.6	2	1		$mT^{-1} \times 10^{-6}$
Power loss density	P_m	16 25	200 200	$\theta = 85^oC$ $\theta = 85^oC$				60 - 100 100 - 150	$\mu W.mm^{-3}$ $\mu W.mm^{-3}$
Curie point	θ_c	< 10	< 0.1		130 - 250	150 - 250	100 - 140	180 - 280	^oC
Temperature factor	$\frac{\Delta\mu_i}{\mu_i^2 \Delta\theta}$	< 10	< 0.1	from 5^oC to 55^oC	0.5 - 1.5	0 - 2			$^oC^{-1} \times 10^{-6}$
Disaccommodation factor	$\frac{\Delta\mu_i}{\mu_i^2}$	< 10	< 0.1	from 10 min to 100 min	1 - 3	3 - 12			10^{-6}
Resistivity	ρ	d.c.			1 - 5	1.5 - 10	0.05 - 0.5	1 - 5	$\Omega.m$

TABLE 3.3. Typical properties of manganese zinc ferrites

Property	Symbol or expression	Measuring conditions: f kHz	Measuring conditions: $\hat{B}$ mT	Measuring conditions: Misc.	Principal Applications: inductors and transformers			Unit
Initial permeability	μ_i	< 10 kHz	< 0.1		400 - 750	160 - 490	70 - 150	
Saturation flux density	B_{sat}			H = 800 $A.m^{-1}$ H = 4000 $A.m^{-1}$	270 - 340	300 - 360	 250 - 400	mT mT
Coercivity	H_c			from saturation	16 - 50	80 - 160	160 - 300	$A.m^{-1}$
Residual loss factor	$(\tan\delta_r)/\mu$	1 MHz 3 MHz 10 MHz	< 0.1 < 0.1 < 0.1		35 - 150	25 - 90 50 - 200	20 - 40 25 - 50 60 - 100	10^{-6} 10^{-6} 10^{-6}
Hysteresis coefficient	η_B	10 kHz	0.3 - 1.2		1 - 2	5 - 15	2 - 10	$mT^{-1} \times 10^{-6}$
Curie point	θ_c				125 - 200	200 - 350	250 - 400	^oC
Temperature factor	$\frac{\Delta\mu_i}{\mu_i^2 \Delta\theta}$	< 10 kHz	< 0.1	from 25°C to 55°C	0 - 15	0 - 8	0 - 8	$^oC^{-1} \times 10^{-6}$
Resistivity	ρ	d.c.			> 10^3	> 10^3	> 10^3	> 10^3

TABLE 3.4. Typical properties of nickel zinc ferrites

CHAPTER 3. REFERENCES

1. Heikes, R.R. and Johnstone, W.D. Mechanism of conduction in Li-substituted transition metal oxides. J. Chem. Phys., (1957), 26, No.3, pp.582-587.
2. Lotgering, F.K. Semiconduction and cation vacancies in manganese ferrites. J. Phys. Chem. Solids, (1964), 25, pp.95-103.
3. Stijntjes, T.G.W., Klerk, J. and Broese van Groenou, A. Permeability and conductivity of Ti-substituted MnZn ferrites. Philips Res. Repts., (1970), 25, pp.95-107.
4. Bongers, P.F. et al. Defects, grain boundary segregation and second phases of ferrites in relation to the magnetic properties, Ferrites (Proceedings of IFC3), pp.265-271. Ed. Watonabe, H., Iida, S. and Sugimoto, M. Centre for Academic Publications, Japan, (1981).
5. Chikazumi, S. Physics of Magnetism. pp.260-264. John Wiley and Sons, Inc., New York, (1964).
6. Hoekstra, B. et al. Initial permeability and intrinsic magnetic properties of polycrystalline MnZn ferrites. J. Appl. Phys., (1978), 49, No.9, pp.4902-4907.
7. Chikazumi, S. Physics of Magnetism. pp.271-274. John Wiley and Sons, Inc., New York, (1964).
8. Knowles, J.E. Permeability mechanisms in manganese zinc ferrites. J. de Physique, (1977), 38, C1, Suppl.4, pp.27-30.
9. Broese van Groenou, A., Bongers, P.F. and Stuijts, A.L. Magnetism, microstructure and crystal chemistry of spinel ferrites. Mater. Sci. Eng., (1968/9), 3, pp.341-343.
10. De Lau, J.G.M. Influence of chemical composition and microstructure on high frequency properties of Ni-Zn-Co ferrites. Philips Res. Repts. Suppl., (1975), No.6, pp.88-91.
11. Stoppels, D. Relationship between magnetocrystalline anisotropy, including second-order contribution, and initial magnetic permeability for monocrystalline MnZn ferrous ferrite. J. Appl. Phys., (1980), 51, No.5, pp.2789-2794.
12. Brough, C. (to be published in 1983).
13. Smit, J., Lotgering, F.K. and Stapele, R.P. van. Anisotropy and relaxation in ferrites. J. Phys. Soc., Japan (1962), 17B, pp.268-272.
14. Giles, A.D. and Westendorp, F.F. The effect of cobalt substitutions on some properties of manganese zinc ferrites. J. Phys. D (GB), (1976), 9, pp.2117-2122.
15. De Lau, J.G.M. Influence of chemical composition and microstructure on high frequency properties of Ni-Zn-Co ferrites. Philips Res. Repts. Suppl. (1975), No.6, pp.47-71.
16. Braginski, A. Magnetic after-effect in iron-rich ferrites containing vacancies. Phys. Stat. Sol., (1965), 11, pp.606-616.
17. Knowles, J.E. Magnetic after-effects in ferrites substituted with titanium or tin. Philips Res. Repts. (1974), 29, pp.93-118.
18. Knowles, J.E. and Rankin, P.J. Disaccommodation of permeability in manganese-zinc-titanium ferrites. J. de Phys., (1971), 32, C1 Suppl. 2-3, pp.845-846.

19. Stoppels, D., Enz, U. and Damen, J.P.M. Stress dependence of the magnetic permeability of MnZn ferrous ferrites. J. Magn. and Magn. Mater., (1980), 20, pp.231-235.
20. Snelling, E.C. Soft Ferrites, Properties and Applications. p.172. Butterworths, London, (1969).
21. Snelling, E.C. ibid. pp.174-175.
22. Snelling, E.C. ibid. pp.29-33.
23. Rayleigh, Lord. Notes on electricity and magnetism III. On the behaviour of iron and steel under the operation of feeble magnetic forces. Phil. Mag., (1887), 23, p.225.
24. Chikazumi, S. Physis of Magnetism. pp.308-319, p.382. John Wiley and Sons, Inc., New York, (1964).
25. Smit, J. and Wijn, H.P.J. Ferrites. pp.289-297. Philips Technical Library, Eindhoven, (1959).
26. Broese van Groenou, A., Bongers, P.F. and Stuijts, A.L. Magnetism, microstructure and crystal chemistry of spinel ferrites. Mater. Sci. Eng., (1968/9), 3, pp.344-354, pp.364-367.
27. Snoek, J.L. Time effects in magnetization. Physica, (1938), 5, pp.663-688.
28. Mizushima, M. Magnetic properties of cobalt-substituted Ni-Zn ferrites. Jap. J. Appl. Phys. (1964), 3, No.2, pp.82-86.
29. Snoek, J.L. Dispersion and absorption in magnetic ferrites at frequencies above one megacycle. Physica.(1948), 14, pp.207-217.
30. Smit, J. and Wijn, H.P.J. Ferrites. pp.84-88. Philips Technical Library, Eindhoven, (1959).
31. Smit, J. and Wijn, H.P.J. ibid. pp.82-84.
32. De Lau, J.G.M. Influence of chemical composition and microstructure on high frequency properties of Ni-Zn-Co ferrites. Philips Res. Repts. Suppl., (1975), No.6, p.28.
33. Néel, L. Some theoretical aspects of rock magnetism. Adv. Phys. (Phil. Mag. Suppl.), (1975), 4, pp.191-244.
34. Street, R. and Wooley, J.C. Irreversible magnetic viscosity effects. Soft Magnetic Materials for Telecommunications. Edited by Richards, C.E. and Lynch, A.C. p.180. Pergamon Press Ltd, (1953).
35. Stacey, F.D. Thermal agitation of ferromagnetic domains. Proc. Phys. Soc., (1959), 73, pp.136-138.
36. Giles, A.D. and Westendorp, F.F. Some loss relationships in Mn-Zn ferro ferrites and their response to magnetic disturbance. IEEE Trans. Magn., (1982), MAG-18, No.4, pp.944-950.
37. König, U. Improved manganese-zinc ferrites for power transformers. IEEE Trans. Magn., (1975), MAG-11, No.5, pp.1306-1308.
38. Knowles, J.E. The origin of the increase in magnetic loss induced by machining ferrites. IEEE Trans. Magn., (1975), MAG-11, No.1, pp.44-50.

CHAPTER 4
Ferrite Cores for Inductors

4.1. INTRODUCTION

Inductance has been one of the essential elements of electrical networks since the beginning of telecommunications and it has had an important role in most branches of electronics. The advent of integrated circuits brought the need to use only those circuit elements that can be realized on a silicon surface and the physical inductor is clearly not a candidate for this technology. In analogue circuits, attempts were made to avoid inductive reactance and if this were not possible then other solutions were sought, e.g. bulk wave resonators, surface wave devices, gyrators, etc. A more powerful trend was the replacement of analogue circuits by digital circuits in which the need for inductance can be virtually eliminated.

However, the modern inductor is the product of a long evolution[1]; its design and application is extremely flexible and it can be inexpensive. It is still used on a large scale. For example, it holds a pre-eminent position in long-distance analogue telephony equipment where millions of high quality inductors have been used annually to provide filtering, most of which is still in service. Recently the introduction of digital transmission has led to a decline, but by no means a cessation, in the procurement of analogue equipment. However the replacement or avoidance of inductors by competitive technologies is usually only cost-effective if there is a very large market for a standardized circuit function; for smaller scale demands, or in cases where the design must remain flexible, the inductor remains an essential circuit element.

In this Chapter the inductor is considered in the context of the high performance appropriate to applications such as telephony; less stringent requirements will therefore be embraced. Ferrite has become the accepted core material for inductors covering a wide range of applications. The requirements of an inductor may be summarized as follows:

- An inductance value which, once adjusted, is substantially constant at a given temperature during its service life.

- A temperature coefficient of inductance that is within close limits about an appropriate nominal value over the required temperature range.
- Very low electrical and magnetic losses.
- Low non-linear distortion.
- Low cost and volume.

In network design, the capacitances are usually set at standard values and the nominal values of the corresponding inductances are precisely calculated. The inductor is designed to provide the nominal inductance but it is usually necessary for this value to be adjustable in circuit. This adjustment is to compensate for the tolerance of the effective permeability of the inductor and of the capacitance of the resonating capacitor, the presence of stray capacitances, the variations in winding geometry and the necessity for the winding to have an integral number of turns. An adjustment range of ± 7% is typical and a setting accuracy of $\pm 10^{-4}$ is desirable.

The values of inductance and resonating capacitance will in general be functions of temperature and time. Unwanted changes of inductance are called variability and may be influenced by the choice of air gap. In considering temperature dependence, it is usually the change of resonant frequency with temperature that is relevant, so where this is important the temperature coefficient (abbreviated to TC) of the inductance is arranged to compensate, at least partially, that of the capacitance. Typically the TC of the LC product may need to be limited to 0 ± 10^{-4}/°C and this might correspond to a TC of inductance of $(+50 \text{ to } +150)\times10^{-6}$/°C. A typical long-term constancy for the LC product might be limited to $\pm 10^{-3}$ over a service life of 20 years and the corresponding drift of inductance might be $\pm 0.5\times10^{-3}$.

Within a given volume, a high Q-factor is usually desirable as this will generally result in a more efficient network design. However, particularly at lower frequencies, high Q-factor is not compatible with low variability. This is because the achievement of a high Q-factor would require a small air gap while low variability (e.g. low TC of inductance) requires a large air gap. Typical Q-factors range from 50 at frequencies below 300 Hz, through values of 50-1000 at 100 kHz, falling to the region of 200 at 10 MHz.

The hysteresis loop is essentially non-linear and this gives rise to some distortion between the current and voltage waveforms. The relevant parameter is the hysteresis loss tangent of the inductor which in turn depends on the hysteresis coefficient of the ferrite material and the length of the air gap. Distortion arising from hysteresis is usually negligible in a good ferrite core and this gives the inductor the advantage of a very large dynamic range, a parameter that is often deficient in active circuits.

To meet the requirements of the inductor core, a series of MnZn ferrites is available for application at frequencies up to about 1 MHz. They have low losses and controlled temperature dependence of permeability; the initial permeabilities range from about 3000

for the lower frequency region to about 700 for applications at about 1 MHz. For even higher frequencies a change-over to low-loss NiZn ferrites ($\mu_i \approx 100$) is an advantage.

Core volume and cost are inter-related and depend on many factors. For a given overall performance, core volumes have been reduced by at least a factor of 20 over the period since ferrites were commercially introduced. This reduction has been mainly due to improved ferrite materials but optimization of core geometry has played a part. The cost of an inductor includes that of the winding, assembly, mounting and adjustment, so great attention has been paid to these aspects as well as the basic cost of the ferrite core.

It is the improvement in all the above aspects that has kept the ferrite core in a competitive position. In the Sections that follow each of these aspects of inductor design will be considered in more detail.

4.2. CORE GEOMETRY

Before the introduction of ferrites, high quality inductors often used powder iron cores. Due to the relatively low permeability, adequate magnetic isolation between adjacent inductors could be obtained only by the use of toroidal core shapes and this resulted in winding and adjustment difficulties. Ferrite materials, having initial permeabilities between about 100 and 3000, can provide adequate magnetic screening when used to enclose a solenoidal winding. From the outset this led to a two-part core assembled round a cylindrical coil former which occupied an annular recess in the core halves. Fig. 4.1 shows the basic cylindrical geometry, which is referred to as a pot core.

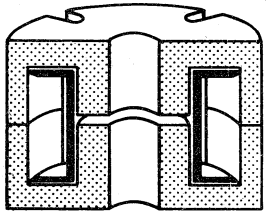

FIG. 4.1. Cross section of a pot core

Many variations have evolved but the pot core exemplifies the essential features. Generally the two core halves are manufactured from identical dies and the plane surfaces, where the outer walls meet, are finely ground to provide a low reluctance contact. The centre poles, which define the magnetic path through the winding, generally do not meet, one or both having been cut back by precision grinding to provide the air gap; this is an essential design variable which will be discussed in the next Section. An axial hole in the centre poles provides access to the air gap for the purposes of inductance adjustment. Access to the coil former is via suitable slots in the outer walls. The assembly generally involves a set of

separate assembly parts such as plates and clips and these vary widely between manufacturers. Cementing with epoxy resin is also used but care must be taken to avoid any significant glue-line thickness on the pole faces. As noted in the previous Section there are a number of criteria of good inductor performance. The Q-factor is the parameter that depends most directly on core proportions. It also depends, of course on a number of other considerations such as the magnetic losses in the core material, the length of the air gap, etc., but assuming these to be constant, it can be shown to a first approximation that the optimum proportions of the core are those which yield the lowest value of the ratio of the d.c. winding resistance, R_{dc}, to the corresponding inductance, L. Clearly these proportions will give the highest Q-factor, $\omega L/R_{dc}$, at low frequencies. At higher frequencies, eddy currents in the winding will change the optimum proportions a little depending on the type of conductor but, since such factors are user-dependent, they cannot be taken into account except where the core is optimised for a specific application.

Considering the low frequency optimum geometry, the inductance of a winding of N turns on a ferrite core having an effective permeability μ_e (see next Section) is

$$L = \mu_o \mu_e N^2 / \Sigma(\ell/A) \qquad \text{H} \qquad (4.1)$$

where ℓ = the incremental length along the magnetic path having a cross-sectional area A.

The summation $\Sigma(\ell/A)$ is called the core factor and has the symbol C_1. It can be regarded as the quotient of an effective length, ℓ_e, of the magnetic path in the core and its effective (uniform) cross-sectional area, A_e. Thus

$$C_1 = \Sigma(\ell/A) = \ell_e/A_e \qquad \text{m}^{-1} \qquad (4.2)$$

Returning to the optimization, the d.c. resistance of the winding, if d is the copper diameter, is given by

$$R_{dc} = \frac{4\rho_c N \ell_w}{\pi d^2} = \frac{\rho_c N^2 \ell_w}{A_w F_w} \qquad \Omega \qquad (4.3)$$

where ρ_c = resistivity of copper (= $1.69 \times 10^{-8}\ \Omega$ m at 20°C)
ℓ_w = mean turn length
A_w = cross-sectional area of the winding space in the coil former
F_w = copper space factor of the winding = $N\pi d^2/4A_w$.

For an ideally packed winding, $F_w = \pi(d/d_o)^2/4$ which is a constant for a given conductor, d_o being the diameter over the insulation. If this ideal value is used then a packing factor $F_p (< 1)$ can be introduced to allow for the practical winding where the packing is non-ideal.

Then $$\frac{R_{dc}}{L} = \frac{\rho_c}{\mu_o \mu_e F_w F_p} \times \frac{\ell_w \ell_e}{A_w A_e} \quad \Omega/H \qquad (4.4)$$

Provided that F_w and F_p are not significantly dependent on the conductor diameter, which is approximately true, this expression is independent of the number of turns. For a given value of μ_e, the first quotient is approximately constant while the second can be expressed in terms of the core dimensions. Clearly the second quotient, as it stands, is inversely proportional to [length]^2 so it is necessary to eliminate the size dependence by multiplying both sides by $V_T^{2/3}$ where V_T is the overall volume of the core. The expression

$$V_T^{2/3} \frac{\ell_w \ell_e}{A_w A_e} \qquad (4.5)$$

may now be expressed in terms of proportions relative, for example, to the overall diameter or equivalent major dimension. There are four basic proportions, namely, core height, and the breadth, outer and inner diameter of the winding space; the expression 4.5 may readily be minimised with respect to these proportions to obtain the optimum shape. One additional proportion, namely, the relative size of the central hole must be a compromise influenced by the needs of the adjustment mechanism. It may be that practical considerations, such as minimum practical ferite wall sections, will lead to some over-riding constraints, but in principle this procedure illustrates the optimisation process which can be applied to core geometries in general.

Several ranges of pot cores have been designed in the past and one in particular has been adopted by the International Electrotechnical Commission as an international standard[2]. The need to increase the packing density of components on printed circuit boards led to the introduction of the square pot core which was also optimised by the above principles. Designated the RM core, a range of sizes has been adopted as an IEC standard[3,9,10]. The RM core type, illustrated in Fig. 4.2, incorporates a coil former having fixed pins, and is provided with spring clips for rapid assembly. It is the core type mainly used for present day high-quality inductors.

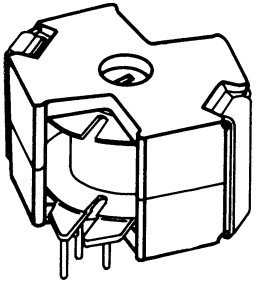

FIG. 4.2. A typical RM core

4.3. THE EFFECT OF AN AIR GAP

The air gap may be regarded as the main moderator in the design of an inductor using a given core. In qualitative terms it reduces the effect, on the inductor performance, of all the core material parameters and it increases the effects due to the winding. For a given set of performance requirements there is, broadly speaking, an optimum value of air gap length; in practice different sub-sets of requirements may lead to somewhat different optimum values so a choice or compromise may then be necessary.

The inductance of a winding on a core that has a core factor C_1, an air gap length/area = ℓ_g/A_g, where ℓ_g is small compared to ℓ_e, and a material with an initial permeability, μ_i, is given by

$$L = \frac{\mu_o N^2}{\ell_g/A_g + C_1/\mu_i} = \mu_o \mu_e N^2/C_1 \quad \text{H} \tag{4.6}$$

where μ_e is the effective permeability and is defined by this equation, i.e. it is the permeability that a core appears to have if the presence of the gap is ignored (see also Eqn. 4.1).

It follows that

$$\mu_e = \frac{C_1}{\ell_g/A_g + C_1/\mu_i} \tag{4.7}$$

If μ_i is large and ℓ_g/A_g is not too small

$$\mu_e \approx A_g C_1/\ell_g \approx \ell_e/\ell_g \tag{4.8}$$

Originally cores were manufactured with standard gap lengths but now it is preferred that the gap is adjusted during manufacture to provide a close-tolerance nominal value of inductance for a given number of turns. This is expressed as the "inductance factor", which in practice is defined as the inductance in nH normalised for one turn, and has the symbol A_L. Thus

$$L = A_L N^2 \quad \text{nH} \tag{4.9}$$

It follows that

$$A_L = \mu_o \mu_e 10^6/C_1 \quad \text{nH for 1 turn} \tag{4.10}$$

where C_1 is in mm^{-1}

Manufacturers usually quote the A_L value for gapped cores. The values are standardised in the R series of standard numbers. Table 4.1 shows the A_L values with the corresponding effective permeabilities of the entire RM range[3] listed in IEC Publication 431[3]. The standardised values of ℓ_e, A_e and C_1 are also included.

Core[1] type	Effective parameters[2]			Effective permeability[3] for A_L (in nH/turn^2) =									
	ℓ_e mm	A_e mm^2	C_1 mm^{-1}	40	63	100	160	250	315	400	630	1000	1600
RM4	21.0	11.0	1.90	60.8	95.7	152	243	380	479				
RM5	20.8	20.8	1.00	31.8	50.1	79.6	127	199	251				
RM6S	26.9	31.3	0.86	27.4	43.1	68.4	109	171	215				
RM6R	25.6	32	0.80	25.5	40.1	63.7	102	159	201	255			
RM7	29.8	40	0.74	23.7	37.4	59.3	94.9	148	-	237			
RM8	35.1	52	0.67	21.5	33.8	53.7	85.9	134	169	215	338		
RM10	42	83	0.50	-	-	40.3	64.4	101	127	161	254	403	644
RM14	71	178	0.40	-	-	-	50.8	79.4	100	127	200	317	508

TABLE 4.1. Effective parameters and effective permeabilities for the range of RM cores

1) As listed in IEC Publication 431

2) Standard IEC values

3) Calculated from $\mu_e = A_L \ell_e 10^{-6}/\mu_o/A_e$ (core without adjuster)

Whereas the A_L value is directly applicable to winding calculations, it is the effective permeability that is the esential parameter that characterizes the core for performance calculations. In practice the value of A_L depends somewhat on the way the coil former is occupied by the winding. The quoted value usually refers to a full winding; a fractionally full winding may result in a deviation of several percent.

Although the main purpose of the air gap is to allow an approximately optimum balance between the influences of the core and winding, it also provides a convenient means of inductance adjustment. It was noted earlier that, in order to compensate for various tolerances, it is desirable to provide inductance adjustment over a range of about ± 7%. The general method of achieving this is to vary the reluctance of the air gap by about the same proportion. By far the most common mechanism is the adjustment of the position of a magnetically soft cylinder on the axis of the central hole so that it shunts the air gap by an amount dependent on its position. The axial position is generally adjusted by a leadscrew action. Fig. 4.3 shows a typical arrangement.

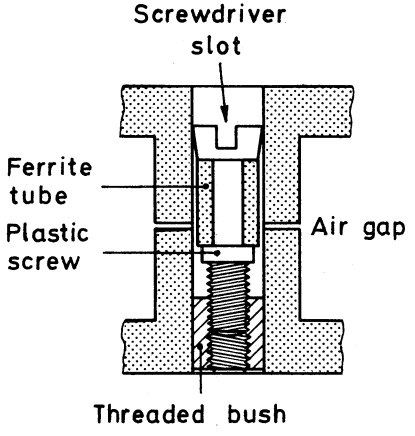

FIG. 4.3. A typical arrangement of an adjuster in an inductor core

The adjusting mechanism is of major technical importance and a detailed consideration of all the aspects of its design and performance is inappropriate in the present context. However the following outline will give an indication of some of the main aspects.

Other things being equal, the higher the A_L value the smaller is the available adjustment range because the core has a smaller air gap and therefore the shunting action of a given shunt is less. However, cores having the higher A_L values have larger manufacturing tolerances on that parameter and therefore need more adjustment range. For a

given A_L, the most effective way of increasing the adjustment range is to reduce the radial clearance between the shunt and the wall of the hole. This rapidly reduces the permissible dimensional tolerances on the diameters controlling the radial clearance. Further, if the rotation of the cylindrical shunt during adjustment is not concentric then the curve of adjustment as a function of rotation may have unacceptable undulations; these will be worse if the radial clearance is small.

While adequate range is necessary, it is important to avoid too much adjustment per revolution as this can exaggerate unwanted variations of inductance with temperature and time. The adjuster can be a major source of unwanted inductance variations and careful design is necessary to minimise such effects. Finally the adjusting mechanism must be very cheap, reasonably robust, easy to operate and capable of providing a high degree of stability under adverse environmental conditions.

4.4. INDUCTANCE VARIABILITY

Unwanted changes of inductance, mainly with respect to time and temperature, are referred to as variability. They may arise from the ferrite material or from mechanical aspects of the assembly. In either case they may be reversible, as in the case of temperature coefficient or irreversible as with a drift with time.

It is relatively easy with modern ferrite inductor cores to achieve a fairly low level of variability, e.g. a TC of inductance that is within $\pm$ 50x10^{-6}/°C of the required value, and a long-term drift of better than 10^{-3}. However, in many professional applications the variability performance is required to be substantially better than this and in such cases great care is needed in the design and construction of the inductor assembly.

4.4.1. VARIABILITY DUE TO THE FERRITE MATERIAL

Inasmuch as the inductance depends on the core material permeability, the variability will depend on the variation of that permeability. In Chapter 3 some factors affecting the permeability of ferrites were considered. In general, the permeability is a function of temperature, time, flux density, frequency, polarizing field strength and mechanical stress.

The relation between a fractional change in the permeability, $\Delta\mu/\mu$, arising from any cause, and the corresponding change in inductance, $\Delta L/L$, of a gapped inductor follows from Eqn. 4.6, by differentiation (the subscript i is dropped since this derivation is not confined to the initial permeability):

$$\frac{dL}{d\mu} = \frac{\mu_o N^2 C_1}{\mu^2}\left(\frac{\ell_g}{A_g} + \frac{C_1}{\mu}\right) = \frac{L}{\mu^2}\mu_e \qquad \text{from Eqn. 4.7}$$

$$\therefore \quad \frac{dL}{L} = \frac{d\mu}{\mu} \cdot \frac{\mu_e}{\mu}$$

or

$$\frac{\Delta L}{L} \approx \frac{\Delta\mu}{\mu} \cdot \frac{\mu_e}{\mu} \qquad (4.11)$$

Thus any change in the permeability of the core material is reduced in its effect on the inductance by the factor μ_e/μ, which is often called the "dilution ratio". For a typical ferrite inductor, μ_e/μ might be 200/2000, so the benefits of a gap giving this dilution ratio would be to reduce the effect of permeability changes by a factor of ten.

In the case of temperature coefficient, the change in permeability is relative to temperature, so Eqn. 4.11 may be adapted:

$$\frac{\Delta L}{L\Delta\theta} = \frac{\Delta\mu_i}{\mu_i^2\Delta\theta} \cdot \mu_e \qquad (4.12)$$

The LHS is the TC of inductance and the RHS consists of an expression referred to as the Temperature Factor (TF) multiplied by the effective permeability. Since filter inductors are generally used at low flux densities, the TC and TF usually relate to the initial permeability, μ_i, so this symbol has been substituted in Eqn. 4.12.

The TF is the TC of the initial permeability normalized with respect to the initial permeability and is the parameter usually quoted to express the temperature dependence of a ferrite inductor core material. A typical value is $(1 \pm 0.5)\times10^{-6}/°C$; if a core having this value were gapped so that $\mu_e = 150$ then the corresponding limits of TC would be (75 and 225) $\times\ 10^{-6}/°C$. These figures would be an appropriate choice if the resonating capacitor were of the polystyrene foil type since such capacitors have a TC of capacitance that is similar in magnitude but opposite in sign so that, to a first order, temperature compensation would be obtained.

The above discussion assumes that the temperature dependence is linear. Fig. 3.7b) on p.39 shows that the $\mu(\Theta)$ curve may be taken as linear only over a small range; similarly the capacitance/temperature curve is non-linear. Consequently temperature coefficient matching can only be approximate even if at some temperature the match is perfect. In practice the designer attempts to match the nominal temperature coefficients and must then calculate the worst case temperature dependence of resonant frequency from the limit TC values for the inductor and capacitor. As stated earlier, other considerations, such as achieving the required Q-factor, may preclude the appropriate choice of μ_e for the attainment of nominal TC matching and in such cases a compromise will be needed. A practical aspect is that the available values of μ_e are limited by the standardization of A_L values, see Table 4.1 on p.79.

In Chapter 3, some of the factors affecting the $\mu(\Theta)$ curve were discussed and it was seen that the curve is very sensitive to a number of factors that depend on the manufacturing conditions. It was also seen that a low linear slope of $\mu(\Theta)$ at a given temperature is incompatible with the attainment of minimum loss at that temperature, (see Section 3.5.7). So for the highest quality cores a compromise is necessary. In the manufacture of such cores the control of temperature factor (and core loss) is a major consideration.

The other cause of inductance variability due to the core material is the time-change of permeability, or disaccommodation. The basic phenomenon, which is in fact common to most magnetic materials has been described in Section 3.4.4. In principle, the initial increase in permeability to a higher, unstable, value may be triggered by any magnetic, thermal or mechanical stimulus which is sufficient to disturb the domain pattern; disaccommodation is the slow relaxation of the permeability back to its lower, stable, value.

This relaxation of permeability is approximately linear with the logarithm of time; the decrease is typically 0.2% per time decade. The effect of an air gap is determined by Eqn. 4.11, i.e.

$$\Delta L/L = (\Delta\mu/\mu^2)\mu_e \qquad (4.13)$$

where the expression $\Delta\mu/\mu^2$ is referred to as the Disaccommodation Factor and is the parameter generally used to express time dependence of the initial permeability of a ferrite. It is referred to a standard time interval, such as the interval between 10 and 100 minutes after the cessation of a standard disturbance[4].

In filter inductor practice, the most likely disturbance is the thermal cycling that may occur during assembly, finishing or subsequent service of the inductor. A large temperature cycle such as might occur, during inductor manufacture, for the purpose of curing adhesive or stabilizing the assembly would typically start a time variation of inductance of 0.02% per time decade. It is good practice to allow a relaxation period of between one and three days between the occurrence of any large disturbance and the final inductance adjustment process. The subsequent inductance decrease at the above rate would then be about 600×10^{-6} over the following three to eight years (depending on material grade) assuming constant temperature. In practice, small temperature fluctuations prevent the permeability from decreasing indefinitely down the disaccommodation curve, so the long term variation would in practice be much less than the above extrapolated value.

The connection between temperature dependence and time dependence is an important aspect of variability. An increase in temperature will normally cause an increase in inductance due to TC of permeability. However, temperature change produces a magnetic disturbance and so causes the permeability to increase further due to the disaccommodation phenomenon. When the temperature change stops, the inductance will be somewhat higher than the value calculated from the TC and it will then decrease with time towards the calculated value, i.e. the inductance/temperature curve will exhibit an overshoot.

When the temperature falls, the inductance will decrease due to TC but again the temperature change will cause the permeability to be higher than its stable value at each temperature due to the disaccommodation phenomenon. When the temperature change ceases, the inductance will be higher than the value calculated from the TC and again it will decrease with time. The effect is shown in Fig. 4.4. It is important to appreciate that this phenomenon can cause significant error in the measurement of the TC of inductance. It is easily avoided by allowing sufficient time at each measuring temperature for the time change to become negligible; usually about 30 minutes is sufficient.

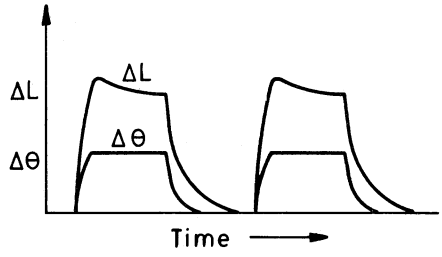

FIG. 4.4. The effect of disaccommodation on the temperature cycling of inductance

Changes in inductance due to other causes, e.g. change of flux density, frequency and polarizing field strength, are generally negligible in filter inductors having ferrite cores; flux densities are usually so low that they have little effect on permeability, the permeability is virtually constant with frequency within the normal design range and polarizing fields are to be avoided in high stability inductors.

4.4.2. VARIABILITY ARISING FROM NON-FERRITE PARTS

Variability can be caused by elements of the inductor assembly acting either directly, e.g. movement of the winding, or via the ferrite core, e.g. change of stress in the core due to the mounting parts. The following list indicates some of the more common effects.

Cause of inductance change	Precaution or remedy
1. Winding movement	Secure coil former to core with soft adhesive so that bond does not stress the core.
2. Unwanted movement of the adjuster:	
a) reversible with temperature	Avoid materials having high coefficients of thermal expansion where they can influence the position of the magnetic shunt.
b) drift with time	Avoid residual stresses in any part of the adjuster mechanism.
3. Stress in the ferrite core	Ensure that the stress is low and constant. Try to match the thermal expansion of the ferrite and the mounting parts. Avoid applying rigid adhesives to the ferrite, and avoid curing such adhesives at elevated temperatures.
4. Relative movement of core halves	Ensure that the core halves are adequately fastened together; this is often incompatible with (3) and requires compromise.

Temperature-reversible effects modify the TC of inductance and can usually be avoided or made small. However, if the design of the adjuster is such that the position of the shunt is reversibly dependent on temperature this can have a significant effect on the TC. Irreversible effects result in long-term drift of inductance and can be serious in some applications unless steps are taken to minimise them. It is generally good practice to subject the completely assembled and finished inductor to a number of temperature cycles, for example, five, extending over, and preferably beyond, the expected operational temperature range. This procedure will relieve stresses and will tend to make incipient drift mechanisms run their courses. The adjuster should be in its nominal mid-range position during the temperature cycling. Final inductance adjustment should be performed several days after the temperature cycling if maximum constancy of inductance is required.

4.5. CONTRIBUTIONS TO THE TOTAL ENERGY LOSS

The Q-factor of an inductor depends on a number of design features that are in principle independent variables. These are: the type of core material (ferrite grade), the size of the core, the effective permeability and the form of winding used. Some of these parameters

may be dictated by considerations other than Q-factor, e.g. limitations of available space or restrictions on the permissible variability, but within such constraints it is generally desirable to maximise the Q-factor.

It is convenient to work in terms of the loss angle, δ, which is the angle by which the phase between the voltage across and the current through the inductor is less than $\pi/2$. If R is the total series loss resistance of an inductor of inductance L

$$1/Q = R/\omega L = \tan\delta_{tot} = \Sigma\tan\delta \qquad (4.14)$$

provided $\tan\delta_{tot} << 1$

The summation is the total of all the contributory loss tangents.

The design problem is to evaluate the loss tangents due to all the separate contributions and to minimize the total. These separate loss contributions will now be considered.

4.5.1. LOSS DUE TO D.C. WINDING RESISTANCE

The loss tangent due to the d.c. resistance of the winding, R_{dc}, is

$$\tan\delta_{dc} = R_{dc}/\omega L \qquad (4.15)$$

$$= \rho_c \ell_w 10^9/\omega A_w F_w F_p A_L \qquad (4.16)$$

from Eqns 4.6, 4.4 and 4.10.

A_L is the inductance factor in nH for 1 turn. If the core size and shape are fixed, then $\tan\delta_{dc}$ depends on A_L and the fullness of the winding. Manufacturers' data sheets either give tables of R_{dc} for a reasonably full winding as a function of overall conductor diameter, d_o, or they give the mean turn length, ℓ_w, and the minimum coil former winding area, A_w. For ideal packing of the conductor, $F_w = \pi(d/d_o)^2/4$, and for fine enamel covered wire this factor lies between 0.5 for very thin wire to 0.7 for 1 mm diameter wire. The corresponding values for F_p are 0.8 and 0.9.

Since $\tan\delta_{dc}$ is inversely proportional to frequency it is the dominant loss at low frequencies. Consequently, high Q-factors at low frequencies can be achieved only by increasing A_L, which increases μ_e and the temperature coefficient, or by increasing the core size which, for a given value of μ_e, increases A_w and A_L.

4.5.2. LOSS DUE TO EDDY CURRENTS IN THE WINDING

As the frequency increases, the resistance of the winding increases due to eddy current effects. Skin effect, which is due to eddy currents generated in a conductor by the alternating magnetic field associated with the current in that conductor acting alone, is not usually very significant. It is the proximity effect[5], which is due to eddy currents generated in the conductors by the leakage field in

the winding as a whole, that can cause the winding resistance to increase to many times the d.c. value. Generally this field is transverse to the conductors so that the resulting eddy currents flow and return in diametrically opposite surfaces along the length of the conductor. Provided the frequency is not so high that the penetration of the flux is affected, the loss tangent due to proximity effect, $\tan\delta_{pe}$, is given by

$$\tan\delta_{pe} = R_{pe}/\omega L = k_e f N d^4/\mu_e \qquad (4.17)$$

where d is the copper diameter of the solid conductor.

The proximity effect constant, k_e, is usually determined experimentally; its value depends on the core and winding geometry and on the effective permeability. Fig. 4.5 gives k_e as a function of A_L for a range of RM cores; the units of k_e are such as to be consistent with d in mm in Eqn. 4.17, (see Table 4.1 on p.79 for the correspondence between μ_e and A_L for RM cores and also Eqns. 4.9 and 4.10).

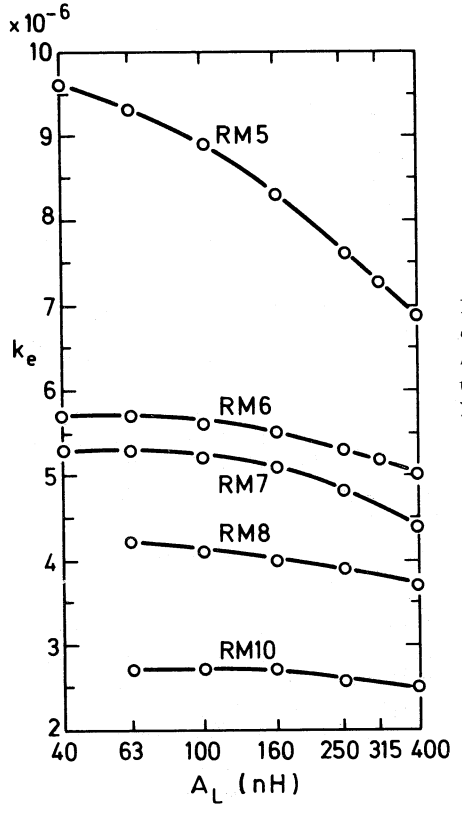

FIG. 4.5. The proximity effect constant, k_e, as a function of A_L for a range of RM cores. The units of k_e correspond to d, in Eqn. 4.17, being in mm.

Proximity effect, in common with many eddy current phenomena, depends on the parameter d/Δ, where Δ is the penetration depth, $= 65.5/\sqrt{f}$ for copper at 20°C, where d and Δ are both in mm and f is in Hz. Eqn. 4.17 is valid for frequencies below the region where d/Δ significantly exceeds unity. Within this range the total copper resistance is,

$$R_{ac} = R_{dc} + R_{pe}$$

$$= 4\rho_c N \ell_w/\pi d^2 + \omega L k_e f N d^4/\mu_e \quad \Omega \qquad (4.18)$$

from Eqns. 4.3 and 4.17.

Since the units of k_e in Fig. 4.5 are consistent with d in mm in the second term, then for consistency the first term should be expressed in mm units and $\rho_c = 16.9 \times 10^{-6}\ \Omega$ mm at 20°C.

By differentiation, following the derivation given in Ref. 6, R_{ac} is a minimum when

$$2\rho_c N \ell_w/\pi d^2 = \omega L k_e f N d^4/\mu_e$$

$$\left.\begin{array}{lll} \text{i.e.} & \text{when} & R_{pe} = \tfrac{1}{2} R_{dc} \\ & \text{or} & R_{ac} = 1.5\, R_{dc} \end{array}\right\} \qquad (4.19)$$

Thus the optimum diameter, d_{opt}, is given by

$$d_{opt} = \left(\frac{\rho_c \ell_w \mu_e}{\pi^2 f^2 L k_e} \right)^{1/6} \quad \text{mm} \qquad (4.20)$$

This optimization is relevant to inductor designs where solid conductors are used in the frequency range from about 10 to 50 kHz. At the lower end of this range the optimum conductor diameter is larger than the core can accommodate, so the design is then the same as for the very low frequency region, i.e. the conductor diameter is chosen to be the largest that can be accommodated. As the design frequency increases, the optimum diameter decreases so beyond a certain frequency it becomes advantageous to fill the winding space only partially.

At even higher frequencies, typically > 50 kHz, the penalty of the proximity effect becomes excessive, the decreasing optimum diameter raising R_{ac} to unacceptable values. The remedy is well-known; the solid conductor, preferred for its lower cost, must be replaced by the much more expensive bunched conductor which consists of a bundle of thin insulated strands twisted together. The twist cancels the emf's induced by the transverse field and the only eddy currents remaining are those in the individual strands which, because d is very small, are often negligible.

If the conductor now consists of s strands of diameter, d, Eqn. 4.18 becomes

$$R_{ac} = \frac{4\rho_c N \ell_w}{\pi s d^2} + \frac{\omega L k_e N s d^4 G_r}{\mu_e} \quad \Omega \qquad (4.21)$$

The factor G_r has now been introduced for reasons of generality. As the frequency exceeds the value where d/Δ becomes greater than unity, the penetration of the magnetic flux into the copper is reduced and the proximity effect resistance becomes less than the value calculated in Eqn. 4.18. Fig. 4.6 shows G_r as a function of d/Δ . In fact, G_r is only likely to be significantly less than unity for solid conductors (s=1) and at high frequencies.

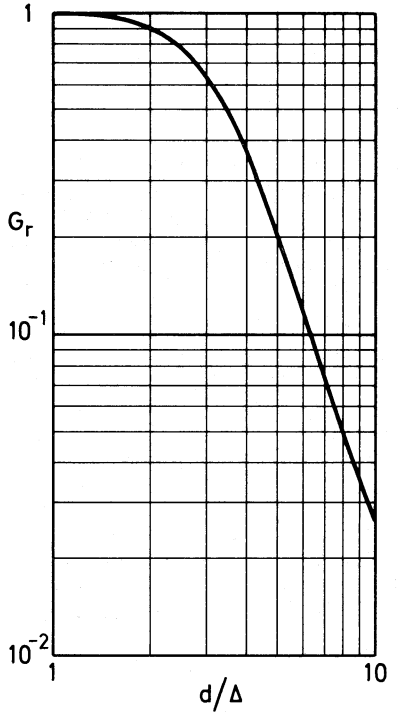

FIG. 4.6. The proximity effect factor, G_r, as a function of d/Δ

Although an expression for optimum strand diameter, corresponding to Eqn. 4.20, can readily be derived from Eqn. 4.21, it would be of little practical use because when bunched conductors having s >> 1 are used, s and d are chosen so that the winding space is filled. It is usual to choose the largest strand diameter, d, that will keep R_{pe} very small compared to R_{dc} and then the value of s is chosen so that the winding space is filled.

4.5.3. LOSS DUE TO STRAY CAPACITANCE

The stray capacitance is composed of three main parts; the inter-turn and inter-layer distributed capacitance, and the capacitances from each end of the winding to the core. It is usual to combine these components into a single capacitance, C_s, appearing in parallel with the winding and to assume an average value for the electrical loss angle, δ_d, of the dielectric. The loss conductance is then

$$G_s = \omega C_s \tan\delta_d \quad \text{S} \tag{4.22}$$

This conductance combines with the inductive reactance to give the dielectric loss contribution, $\tan\delta_{cp}$, to the overall loss tangent of the inductor

$$\tan\delta_{cp} = \omega L G_s = \omega^2 L C_s \tan\delta_d$$

$$= (C_s/C_{res})\tan\delta_d \tag{4.23}$$

where C_{res} is the total capacitance required to resonate the inductor at the frequency $\omega/2\pi$. Usually $C_s << C_{res}$ so the effect of $\tan\delta_d$ is considerably reduced; it is important to ensure a good reduction by making the stray capacitance small compared to C_{res} since a typical value for $\tan\delta_d$ is 0.015 which would be equivalent to a Q-factor of 67 if undiluted.

In addition to this direct contribution there is, in a series resonant circuit, a contribution[7] due to the small rise in inductor current resulting from current circulating in the parallel circuit consisting of LC_s. This increases the inductor loss tangent by a factor $2C_s/C_{res}Q$, where Q is the Q-factor of the inductor.

4.5.4. CORE LOSS

If G is the conductance appearing across the inductor due to the magnetic loss in the core when an RMS voltage U is applied, then the power loss is $P = U^2G$. The induced emf $\approx U$ if $\tan\delta << 1$, and it is related to the frequency and the effective flux density, $\hat{B}_e$, by the induction equation

$$U = \omega \hat{B}_e A_e N/\sqrt{2} \quad \text{V} \tag{4.24}$$

This equation defines $\hat{B}_e$ when the effective core area A_e is used. The loss tangent due to the magnetic core is

$$\tan\delta_m = \omega L G = \omega L P/U^2$$

If there is no air gap

$$L = \mu_o \mu_i N^2 A_e/\ell_e \quad \text{H}$$

$$\therefore \quad \tan\delta_m = \omega \mu_o \mu_i N^2 A_e P/\ell_e U^2$$

Putting $P = P_m A_e \ell_e$ where P_m is the power loss per unit volume, and substituting for U from Eqn. 4.24

$$\tan\delta_m = \mu_o \mu_i P_m / \pi f \hat{B}_e^2 \qquad (4.25)$$

If a small air gap is now introduced and the reduction of core material volume is negligible, and if U, ω and N are unchanged, the flux density will remain constant (by Eqn. 4.24). Since $\hat{B}_e$ and f are unchanged by the air gap, the core loss density P_m is unchanged. In the above expression for L, the initial permeability must be replaced by the effective permeability (see Eqn. 4.6), so Eqn. 4.25 becomes, for a gapped core,

$$(\tan\delta_m)' = \mu_o \mu_e P_m / \pi f \hat{B}_e^2 \qquad (4.26)$$

where the prime refers to the presence of an air gap.

$$\therefore \quad (\tan\delta_m)'/\mu_e = (\tan\delta_m)/\mu_i \qquad \text{(from Eqn. 4.25)}$$

or

$$(\tan\delta_m)' = (\tan\delta_m)\mu_e/\mu_i \qquad (4.27)$$

So again the contribution of the core is reduced by the dilution ratio, μ_e/μ_i.

In an inductor core, the main loss component when $B_e \to 0$, is the residual loss, denoted by subscript r, so

$$(\tan\delta_r)' = [(\tan\delta_r)/\mu_i]\mu_e \qquad (4.28)$$

The expression $(\tan\delta_r)/\mu_i$ is the residual loss factor and is, as described in Chapter 3, the main core loss factor at low flux densities. It is independent of core shape.

Another, generally much smaller, contributory loss arises from eddy currents in the bulk of the ferrite core due to the time-changing flux in a material of finite conductivity. This loss, denoted by subscript F, depends on the size and shape of the core and its conductivity; it is also proportional to μ_e:

$$(\tan\delta_F)' = \text{const.} f . \mu_e \qquad (4.29)$$

In practice, for a given core type, $\tan\delta_r$ and $\tan\delta_F$ are almost inseparable by straightforward measurement, so in a core specification they are usually combined into a single low-flux-density core loss parameter

$$(\tan\delta_{r+F})' = [(\tan\delta_{r+F})/\mu_i]\mu_e \qquad (4.30)$$

The remaining loss contribution is that due to hysteresis. In terms of the loss tangent it is proportional to the flux density and, since filter inductors are usually operated at low signal levels, the hysteresis component of the total core loss is usually small. In terms of the hysteresis coefficient of the core material, η_B, (see Eqn. 3.5.1) the hysteresis loss tangent of a gapped core is

$$(\tan\delta_h)' = \mu_e \eta_B \hat{B}_e \qquad (4.31)$$

4.5.5. THE TOTAL LOSS TANGENT

In general, the total loss tangent $(=1/Q)$ is the sum of the contributory loss tangents introduced above. The loss tangent due to d.c. resistance of the winding is proportional to 1/f and all the others increase with f. In general, therefore, there will be a frequency at which the total loss tangent has a minimum if μ_e remains constant. Similarly, the loss tangents due to losses in the winding decrease if μ_e is increased while those due to core losses are proportional to μ_e. Therefore at a given frequency there will be a value of μ_e at which the total loss tangent is a minimum.

Fig. 4.7 shows diagrammatically the contributory and total loss tangents as functions of frequency for a typical fixed inductor design. The hysteresis loss has been omitted, now and subsequently, because, as stated earlier, it is usually negligible in filter inductors; it may be readily added to the total loss if it proves to be significant.

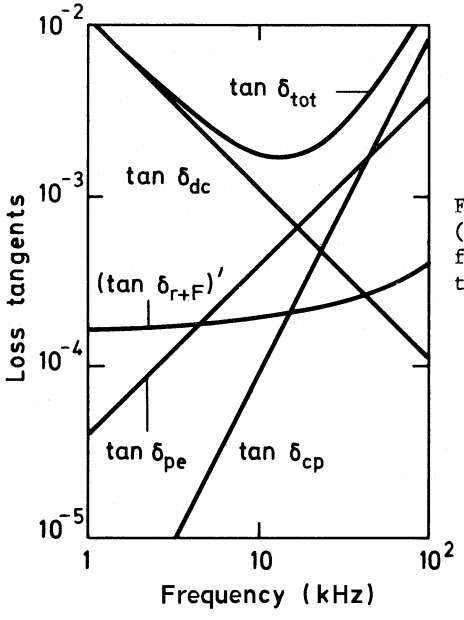

FIG. 4.7. Typical contributory (and total) loss tangents as functions of frequency for a typical inductor design

At low frequencies the loss is due almost entirely to the d.c. resistance of the winding. At the higher frequency end of the range the loss is dominated by one or more of the other contributions. If the inductance is large the stray capacitance loss will be the largest contribution; if the winding has relatively large diameter

conductor the major loss could be that due to proximity effect, but in a typical inductor design it is usually the magnetic loss in the core that dominates the high frequency performance.

4.6. Q-FACTOR

For a given inductor design, the Q-factor may be presented as a function of frequency. Fig. 4.8 shows such curves for a set of specific designs using the standard RM cores. Performance data in this form, provided by the manufacturer, gives useful application information to the designer. The curves may be based on measurement or calculation. Measurement either involves the determination of R and L of Eqn. 4.14 or the value of the Q-factor directly by means of a Q-meter. The calculation may be performed by applying the relevant equations of the foregoing Section and requires a knowledge of the following design parameters:

$$A_L,\ A_w,\ C_s,\ d,\ F_p,\ F_w,\ k_e,\ \ell_w,\ N,\ s,\ \mu_e,\ \rho_c,\ \tan\delta_d,\ (\tan\delta_{r+F})/\mu_i$$

These parameters are either known or may be determined experimentally for a given core type, in which case nominal, average or safe values may be assigned. Once accurately determined, their use in all subsequent calculations ensures reliable results.

On the other hand the measurement of Q-factor will provide an average result only if it is ensured that the winding and core are chosen so that all the above parameters have average values. The alternative is that many inductors of the same design embracing all the parameter spreads must be measured and the results averaged. Either way, the measurement of nominal or average Q-factor can be laborious.

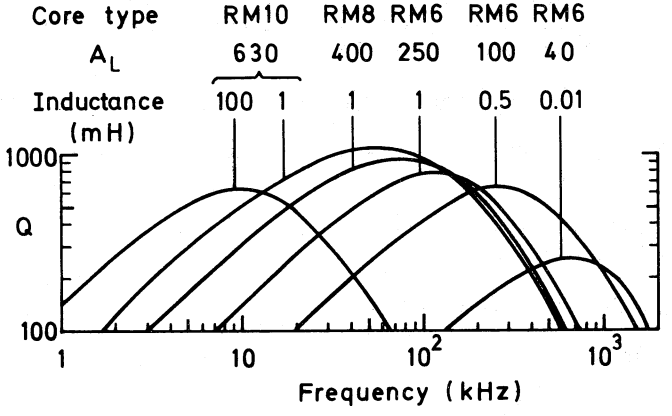

FIG. 4.8. Q-curves of some typical inductors based on cores from the standard RM range

In contrast, once the above parameters have been determined, the calculation of Q-factor for the relevant core type may be programmed so that it may be computed over any range of frequency or inductance for which the parameters are valid. This leads to the construction of the well-known Q-maps[8,9]; Fig. 4.9 shows two typical examples. Such Q-maps may be computed for all available ferrite grades, core sizes, A_L values, conductor types (solid or bunched) and numbers of turns. The designer may therefore read-off the Q-factor at a given frequency for almost any trial design and rapidly decide the best compromise bearing in mind any size or variability restrictions.

The Q-maps generally have the form of hills. Reference to Fig. 4.7 shows that the western slope is determined by the d.c. resistance of the winding. Since the copper packing factor, F_p does not vary much with the number of turns, the contours on this slope run approximately parallel in a north-south direction. The step observed in Fig.4.9(b) is due to the change from single to double textile covering on the bunched conductor.

The north-eastern slope is due to the influence of the self-capacitance loss on the relatively large inductance values. The eastern slope is generally due to a combination of core loss, self-capacitance loss and proximity effect loss in proportion depending on the design. The south-eastern slope, apparent in the Q-map for solid conductors, Fig. 4.9(a), is due mainly to proximity effect loss. The position of the maximum Q-factor moves to a lower frequency if the A_L value, or μ_e, is increased.

For solid conductor windings, the maximum Q-factor is, for most filter inductors, determined by the sum of the d.c. winding resistance and the proximity effect resistance. The optimum combination was discussed in the previous Section.

When the winding consists of bunched conductor then, in the majority of filter inductor designs, the maximum Q-factor is mainly controlled by the sum of the d.c. winding loss and the core loss. When this is so, it can be seen by reference to Eqns. 4.15 and 4.30 that

$$\tan\delta_{tot} = R_{dc}/\omega\mu_e L_o + [(\tan\delta_{r+F})/\mu_i]\mu_e \qquad (4.32)$$

where $L_o = L/\mu_e = \mu_o N^2/C_1$ and is a constant for a given winding and core

Clearly by differentiating with respect to μ_e, the total loss tangent will be minimum when

$$R_{dc}/\omega\mu_e L_o = [(\tan\delta_{r+F})/\mu_i]\mu_e \qquad (4.33)$$

and this occurs when

$$\mu_e^2 = \frac{R_{dc}}{\omega L_o \left(\frac{\tan\delta_{r+F}}{\mu_i}\right)} \qquad (4.34)$$

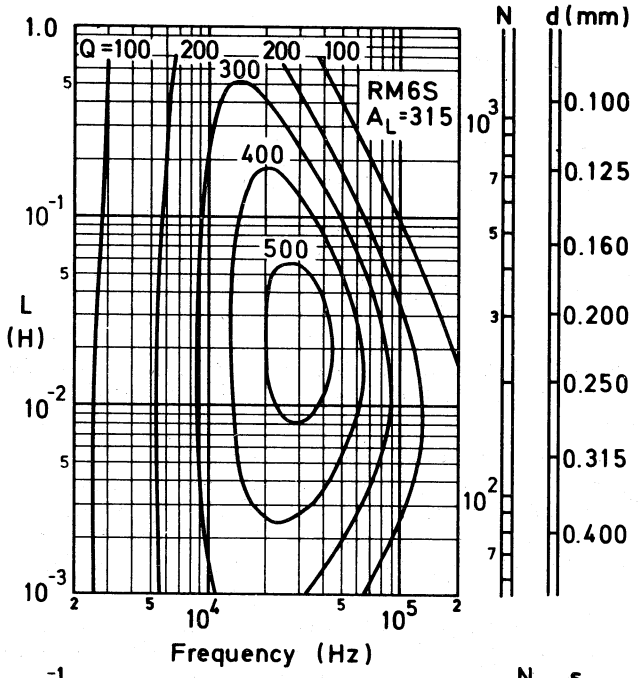

a)

for RM6S, A_L315, fully wound with N turns of solid conductor of diameter, d.

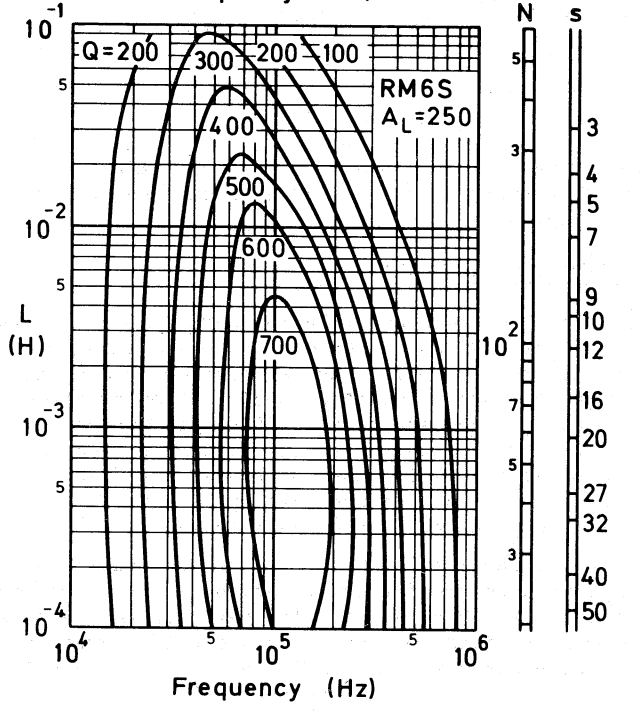

FIG. 4.9. Typical Q-maps (loss contribution from $\tan\delta_h$ omitted)

(Courtesy: Mullard Ltd)

b)

for RM6S, A_L250, fully wound with N turns of s x 0.071 mm bunched conductor

This is the value of effective permeability for maximum Q-factor. From these equations

$$Q_{max} = \frac{\omega \mu_e L_o}{2R_{dc}} = \frac{\omega L_o}{2R_{dc}} \left(\frac{R_{dc}}{\omega L_o \left(\frac{\tan\delta_{r+F}}{\mu_i} \right)} \right)^{\frac{1}{2}}$$

$$\therefore \quad Q_{max} = \left(\frac{\omega L_o}{R_{dc}} \right)^{\frac{1}{2}} \times \frac{1}{2\left(\frac{\tan\delta_{r+F}}{\mu_i} \right)^{\frac{1}{2}}} \qquad (4.35)$$

At a given frequency, the term involving the core loss is a constant for a given ferrite material and the first term depends only on the core and winding geometry.

It can be seen from Eqn. 4.4 that L_o/R_{dc} is proportional to $(\text{length})^2$, so Q_{max} at a given frequency is proportional to the linear dimensions of the core and winding assembly. On the other hand, for a given core shape and size, the value of Q_{max} at a given frequency is inversely proportional to the square root of the core material loss factor.

In practice, the Q-factor requirements tend to remain constant for a particular class of application, so from Eqn. 4.35 it may be seen that for a specified value of Q_{max} at a given frequency:

$$\text{linear dimensions} \propto \left(\frac{\tan\delta_{r+F}}{\mu_i} \right)^{\frac{1}{2}} \qquad (4.36)$$

Developments in ferrite materials have progressively reduced the loss factor and this has led to a corresponding reduction in core size for a given class of application.

4.7. MAGNETIC PROPERTIES OF A FERRITE CORE

In the foregoing Sections, expressions relating core performance to ferrite properties have been given. Such expressions are particularly useful when it is necessary to predict the performance of a core, such as a core under development, where no core specification exists. However, when a core becomes a commercial item, its performance is specified by the manufacturer in terms of core parameters such as loss tangents and temperature coefficient for the standardized values of inductance factor[9,10]. It is then unnecessary, and indeed inadvisable, to derive core parameters from the material data.

The ferrite material properties, such as those discussed in Chapter 3, are published by manufacturers for their various material grades. The values, and their limits where applicable, refer to the ferrite made from specified compositions, processed in a specified way and made into relatively simple shapes, generally toroids, suitable for basic measurements. Under these conditions the full potential of the ferrite grade may be realized.

However, when the same material is pressed into the relatively complex geometries of practical core shapes and processed as required to produce assemblies suitable for the construction of inductors, the properties of the basic material are modified and, in general, somewhat degraded.

The causes of these discrepancies between toroidal properties and those of the inductor core are complex and remain an active area of investigation. Among the more important causes are inhomogeneity in the core due to variations in pressed density resulting from difficult die geometries, uneven exposure to kiln temperature and atmosphere, grinding operations during core finishing, and stress due to assembly operations. Some of these influences will now be discussed in a little more detail.

The $\mu(\Theta)$ curve, as shown in Chapter 3, is strongly dependent on the temperature and oxygen pressure during firing. If the core is not uniformly dense or it is non-uniformly exposed to kiln conditions, the $\mu(\Theta)$ curve will be different in different parts of the core. The overall temperature coefficient of permeability is then more difficult to control than it is for a simple toroid.

It was also seen in Chapter 3 that stress has a strong effect on the $\mu(\Theta)$ curve and on the magnetic losses. Stress is one of the most important factors influencing the properties of a finished core. Knowles[11] has shown that surface grinding has the effect of stretching the surface so that it is put into compression and thus exerts a tensile stress on the interior of the core. The effect of this stress depends on the ferrite composition, the shape of the core and the method of grinding. In general it modifies the $\mu(\Theta)$ curve and therefore changes the TC of permeability. Fortunately the stress, once established, is stable with time and therefore the resultant TC is constant.

The residual surface stress after grinding approximates to the ultimate compressive stress of the ferrite; this residual stress has been measured by Knowles[12] and found to be typically 600 MN/m^2, decreasing to zero at a depth of approximately 5 μm below the surface. The permeability in this layer is greatly reduced and since the loss factor equals $(\tan\delta)/\mu$, this is greatly increased.

A ferrite inductor core invariably has the contact faces ground flat to ensure a stable, low-reluctance, joint and in addition a grinding operation is used to provide the air gap. So a significant increase in both hysteresis and residual loss and an alteration in the TC is to be expected from these operations and these effects must be taken into account in specifying the performance of the finished core. The stresses may in principle be relieved by polishing out the stressed surfaces and this will restore the ferrite properties towards their basic toroidal values. However, even if practicable, the polishing process is expensive and is only justified under special circumstances.

Other causes of change of properties arise from the use of clips, clamps or adhesives for assembly. A thin layer of epoxy resin applied to the ferrite surface and cured at an elevated temperature will appreciably change the TC. Excessive clamping pressures cause similar changes. Unfortunately, the sensitivity of ferrite to stress effects is greater for those ferrites that have been developed to have specially low losses, i.e. for high quality inductor cores. However, with proper care, the degradation due to these effects can be small compared with the improvements due to material development, so there is in fact a significant gain in the use of the better quality materials.

Grinding and clamping or gluing appear to be unavoidable operations and generally the modified parameters have to be accepted. The manufacturer usually quotes the toroidal properties which characterize the material grade but, to allow for the process effects just described, somewhat different limits will be used when calculating the properties of the finished core. These core properties are then the subject of the core (i.e. component) specification; their values are maintained within the specification limits by production control and quality assessment.

4.8. EXAMPLES OF INDUCTOR DESIGN

In this Section, two examples of inductor design will be used to illustrate the typical performance that can be achieved with modern ferrite inductor cores. The Q-factors are taken from published Q-maps and some of the other parameters are calculated from the material data as it applies to the finished core.

4.8.1. LOW FREQUENCY INDUCTOR

The specification given below is typical of an inductor used in the channel filters of the sub-group translating equipment of Frequency Division Multiplex telephony systems[13].

Requirements

L = 20 mH, Q > 500 at 30 kHz, TC < 300×10^{-6}/°C,
Applied voltage, U = 0.5V

Core type

Reference to Fig. 4.9a) on p.95 shows that the required Q-factor may be obtained with core type RM6S with A_L = 315 (without adjuster) and μ_e = 215 (from Table 4.1 on p.79).

Core properties

The above core is made from a ferrite grade giving the following core parameters:

$(\tan\delta_{r+F})/\mu_i$ at 30 kHz < 2.6×10^{-6}

Hysteresis coefficient, η_B < 0.83×10^{-6} mT^{-1}

Temperature Factor, 5 to 70°C, = $(0.34 \text{ to } 1.17)\times10^{-6}$/°C

If it is assumed that the adjuster in its mid-range position will increase the inductance by 7%, then the new μ_e will be 230 and the required inductance without the adjuster is 18.69 mH.

Winding

Number of turns = $\sqrt{18.69 \times 10^6/315} = 244$ (from Eqn. 4.9)

Conductor: Enamelled copper wire, d = 0.224 mm (from Q-map)

Note: This diameter happens to be almost equal to d_{opt} calculated from Eqn. 4.20)

Temperature coefficient of inductance

$$TC = \mu_e \times TF$$

$$= 230\ (0.34 \text{ to } 1.17) \times 10^{-6}/°C \simeq (78 \text{ to } 269) \times 10^{-6}/°C$$

Hysteresis loss tangent

$$B_e = \sqrt{2}U/\omega A_e N$$

Putting U = 0.5V, $A_e = 31.3 \times 10^{-6}$ (from Table 4.1 on p.79)

and N = 244, then $B_e = 0.5$ mT;

$$\therefore \quad (\tan\delta_h)' = \mu_e \eta_B B_e \qquad \text{(from Eqn. 4.31)}$$

$$= 230 \times 0.83 \times 10^{-6} \times 0.5 = 95 \times 10^{-6}$$

This is equivalent to a Q-factor of 10500, so the hysteresis loss will reduce the total Q-factor by less than 5%.

Third harmonic distortion

The ratio of the generated third harmonic emf to the applied emf is given by[14]

$$0.6\tan\delta_h < 0.6 \times 95 \times 10^{-6} = 57 \times 10^{-6}$$

which is equivalent to 85 dB

4.8.2. MEDIUM FREQUENCY INDUCTOR

The specification given below is typical of an inductor used in the channel filters of a group translating equipment of Frequency Division Multiplex telephony systems[13]. The procedure is identical with that of the previous example and it will therefore be abbreviated.

Requirements

L = 1 mH, Q > 700 at 100 kHz

TC between 60 and 230 ($x10^{-6}/°C$)

Applied voltage, U = 0.5V

Core type

Reference to Fig. 4.9b) on p.95 shows that a Q-factor greater than 700 can be obtained with core type RM6S with A_L = 250 and μ_e = 172 (without adjuster)

Core properties

As before

Again assuming a 7% increase in inductance due to the adjuster, μ_e will be 184 and the required inductance without the adjuster is 0.935 mH

Winding

Number of turns = $\sqrt{0.935x10^6/250}$ = 61

Conductor: 20 x 0.071 mm bunched conductors

Temperature coefficient of inductance

TC = (62.5 to 215) x $10^{-6}/°C$

Hysteresis loss tangent

$\hat{B}_e$ = 0.6 mT

$\tan\delta_h < 92 \times 10^{-6}$

Resulting Q-factor degradation = 6.3%

Third harmonic distortion

$0.6\tan\delta_h < 55 \times 10^{-6}$

which is equivalent to 85 dB

4.8.3. COMMENTARY

These two examples are not very different in their requirements but they illustrate several significant points. At frequencies up to about 30 kHz, depending on core size, the highest Q-factor is obtained with solid conductors, because they have higher copper packing factors

than bunched conductors. As solid conductors are much less expensive than bunched conductors there may be economic reasons for using them even at somewhat higher frequencies, where consideration of Q-factor alone would favour bunched conductors.

In the first example the core loss tangent is $2.6\times10^{-6}\times230 = 0.0006$. $R_{dc} = 3.29\Omega$ and $R_{pe} = 1.68\Omega$ giving an a.c. winding resistance loss tangent is 1.3×10^{-3}. Ignoring other losses, this gives a total loss tangent of 1.9×10^{-3} and therefore a Q-factor of 530, which agrees with the Q-map. A higher Q-factor could have been obtained by using a higher A_L value but this would have increased the TC.

If the required inductance had been lower this would have resulted in fewer turns of thicker conductor and then it would have been preferable to use the optimum conductor diameter (Eqn. 4.20) rather than use the thickest conductor that could be accommodated.

The second example shows the need to use bunched conductors at the higher frequencies. The use of a lower A_L value places the tolerance zone of the TC of inductance in a position of approximate compensation for the TC of a polystyrene capacitor.

Both the examples have the applied voltage specified as 0.5V. In the case of a filter this is the voltage across the inductor at resonance. Because of the differences between the two inductance values, the A_L values and the frequencies, the operating flux densities are approximately equal. The effect of hysteresis is seen to be very small and the associated harmonic distortion is correspondingly small.

Turning briefly to higher frequencies, inductors operating at, for example, 10 MHz usually employ cores made of NiZn ferrite having initial permeabilites of about 100 and effective permeabilities of about 25. A typical inductance would be about 10 μH. Q-factors would be typically 150, obtained with a single layer of bunched conductor preferably spaced mid-way between the inner and outer diameters of the coil former.

CHAPTER 4. REFERENCES

1. Welsby, V.G. The Theory and Design of Inductance Coils. Macdonald and Co. (Publishers) Ltd., London, 2nd Edition,(1960).
2. International Electrotechnical Commission. Publication 133, Dimensions of Pot-Cores Made of Ferromagnetic Oxides and Associated Parts. Geneva, (1967), with Supplements A (1970) and B (1971), and Amendment No.1 (1975).
3. International Electrotechnical Commission. Publication 431, Dimensions of Square Cores (RM-cores) Made of Magnetic Oxides and Associated Parts. Geneva, (1973), with Supplements A (1976) and B (1978).
4. International Electrotechnical Commission. Publication 367-1, Cores for Inductors and Transformers for Telecommunications, Part 1, Measuring Methods. p.27, Geneva, (1982).
5. Snelling, E.C. Soft Ferrites, Properties and Applications. p.344 et seq. Butterworths, London, (1969).

6. Snelling, E.C. Ferrites for power applications. Paper No.6 in Colloquium on Trends in Forced Commutation Components, Instn elect. Engrs., (1978), Digest No. 1978/3.
7. Snelling, E.C. Soft Ferrites, Properties and Applications. p.212, Butterworths, London, (1969).
8. Snelling, E.C. ibid. p.216.
9. Mullard Technical Handbook. Book 3, Part 4, Mullard Ltd., Torrington Place, London, WC1E 7HD, (1979).
10. Philips Data Handbook, Components and Materials. Part 4a, Eindhoven, (1978).
11. Knowles, J.E. The effect of surface grinding upon the permeability of manganese-zinc ferrites. J.Phys. D (GB), (1970), 3, pp.1346-1351.
12. Knowles, J.E. The origin of the increase in magnetic loss induced by machining ferrites. IEEE Trans. Magn., (1975), MAG-11 No.1. pp.44-50.
13. Freeman, R.L. Telecommunication System Engineering. p.165. John Wiley & Sons, Inc., (1980).
14. Snelling, E.C. Soft Ferrites, Properties and Applications. p.181, Butterworths, London (1969).

CHAPTER 5
Ferrite Cores for Transformers

5.1. INTRODUCTION

Transformers are used in electronic equipment to provide matching of circuit impedances, to establish accurate voltage or current ratios, for coupling balanced to unbalanced circuits and to provide electrical isolation. As in the case of the inductor, the transformer has become increasingly incompatible with modern microelectronic technology and some of the above functions can now be implemented, or the need for them be obviated, by active circuits in which complexity is no longer an inhibiting factor. However, efficient electrical isolation is one transformer function that is not easily provided by microelectronic circuits and so, in fact, modern systems still employ significant numbers of transformers, particularly for interconnexion and for power supply.

When ferrites were first introduced, their value as core material to replace the traditional laminated metal cores was immediately apparent, particularly at frequencies above the audio range. They were first used in wide band analogue signal transformers for telephony and soon after found a mass market as cores for line output transformers in television receivers. Later they were used for low power pulse transformers, H.F. balun transformers and then in high power, high frequency transformers. In addition, they now play an essential role as cores for transformers in Switched Mode Power Supplies.

A fundamental function of a transformer core is to provide the maximum magnetic coupling between the windings. In the absence of a core, only a small fraction of the magnetic flux generated by the primary couples with the secondary winding. A high permeability core results in a large additional flux, most of which is confined to the core and is thus constrained to couple completely with both windings. The higher the permeability, the more complete is the coupling of the total flux. It is also important to achieve this coupling with the minimum loss of power, so it is usually desirable for the core loss to be small. Winding losses are also important and these can to some extent be minimized by the proper choice of core properties.

It is not the purpose of this Chapter to provide a set of equations, data or procedures by which transformers can be designed; this aspect of the subject is adequately dealt with in textbooks on transformer design, see for example references 1-3. The intention of this Chapter is to outline some of the more important aspects of ferrite cores in their application to the main types of transformers.

It will be a useful preliminary to recall the equivalent circuit of a transformer and to define some of the basic terms and relations. Fig. 5.1 shows the main elements of a somewhat simplified equivalent circuit.

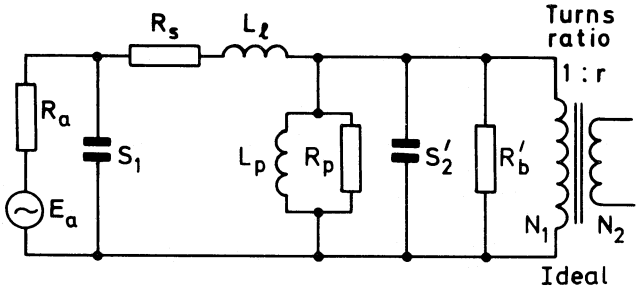

FIG. 5.1. A simplified equivalent circuit of a transformer; see text for element definitions

The elements of this circuit may be defined as follows (the secondary elements being referred to the primary):

E_a = source voltage, R_a = source resistance.

R_s = total winding resistance = $R_1 + R_2'$ where R_1 is the primary winding resistance and R_2' is the secondary winding resistance referred to the primary

L_ℓ = total leakage inductance ≈ the primary inductance with the secondary shorted. This may be calculated by well-known formulae[4].

L_p = open circuit inductance, which may be calculated from Eqns. 4.1 or 4.9.

R_p = the shunt loss resistance representing the core loss.

S_1, S_2' = the primary and referred secondary self or stray capacitances respectively. These may be calculated by well-known formulae[5].

R_b' = load resistance referred to the primary

r = turns ratio.

This equivalent circuit is applicable to most types of transformer and provides a basic reference in the following Sections. In the first of these, consideration will be given to low power transformers in which the transmission of information with the minimum distortion is the main concern. This is followed by a Section dealing with higher power transformers in which the main constraint is the power loss as it affects the efficiency or the operating temperature.

5.2. LOW POWER, WIDE BAND TRANSFORMERS

5.2.1. GENERAL

In the context of this Section, the term "analogue transformer" will be used to describe a transformer designed to carry a wide band, low power analogue signal and the term "pulse transformer" will describe one which carries a digital or pulse signal. Both types are widely used in electronic equipment.

Since a pulse train has a definable frequency spectrum, the design considerations for the two types of transformers are similar. However, the analogue transformer is specified in the frequency domain whilst the pulse transformer is specified in the time domain. The analogue transformer is usually required to transmit a specified bandwidth over which the attenuation should not exceed specified values. The pulse transformer is required to transmit a given pulse shape with specified limits on the shape distortion. Fig. 5.2 shows the main features of the transmission spectrum of the analogue transformer and Fig. 5.3 shows, in simplified form, the main distortions of an ideal rectangular pulse introduced by a pulse transformer.

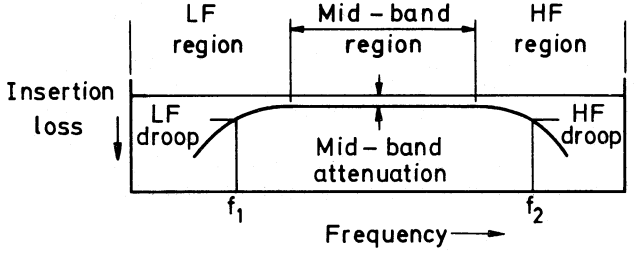

FIG. 5.2. Idealized transmission characteristic of a wide band transformer

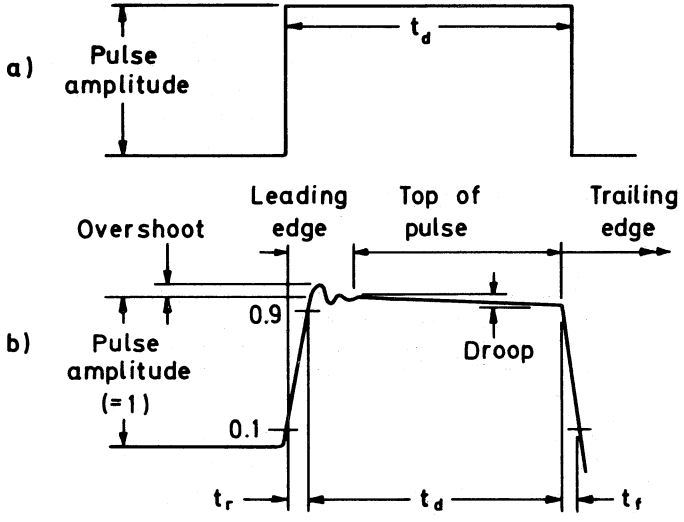

FIG. 5.3. a) An ideal rectangular pulse and b) the main pulse distortions that may be introduced by a transformer

Generally speaking, a transformer design that gives a good, wide, frequency response will also, under appropriate conditions, give a good pulse response. This Section is concerned with the influence of the core and windings on these responses and later it will be necessary to express in a little more detail the relations between the parameters of the core and windings, and the transformer responses. However, it is useful at this stage to indicate a few qualitative relations.

Shunt inductance, L_p, is responsible for the low frequency droop in the analogue transformer since its reactance progressively shunts the circuit as the frequency decreases. In the case of the pulse transformer, the shunt inductance causes the top of the pulse to droop because, during the pulse, the magnetizing current in L_p rises approximately linearly with time causing an increasing voltage drop across the source resistance.

The winding resistance is the main cause of the mid-band attenuation in low frequency analogue transformers. In a pulse transformer it attenuates the output pulse but usually has little effect on the pulse distortion.

The high frequency droop of an analogue transformer may be due to either the increasing series reactance of the leakage inductance or the decreasing shunt reactance of the self-capacitances, or a combination of both, as the frequency increases. In a pulse transformer the leakage inductance, self-capacitances and the source or load resistance combine to slow down, or otherwise distort, the leading and trailing edge responses.

Obviously the effect of the transformer reactances and resistances depend on their relation to the circuit impedance. For the purpose of design, an important parameter is the parallel combination of the source and load resistances, designated R.

$$R = R_a R_b' / (R_a + R_b') \qquad \Omega \qquad (5.1)$$

If the transformer matches the load to the source then $R_a = R_b'$ and

$$R = R_a/2 \qquad \Omega \qquad (5.2)$$

5.2.2. THE EFFECT OF CORE PERMEABILITY AND SHAPE ON TRANSFORMER PERFORMANCE

The shunt, or open circuit, inductance of a transformer is the circuit element that is associated with the magnetizing current. Ideally this inductance should be as large as possible so that the magnetizing current is correspondingly small.

In the case of the analogue transformer, attenuation in the low frequency droop region due to the shunting effect of L_p, is

$$A_i = 10 \log_{10}[1 + (R/\omega L_p)^2] \qquad \text{dB} \qquad (5.3)$$

Thus the lower frequency of the transmission band, f_1, (see Fig. 5.2) depends on the ratio R/L_p.

For a pulse transformer, the droop D expressed in percent, is approximately related to L_p as follows

$$t_d R/L_p \approx D/100 \qquad (5.4)$$

where t_d is the pulse duration

Again R/L_p is the important parameter.

The mid-band attenuation of an analogue transformer and the pulse amplitude attenuation of a pulse transformer are both functions of $R_s/(R_a + R_b')$.

From Eqns. 5.3 and 5.4 any core can, in principle, be used to achieve the required low frequency droop or pulse droop by merely using enough turns in the windings. However, if the core is too small, this will lead to an excessive winding resistance, R_s, and cause high mid-band or pulse attenuation. From Eqn. 4.4, adapted for the transformer case

$$R_s/L_p \propto (\ell_w \ell_e / A_w A_e) \times 1/\mu_e \qquad (5.5)$$

This is independent of the number of turns so, for a given core, R_s is proportional to L_p, thus demonstrating that the droop performance can be improved at the expense of the mid-band or pulse attenuation. For a given size of core it is clearly desirable to have the highest possible effective permeability since this will reduce R_s/L_p. In

general, this ratio, from Eqn. 5.5, depends on the core permeability and the geometry and may be calculated for each core type and size. Such a figure, often calculated for one winding occupying half the available space, is used as a figure of merit for transformer cores. If this were the only criterion then, as described in Section 4.2 for inductor cores, the geometry could be optimized. Indeed, an inductor core, optimised in this respect, will make a reasonably good transformer core.

However there is another, somewhat conflicting, consideration for the transformer core. The high frequency or transient response depends, at least in part, on the leakage inductance. The formula for leakage inductance[4] referred to the primary, N_1, has the form

$$L_\ell \propto N_1^2 \ell_w h_w / b_w \qquad (5.6)$$

where h_w = total height of the windings
b_w = breadth of the windings
ℓ_w = mean turn length

To a first approximation the bandwidth of an analogue transformer and the pulse distortion of a pulse transformer depend on the ratio L_p/L_ℓ. From Eqns. 5.6 and 4.1 this ratio is independent of N. So, for an analogue transformer, any increase of N to decrease f_1 will also decrease f_2 (see Fig. 5.2, p.105) and in addition increase the mid-band attenuation as described above; the bandwidth stays constant. To increase the bandwidth it is necessary to increase L_p/L_ℓ and there are several options:

- Increase μ_e
- Optimise the geometry. It can be shown that

$$L_p/L_\ell = 3\mu_e b_w / \ell_w h_w C_1 \qquad (5.7)$$

  so a broad shallow winding is desirable. This is incompatible with the optimum geometry for minimum R_s/L_p. In practice a compromise may be sought, whereby the latter optimum is modified to increase b_w and decrease h_w by amounts that do not seriously increase R_s/L_p.

- Interleave the primary and secondary windings[4]; this reduces L_ℓ without affecting L_p.

From the above considerations it is clear that in respect of attenuation, bandwidth and pulse distortion, the performance of a core of given shape and size depends on the effective permeability which in turn depends on the initial permeability of the core material. These two permeabilities differ, not, as in the case of the inductor core due to deliberate gapping, but due to the residual gap at the contacting pole faces. Even with very fine grinding the gap is not zero because of residual surface roughness and departure from perfect flatness. Associated with the grinding is the surface stress effect observed by Knowles[6], already mentioned in Sections 3.4.5 and 4.7.

This results in a low permeability skin several micrometres deep on each ground surface.

The residual gap will dilute the available permeability as shown in Eqn. 4.7. The magnitude of this reduction is illustrated in Fig. 5.4.

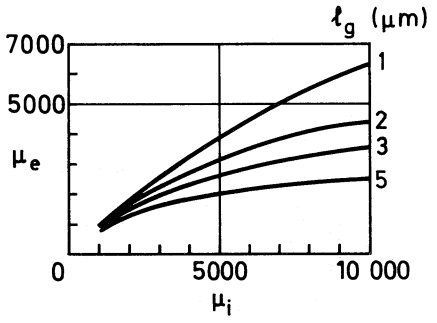

FIG. 5.4. The effective permeability of a typical transformer core* as a function of the material permeability for several values of residual gap length ℓ_g

(*RM8, see Section 5.2.3)

Clearly the loss of permeability becomes large for high values of μ_i. One remedy, which is partially effective but expensive, is to diamond polish the contacting pole faces and this is often done in the manufacture of the higher quality transformer cores.

The permeability referred to so far is the permeability at low flux density obtained in the absence of any polarizing, or static, magnetization, i.e. corresponding to the initial permeability. If there is a net d.c. mmf in the windings the initial permeability of an ungapped core will be reduced to a value referred to as the incremental permeability, μ_Δ, as shown in curve A of Fig. 5.5. An air gap has the effect shown. It can be seen that for a given value of NI there is an air gap that will maximize the (effective) incremental permeability. The design of a transformer carrying d.c. involves choosing the optimum air gap so that the number of turns for a given inductance is at a minimum. Manufacturers' catalogues usually provide design curves derived from data such as shown in Fig. 5.5. These are called Hanna curves and a typical set for the RM range of cores is shown in Fig. 5.6. Given the required inductance, L, and the direct current, I_{dc}, the curves indicate the optimum values of N and air gap. For transformers, the air gap is most conveniently provided by inserting spacers between the pole faces, in which case the air gap is twice the spacer thickness. Design curves are usually expressed in terms of spacer thickness.

Returning to the more usual unpolarized transformer, the effective permeability will vary with temperature, following the general shape of the $\mu_i(\theta)$ curve for the material (see Section 3.4.3). Generally it is required that the effective permeability shall exceed a specified value over a given temperature range. As in the case of inductor cores, the component specification is usually in terms of the inductance factor, A_L.

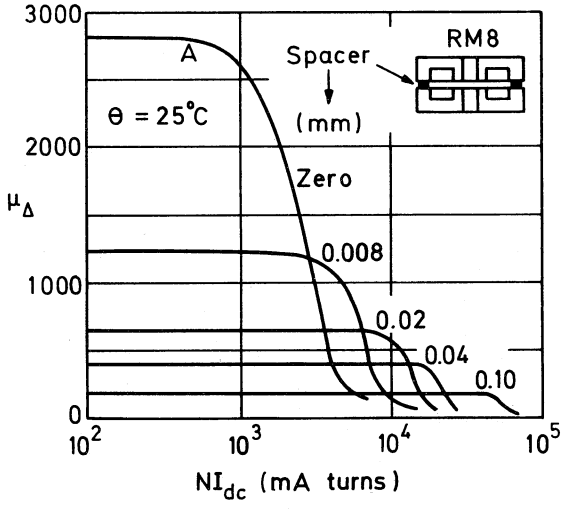

FIG. 5.5. Incremental permeability of a typical transformer core* as a function of d.c. ampere turns with spacer thickness as a parameter

(*RM8, see Section 5.2.3)

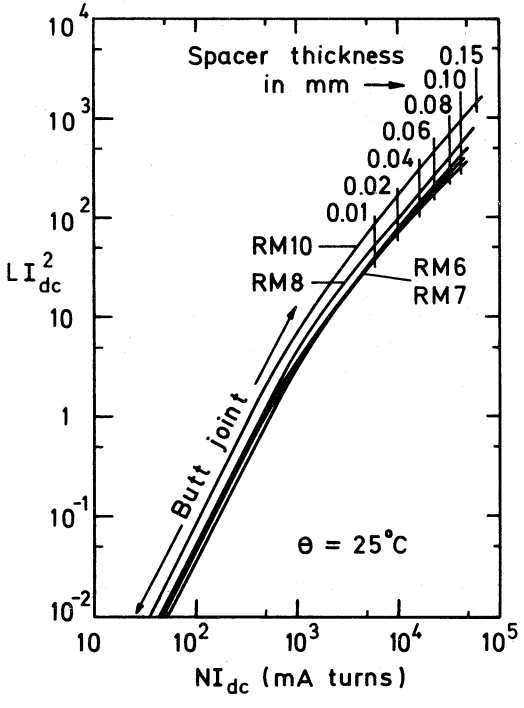

FIG. 5.6. A set of Hanna curves, LI_{dc}^2 vs NI_{dc}, for a range of RM cores; I_{dc} in mA, L in H

For transformers having the lower cut-off frequency below about 0.1 MHz, special MnZn ferrites having initial permeabilities greater than 5000 over the normal operating temperature range have been developed. Even permeabilities greater than 10000 are available but, for the reason illustrated in Fig. 5.4, they are supplied only in toroidal form. Ferrites having such high permeabilities are rather sensitive to stress and care with winding and mounting is necessary if some loss of permeability is to be avoided.

The significance of core losses will be considered in Section 5.2.4.

5.2.3. PRACTICAL CORE SHAPES

Most ferrite transformer cores, with the exception of toroids, consist of two parts with ground pole faces abutting. Usually some attempt has been made to obtain a reasonable compromise on optimum geometric proportions but often practical considerations, such as the need for a particular arrangement of terminals, will strongly influence the shape.

The first ferrite transformer cores copied the E core lamination shapes. This provided interchangeability but did not exploit the ability of the ferrite core to be made in more versatile shapes. E cores with round centre limbs followed resulting in improved R_s/L_p, lower leakage inductance and improved ease of winding. The pot core, already developed and optimised for inductor applications, presented an attractive alternative. It provided standardization of core shapes and accessories for both applications, but it had the disadvantage that access for lead-outs and the provision of terminals were restricted. The RM range (see also Section 4.2) largely removes these disadvantages and provides terminal pins compatible with printed circuit boards. This range is now internationally accepted for both inductor and transformer applications; cores for the latter application are usually made in the higher permeability ferrites and are supplied without air gap.

Table 5.1 shows typical values of properties for a range of transformer RM cores; see Table 4.1 (p.79) for the effective (dimensional) parameters.

The last column of Table 5.1 lists the ratio of the d.c. resistance to inductance for a winding occupying half the available winding space, e.g. a primary winding, based on the nominal mean turn length, ℓ_w, for the total winding space. This figure is obtained from the following expression

$$\left(\frac{R_{dc}}{L}\right)_{\frac{1}{2}} = \frac{2\rho_c \ell_w 10^9}{F_w A_w F_p A_L} \quad \Omega/H \qquad (5.8)$$

where the copper space factor of the winding, F_w, is put equal to 0.56 and F_p is put equal to 0.85; A_w and A_L are minimum values.

Core type	Mean turn length ℓ_w mm	Winding breadth b_w (min) mm	Winding height h_w (min) mm	Winding area A_w (min) mm^2	μ_e (min)	A_L (min) nH/N^2	$(R_{dc}/L)^{\frac{1}{2}}$ (min) Ω/H
RM4	19.8	6.0	1.35	8.1	2820	2090	84
RM5	24.9	5.2	1.98	10.3	2775	3450	49
RM6	30.7	6.6	2.33	15.4	2850	4125	34
RM7	35.6	7.2	3.05	22.0	2450	4200	27
RM8	41.9	9.35	3.38	31.6	2890	5325	17.6
RM10	52.3	11.0	4.15	45.7	3140	7500	11
RM14	71.3	18.9	5.90	111.5			

TABLE 5.1. Typical properties of a range of transformer RM cores based on dimensions listed in IEC Publication 431 and typical permeability specifications, i.e. $\mu_i \approx 5000$.

Many different core shapes have, over the years, been developed for low power transformers; Fig. 5.7 shows a selection. Although the RM core shape has, due to its acceptance in both transformer and inductor applications, superseded most of the other core shapes, some of these alternative types are still used and can offer certain advantages.

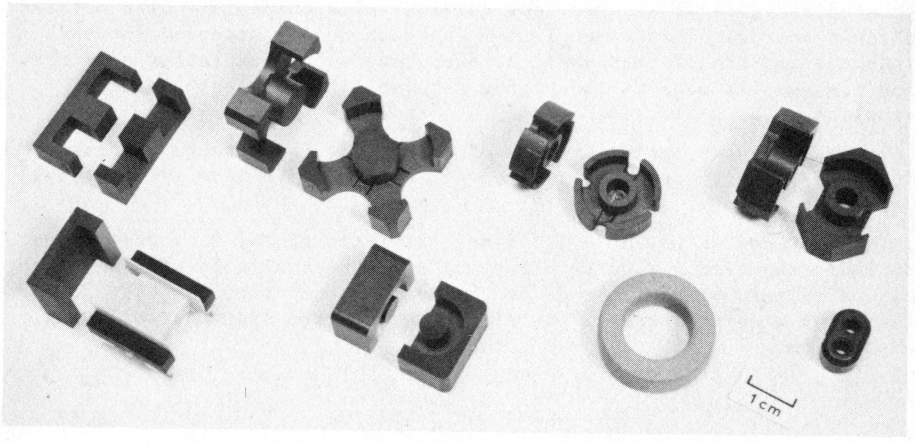

FIG. 5.7. Some low power ferrite transformer cores:
E core. X core. Pot core. RM core.
H core. EP core. Toroid. 2-hole bead.

The X core provides generous access for the lead-outs and its coil former offers a relatively large number of fixed terminal pins.

The H-core exploits the high initial permeability of its ferrite by making the effective air gap negligible. It achieves this by making the pole face area (the upright limbs of the H) very large compared to the core cross-section embraced by the winding (the horizontal limb of the H). Also the residual gap length is reduced by lapping the contact surfaces to a high polish. As a result the effective permeability almost equals the initial permeability (which is typically greater than 5000).

The EP core is a square pot core sectioned in a plane parallel to one side of the square to provide access to the winding. It is mounted with its axis horizontal and the fixed pins on the coil former enable the winding to be terminated symmetrically on either flange, the pins inserting into the printed circuit board. This highly symmetrical arrangement is particularly useful when making higher frequency balanced transformers, where it is often desirable to terminate each end of a layer without the need to pass one end back to the other flange.

For high frequency transformers, requiring only a few turns, there are a variety of one- and two-hole bead-shaped cores. Such cores provide matching or balance/unbalance at frequencies up to about 100 MHz.

Finally there is the simple toroid. This has always been the preferred shape for measuring the basic ferrite properties but its use as a practical core is somewhat limited by the need to employ rather expensive toroidal winding machines. However, the absence of a gap offers the considerable advantage that the effective, or usable permeability equals the initial permeability. As noted in the previous Section, toroids with initial permeabilities greater than 10000 are commercially available. The resulting high inductance factors enable transformer specifications to be met in smaller volumes or with fewer turns. Further, the toroidal shape, when wound uniformly round its entire circumference, has a very low leakage flux and this results in low leakage inductance. Thus the high permeability toroid is superior in principle to the more usual two-part cores in that it enables the largest possible bandwidths (or least pulse distortion) to be obtained. For these reasons the toroidal core will remain an important shape for transformer applications.

5.2.4. THE EFFECT OF LOSSES

This Section is mainly concerned with energy losses in the core but some comments on the effect of a.c. winding losses will be given in the concluding paragraphs.

So far in this Chapter, it has been tacitly assumed that the transformer passband, in the frequency domain, is situated at relatively low frequencies. In terms of high permeability transformer cores this means that the lower end of the passband is below about 0.5 MHz, although this boundary must be regarded as very approximate. For most MnZn ferrites, the initial permeability is very nearly constant below this frequency and the core loss, at low signal strengths, can be

neglected. This can be inferred from the series complex permeability curves shown in Fig. 5.8 (see also Section 3.5). In this, and subsequent, figures, data is given for two MnZn ferrites, a) having $\mu_i \approx$ 5000 and b) having $\mu_i \approx$ 10000, and a NiZn ferrite, c) having $\mu_i \approx$ 100. The latter is included for comparison and also because at higher frequencies NiZn ferrite may be the best material to use.

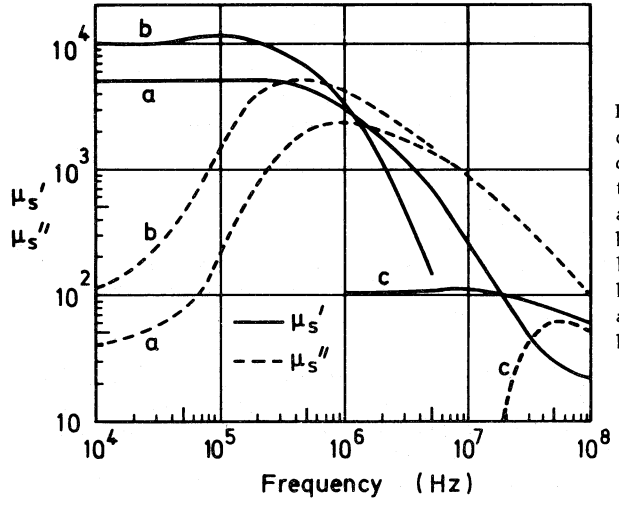

FIG. 5.8. Series complex permeability curves for three typical ferrites; a) MnZn ferrite having $\mu_i \approx 5000$, b) MnZn ferrite having $\mu_i \approx 10000$, and c) NiZn ferrite having $\mu_i \approx 100$.

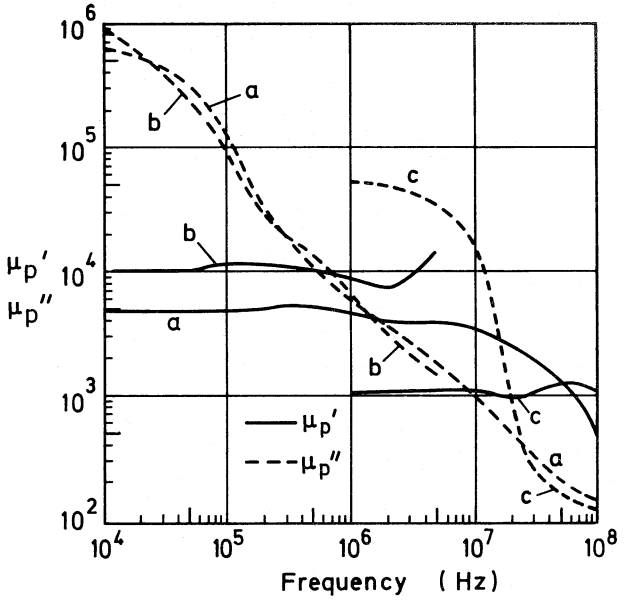

FIG. 5.9. Parallel complex permeability curves corresponding to those of Fig. 5.8.

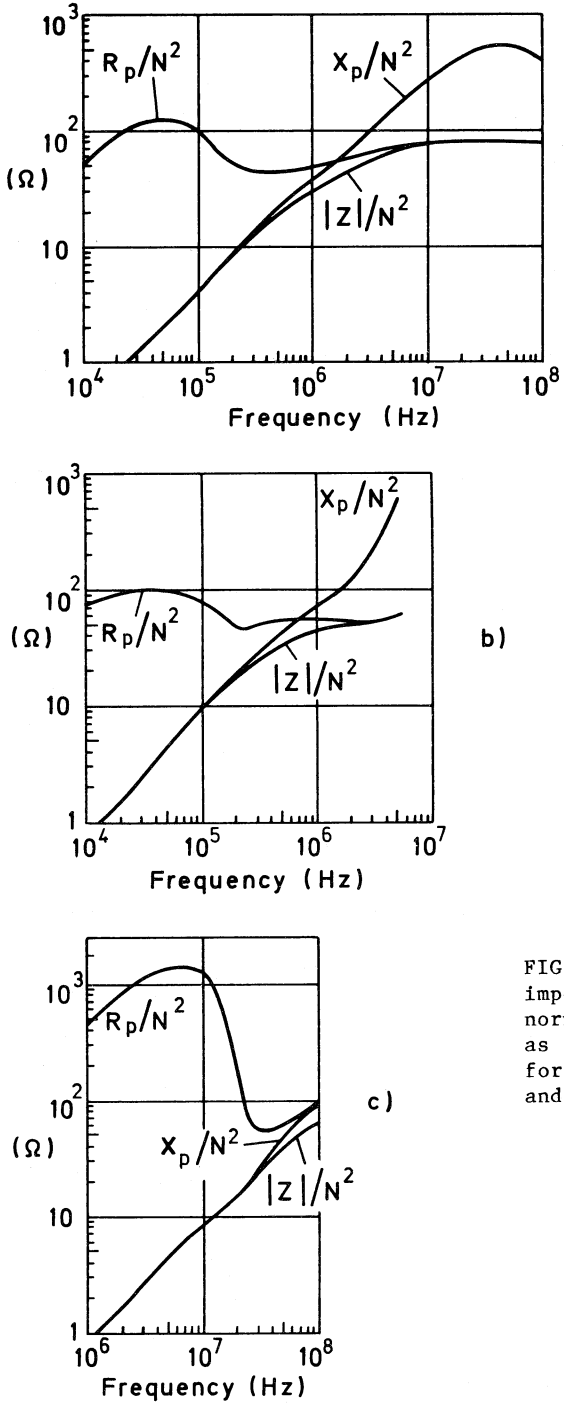

FIG. 5.10. The parallel impedance parameters, normalized for $C_1 = 1\ mm^{-1}$ as functions of frequency, for the materials a), b) and c) of Fig. 5.8.

For transformer applications, the corresponding parallel complex permeability curves shown in Fig. 5.9 (see also Section 3.5) are more relevant because in the design it is ωL_p and R_p that are of interest

$$\left.\begin{aligned} \omega L_p &= \omega L_o \mu_p' \\ R_p &= \omega L_o \mu_p'' \end{aligned}\right\} \qquad (5.9)$$

where $L_o = \mu_o N^2 / C_1$

The parallel impedance parameters may be presented directly, normalized with respect to the square of the number of turns.

$$\left.\begin{aligned} X_p/N^2 &= \omega \mu_o \mu_p'/C_1 \\ R_p/N^2 &= \omega \mu_o \mu_p''/C_1 \\ |Z|/N^2 &= (X_p^2 + R_p^2)^{\frac{1}{2}}/N^2 \end{aligned}\right\} \qquad (5.10)$$

Fig. 5.10 shows these parameters, normalized for $C_1 = 1\ mm^{-1}$, as functions of frequency.

It is seen that for MnZn ferrites the shunting effect of R_p is negligible up to a frequency of about 0.5 MHz; R_p/N^2 does not depart greatly from its value at about 10 kHz. X_p/N^2 rises approximately in proportion to frequency up to about 10^3 MHz. This behaviour means that if a transformer meets the insertion loss specification at f_1 (see Fig. 5.2, p.105) then the influence of L_p and R_p at higher frequencies will be negligible provided f_1 lies below about 0.5 MHz (for MnZn ferrite cores). The situation when f_1 is at a higher frequency will be considered later.

It is assumed in the foregoing discussion that the flux density is so low that there is negligible hysteresis loss. This is usually true for a signal transformer, but it must be remembered that at the lower frequencies the flux density, which for a given voltage is proportional to 1/f, may be sufficient to result in some waveform distortion or even insertion loss. As in the case of the inductor, see Section 4.8, the waveform distortion can be expressed in terms of a third harmonic voltage generator, E_3, inserted in series with the primary inductance.

$$E_3 = 0.6 E_1 \tan\delta_h = 0.6 E_1\ \mu_e\ \eta_B\ \hat{B}_e \qquad (5.11)$$

where E_1 is the applied emf at the fundamental frequency.

In designs where the harmonic distortion is a critical factor, the number of primary turns may be determined by the need to limit $\hat{B}_e$ to meet the distortion specification.

Occasionally the hysteresis loss may make a significant contribution to the very low frequency insertion loss. Its contribution may easily be assessed by determining the extra R_p, $= \omega L_p / \tan\delta_h$, and adding it in parallel to the R_p due to residual loss. For a given applied

voltage the R_p due to hysteresis will, of course, decrease as the frequency falls. The insertion loss due to R_p is given by

$$A_i = 20 \log_{10} (1 + R/R_p) \quad \text{dB} \qquad (5.12)$$

where R is defined in Section 5.2.1.

In addition to hysteresis, the effect of the relatively slow velocity of propagation of electromagnetic waves within the core can give rise to a dispersion of the core impedance under some circumstances. This will be considered later, but first the effect of residual losses in higher frequency transformers will be examined.

It has been noted that if the lower limit of the transmission band (f_1) is below a frequency of about 0.5 MHz then, for MnZn ferrite cores, the shunting effect of X_p and R_p diminish with increasing frequency giving rise to the normal low frequency droop shown in Fig. 5.2 (p.105). It is evident from Fig. 5.10 a) and b) that at frequencies in excess of about 1 MHz the core impedance begins to level off and indeed it can even show a decrease with frequency. If the lower end of the transmission band is situated in this region the insertion loss which is normally observed as a low frequency droop will persist throughout the transmission band. In practice the insertion loss in the transmission band will undulate as the shunt impedance varies with frequency.

As a transformer design parameter, $|Z|$ is of limited use because the effect of impedance on the attenuation depends on the phase angle, or $\omega L_p/R_p$. Using the method described in Ref. 7, the insertion loss due to the shunt impedance Z is given by

$$A_i = 20 \log_{10} \left|1 + \frac{R}{Z}\right|$$

$$= 20 \log_{10} \left|1 + \frac{1}{2Z}\right| \quad \text{dB} \qquad (5.13)$$

when $R_a = R_b' = 1\Omega$

In general

$$Z = \frac{j\omega L_p R_p}{R_p + j\omega L_p} = \frac{R_p}{1 - jQ} \qquad (5.14)$$

where $Q = R_p/\omega L_p$

Putting these two equations together, the insertion loss of a transformer between a 1Ω source and load is

$$A_i = 10 \log_{10} F \quad \text{dB} \qquad (5.15)$$

where $$F = 1 + 1/R_p + (1 + Q^2)/4\ R_p^2 \qquad (5.16)$$

Following the treatment given in Ref. 8, it is seen that for any given value of Q-factor there will be a particular value of R_p which will result in a given insertion loss, e.g. 1 dB. At a given frequency the Q-factor of a particular ferrite is known from the complex permeability data, so the R_p for a given insertion loss may be calculated. From this the required number of turns can be obtained

$$R_p = \omega\mu_o\mu_p''N^2/C_1 \qquad (5.17)$$

It is convenient to put $C_1 = 1\ mm^{-1}$ so that the resulting number of turns (to give R_p) is normalized; this is designated N_a.

$$N_a^2 = R_p 10^3/\omega\mu_o\mu_p'' \qquad (5.18)$$

For a practical design, where the circuit impedance is R $(= R_aR_b'/(R_a + R_b'))$ and the core factor is $C_1\ mm^{-1}$, the actual number of turns required for the given insertion loss is

$$N = N_a(2RC_1)^{\frac{1}{2}} \qquad (5.19)$$

Fig. 5.11 shows N_a as a function of frequency for the same three ferrites, with attenuation A_i as a parameter. If A_i is specified at the lower end of the transmission band then the required number of turns may rapidly be found. If the frequency f_1 is found to be in the undulating, approximately horizontal region of the curve, then, as previously stated, the core impedance will cause undulations over the whole transmission band. The shape of the transmission characteristic may be found at the appropriate value of N_a and estimating the value of A_i at each frequency. Alternatively, R_p and Q may be obtained from Fig. 5.10 at each frequency and the attenuation calculated from Eqns. 5.15 and 5.16.

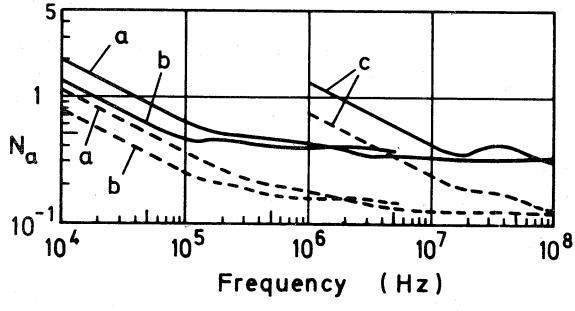

FIG. 5.11. Normalized number of turns as a function of frequency. Solid curve: min. N_a for A_i = 0.5dB. Broken curve: min. N_a for A_i = 3dB. Materials a), b) and c) as in Fig. 5.8, (p.114)

As stated earlier, there are circumstances in which the relatively slow velocity of propagation, v, of electromagnetic waves in MnZn ferrite, due to high permeability, μ, and high effective permittivity, ε, can give rise to a dispersion of the core impedance, a phenomenon called dimensional resonance, see Section 3.5.2.1. The propagation velocity[9] is given by

$$v = (\mu_o \mu \varepsilon_o \varepsilon)^{-\frac{1}{2}} = f\lambda \qquad (5.20)$$

Since for a typical MnZn ferrite $\mu \approx 5000$ and $\varepsilon = 200000$, $v \approx c/30000$ where c is the velocity in free space, (λ = wavelength).

At low frequencies the alternating flux density has the same phase at all points in a core cross-section but at higher frequencies the relatively slow propagation causes the flux density in the interior to be retarded in phase. When the smallest cross-sectional dimension of the core equals half a wavelength a standing wave is established and the net in-phase flux is zero. The effect is that the series impedance of the core, as seen at the terminals of a winding, changes from substantially inductive at low frequencies to resistive when the resonance is established. The modulus of the impedance does not change by a large factor, so provided the dimensional resonance does not occur near f_1 in Fig. 5.2 (p.105) the phenomenon can usually be ignored in transformer applications; in practice it is only observed in large MnZn ferrite cores operating at frequencies above about 50 kHz.

In general, μ and ε in Eqn. 5.20 are complex functions of frequency. Using such data, the resonance dimension, D_r, has been calculated for the previously mentioned MnZn ferrites as functions of frequency. The results are shown in Fig. 5.12. For a rectangular cross-section, D_r, is the smaller dimension; for a circular cross-section it can be taken as the diameter.

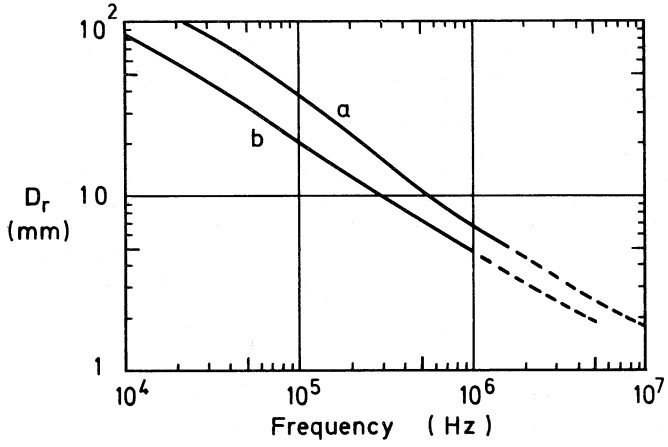

FIG. 5.12. Dimensional resonance in MnZn ferrites. To avoid dimensional resonance at a given frequency the smallest cross-sectional dimension of the core must be significantly less than D_r at that frequency. a) and b) are as in Fig. 5.8 (p.114).

From this account of dimensional resonance it is clear that the data in Figs. 5.8, 5.9, 5.10 and 5.11 relating to MnZn ferrites apply only when the least cross-sectional dimension of the core is significantly less than D_r at a given frequency, i.e. the higher the frequency the smaller must be the core. This constraint is more restrictive for the higher permeability ferrites.

Although in practice there is a natural tendency to avoid dimensional resonance, since it is usual to use smaller cores at the higher frequencies, there are situations where this resonance effect can preclude the use of MnZn ferrite. The alternative is to use one of the NiZn ferrites. Permeabilities of about 1000 are available but as the permittivity is generally < 50, dimensional resonance is moved to frequencies beyond the range being considered here.

Figs. 5.8, 5.9, 5.10 and 5.11 have curves for a commonly available NiZn ferrite with a permeability of 100. If dimensional resonance can be avoided by using suitably small cores then MnZn ferrite cores give a better performance than NiZn ferrite cores, i.e. N_a in Fig. 5.11 is smaller, up to frequencies in the region of 50 MHz.

Finally, the effect of eddy current loss in the windings may be considered very briefly. At low frequencies it may be assumed that, for a transformer, the resistance of the winding is constant over the transmission band and, in that band, the insertion loss, which from Eqn. 5.21 is a function of $R_s/(R_a + R_b')$, is correspondingly constant. At higher frequencies the winding resistance will rise mainly due to proximity effect. This effect has been described for inductor cores in Section 4.5.2 and it will be considered in more detail in Section 5.3.4 when dealing with power transformers.

If the winding resistance is such that it causes a significant insertion loss at the lower end of the transmission band and if it rises with frequency over the band, then the insertion loss will increase with frequency, in other words the mid-band characteristic will be tilted. As with dimensional resonance there is a natural tendency to avoid this effect because, as the application frequency moves to higher values, fewer turns are needed to obtain the required inductance so the d.c. resistance becomes smaller in relation to the circuit impedance. The mid-band attenuation may then be very small and its variation due to eddy currents would be negligible. If this is not the case and a level transmission band is essential then either the conductor diameter must be decreased to give a higher, more constant, resistance or bunched conductor must be used.

5.2.5. SOME DESIGN EXAMPLES

To illustrate the relations between the parameters of the core and windings, and the transformer performance, two simple examples will now be given.

The first is an analogue transformer matching a 600Ω source to a 150Ω load and having a maximum insertion loss of 0.5 dB at f_1 = 100 Hz. An RM8 transformer core (material 'a' of Fig. 5.8, p.114) will be used and it is required to estimate the characteristics of the transmission band.

From Eqn. 5.2, $R = 300\ \Omega$

From Eqn. 5.3, $10 \log_{10}[1 + (300/200\pi L_p)^2] < 0.5$ dB

$\therefore \quad L_p > 1.37H$

From Table 5.1 (p.112), for RM8, $A_L > 5325$ nH/N^2

$\therefore \quad N = (1.37 \times 10^9/5325)^{\frac{1}{2}} = 507$

The minimum winding area, A_w, from the same Table is 31.6 mm^2; half of this is available for the primary winding. Assume a copper packing factor, F_p, of 0.85, then

$$d_o = (15.8 \times 0.85/507)^{\frac{1}{2}} = 0.163 \text{ mm}$$

Wire tables show that d = 0.14 mm copper wire having a fine enamel insulation has d_o = 0.163 mm, therefore this gauge may be used. It has a resistance of 1.12Ω/m. Therefore the total d.c. resistance of the winding, R_1, will be $507 \times \ell_w \times 1.12 \times 10^{-3}$ where, from Table 5.1 (p.112), ℓ_w = 41.9 mm. From this $R_1 = 23.8\Omega$.

The R/L quotient for this half winding is 23.8/1.37 = 17.4Ω/H; this compares with 17.6 from Table 5.1.

The mid-band attenuation is given by

$$20 \log_{10}[1 + R_s/(R_a + R_b')] \quad \text{dB} \qquad (5.21)$$

where R_s is the total winding resistance referred to the primary ($\approx 2R_1$).

This yields a mid-band attenuation of 0.34 dB.

Assuming that the primary and secondary windings are simply wound one above the other, the leakage inductance is approximately given by[4]

$$L_\ell = 4\pi 10^{-7} N^2 \ell_w h_w / 3b_w \quad \text{mH} \qquad (5.22)$$

where the dimensions are in mm.

Substituting the winding dimensions from Table 5.1 (p.112), gives a leakage inductance of 1.63 mH. The corresponding attenuation is given by

$$A_i = 10 \log_{10}[1 + (\omega L_\ell/(R_a + R_b'))^2] \quad \text{dB} \qquad (5.23)$$

For 0.5 dB top-end droop, this expression gives f_2 = 41 kHz.

Finally, to check the significance of the core loss, Fig. 5.10a) on p.115 gives $R_p/N^2 = 50$ at 10 kHz for $C_1 = 1$ mm^{-1}. For an RM8 core with $C_1 = 0.67$ mm^{-1}

$$R_p = \left(\frac{R_p}{N^2}\right) \times \frac{N^2}{C_1} = \frac{50 \times 507^2}{0.67} = 19\ \text{M}\Omega$$

This shunt resistance will clearly give a negligible attenuation in a 600Ω circuit.

If an RM6 core had been used instead of an RM8 core the results would have been as follows (RM8 results in brackets)

N	=	576 (507)	
d	=	0.09 (0.14)	mm
R_1	=	47.9 (23.8)	Ω
Mid-band attenuation	=	0.67 (0.34)	dB
L_ℓ	=	1.5 (1.63)	mH
f_2	=	44.6 (41)	kHz

It is seen that smaller core has increased the mid-band attenuation but has made very little difference to the transmission bandwidth. The latter is to be expected because, in Eqn. 5.7 the expression is dimensionless, so for the same basic shape, L_p/L_ℓ is independent of size.

The second example is a wideband transformer to provide isolation between two 50Ω circuits, the insertion loss to be less than 0.5 dB at f_1 = 1 MHz. The given core is a 2-hole bead in a ferrite having a nominal initial permeability of 5000; the core factor $C_1 = 0.625\ \text{mm}^{-1}$.

From Fig. 5.11 on p.118, the 0.5 dB curve for the μ_i = 5000 MnZn ferrite (curve a) gives $N_a = 0.43$ at 1 MHz.

∴ From Eqn. 5.19

$$N = 0.43\ (2 \times 25 \times 0.625)^{\frac{1}{2}} = 2.4$$

In practice two 3-turn windings could be used. Inspection of Fig. 5.11 shows that, as far as the core is concerned, the bandwith will extend beyond 100 MHz. Leakage inductance will eventually limit the transmission band but for a transformer configuration such as this it is not practicable to calculate the value that the leakage inductance might be. It can be seen that, due to the relative flatness of the curve in the region of 1 MHz, the bandwidth will extend down to frequencies well below 1 MHz. See also Refs. 10 and 11 for examples of an alternative approach using transmission line principles.

5.3. POWER TRANSFORMERS

5.3.1. APPLICATIONS

For the purposes of this Section, a power transformer may be defined as one for which the performance is limited by temperature rise or magnetic saturation of the core. As core materials, ferrites offer lower power losses than most alloy laminated cores operating at the same flux densities, this advantage increasing with frequency. However, the saturation flux density of ferrites is only about a quarter

of that for alloy cores so the ferrite core cannot compete at very low frequencies. These two characteristics of ferrite lead to their advantageous use as cores for power transformers operating at frequencies above about 5 kHz. Power transformers play an essential role in electronic equipment, particularly in circuits involving power conversion from the mains supply where electrical isolation is an essential requirement.

The first power application for ferrite cores was in the output transformers of line time-bases in television receivers. In the professional sector they were used in smaller numbers for a wide variety of purposes, notably in matching transformers for ultrasonic transducers and, in radio transmitters, for matching the RF power to the antenna. The size and weight advantage of ferrite cores in power transformers operating at frequencies in excess of 20kHz led to the use of frequency conversion being considered for mains power supplies for electronic equipment, a function traditionally performed by heavy silicon-iron cored transformers operating at 50-60 Hz. This could in principle be achieved by rectifying the a.c. mains voltage, chopping the resultant d.c. voltage at a high frequency, typically 25 kHz, performing the transformation by a ferrite-cored transformer and then converting the output to d.c. in the conventional way. The main obstacles to implementing this development were the non-availability of suitable semiconductors and capacitors, and the complexity of the necessary control and regulation circuits. These obstacles have now been overcome by developments in power semiconductor devices, capacitors and integrated circuits. Power supplies based on this principle are now widely accepted and are referred to as Switched Mode Power Supplies (SMPS). Typically the output is at a low voltage, e.g. 5 to 15V d.c. to feed the supply rails of equipment employing integrated circuits; currents tend to be high, e.g. ten to several hundred amperes.

This development has opened up a large new application for ferrite and for some years several ranges of SMPS cores have been available commercially. Ferrite power transformer cores, for whatever application, represent an important sector of present-day ferrite production.

5.3.2. GENERAL CONSIDERATIONS

The properties of ferrites intended for application in power transformers have, of course, been specially developed to meet the design requirements of power transformers, so it is necessary to consider such design requirements inasmuch as they relate to the core properties and characterization. Design procedures as such are not within the scope of this treatment. Although power transformers considered in this Section have a wide range of potential applications, and the excitation may be substantially sinusoidal or pulse, symmetrical or unidirectional, there are many common aspects of their design and performance.

5.3.2.1. Temperature Rise

Temperature rise is perhaps the most important aspect of design common to all power transformers. While it is not appropriate to discuss heat transfer here in any detail it is useful to quote formulae[12] for

the two main processes of heat loss in order to deduce some approximate relation between power dissipation, size and temperature. For natural air convection, the rate of heat transfer, P_{conv}, for bodies up to about 200 mm across, is given approximately by the following empirical expression:

$$P_{conv} = 7.5\ \theta^{1.25}/d^{0.25} \qquad \mu W.mm^{-2} \qquad (5.24)$$

where θ = the temperature difference in °C between the transformer surface and the ambient air

and d = the diameter in mm. of a sphere which approximates to the size of the body.

The corresponding expression for radiated power, P_{rad}, is:

$$P_{rad} = 5.67\ 10^{-8} E(T_s^4 - T_o^4) \qquad \mu W.mm^{-2} \qquad (5.25)$$

where E = emissivity of the surface ≈ 0.95 for ferrites
T_s = surface temperature in K
T_o = temperature of surrounding objects in K.

If T_s is not much larger than T_o in relative terms then it readily follows that

$$P_{rad} \approx 5.67\ 10^{-8} \times 4ET_s^3(T_s - T_o)$$
$$\approx 5.67\ 10^{-8} \times 4ET_s^3\theta \qquad \mu W.mm^{-2} \qquad (5.26)$$

if the surrounding objects are at ambient air temperature.

Therefore the total dissipation of the transformer, P_{tot}, which is the sum of the core loss, P_c, and the winding loss, P_w, equals $(P_{conv} + P_{rad})A_c$, where A_c is the total surface area of the transformer assuming that this is at uniform temperature.

$$\therefore \quad P_{tot} \approx A_c(7.5\theta^{1.25}/d^{0.25} + 5.67 \times 10^{-8} \times 4ET_s^3\theta)$$

Assuming that the transformer shape remains constant and its size is characterized by a linear dimension L, then $A_c \propto L^2$ and provided the fractional change of T_s is not large,

$$P_{tot} \propto \theta^{1.25} L^{1.75} + k\theta L^2 \qquad \text{(approx)}$$

For the purpose of the present discussion this may be approximated to

$$P_{tot} \propto \theta L^2 \qquad \text{(approx)} \qquad (5.27)$$

It can be shown[13] that the output power, P_o, of a transformer that is core-loss limited is proportional to $P_{tot}L$. Combining this with Eqn. 5.27 gives

$$P_o \propto \theta L^3 \qquad \text{(approx)} \qquad (5.28)$$

Therefore to obtain the smallest transformer for a given output power, or the maximum output power for a given size, it is obviously desirable to allow the temperature rise to be the maximum permitted by the material properties. In practice the ferrite properties generally impose the limit on temperature rise. This is not due to any irreversible effects on the ferrite (the ferrite can be operated up to temperatures of at least 300°C without permanent effect) but primarily because the saturation flux density falls with increasing temperature. This is illustrated for a typical power ferrite in Fig. 5.13. For most power ferrites the recommended maximum operating temperature is 100°C and the properties are often quoted for this temperature.

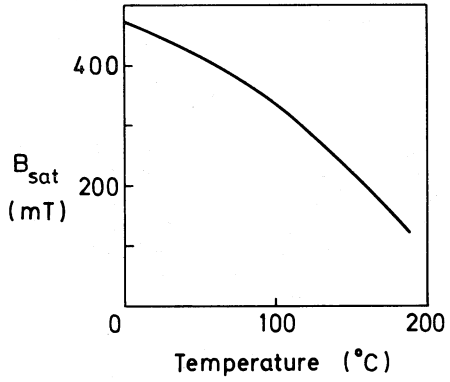

FIG. 5.13. B_{sat} as a function of temperature for a typical power (MnZn) ferrite.

Of course, the relevant temperature, as far as the core is concerned, is the temperature of the hottest point and this is invariably the centre of the interior of the limb embraced by the winding. Fig. 5.14 shows this "hot spot" temperature rise for a standard range of round-leg E cores (EC cores). It may be mentioned in passing that the thermal conductivity of ferrite is relatively high (e.g. 4 $mW.mm^{-1}.°C^{-1}$ at 20°C) so that the temperature at the centre of a ferrite core is rarely more than a few degrees above that of the surface.

5.3.2.2. Maximum Flux Density

The designer will normally wish to use the maximum permissible flux density excursion, since this will minimize the number of turns.

From the induction equation

$$\overline{E}\Delta t = NA_e\Delta B_e \quad \text{V.s} \qquad (5.29)$$

where $\overline{E}$ = applied emf averaged over time Δt.

ΔB_e = corresponding change in effective flux density.

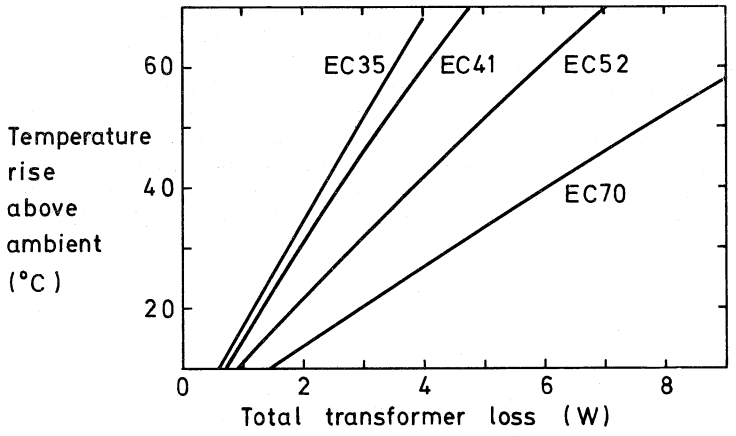

FIG. 5.14. Hot-spot temperature rise above ambient as a function of total transformer loss for each core in the EC range (see Section 5.3.5). This temperature is measured on the cylindrical surface of the centre leg at the junction of the two half-cores, the surrounding winding dissipating approximately half the total loss (the core dissipating the other half). The core is lying horizontally and exposed to natural convection.

For a symmetrical square wave having equal half-cycles, each of duration t_d, and therefore a repetition frequency of $1/2t_d$:

$$\hat{B}_e = Et_d/2A_eN = U/4A_eNf \quad T \qquad (5.30)$$

where $\hat{B}_e$ = peak flux density in one direction.
E = emf pulse amplitude.
≈ applied voltage U.

For a sine wave of rms amplitude U

$$\hat{B}_e = \sqrt{2}U/\omega A_eN \quad T \qquad (5.31)$$

There are two independent factors that may limit the maximum operating flux density; the permissible rise in magnetizing current, and the power dissipation.

During the magnetization cycle, as the flux density rises, the magnetizing current will rise in accordance with the shape of the magnetization curve, see Fig. 5.15a). As the flux density approaches saturation the current will begin to rise sharply; this is illustrated for both square and sine waves in Fig. 5.15b) and c). Invariably the electrical circuit design will impose some limit on this rise in current and this will place some limit on the peak flux density. Typically the maximum recommended operating flux

density will be put at about 5% below the minimum technical saturation flux density limit (e.g. the minimum value at H = 800 $A.m^{-1}$) at the operating temperature. For a typical power ferrite operating at 100°C this maximum recommended flux density would be about 320 mT.

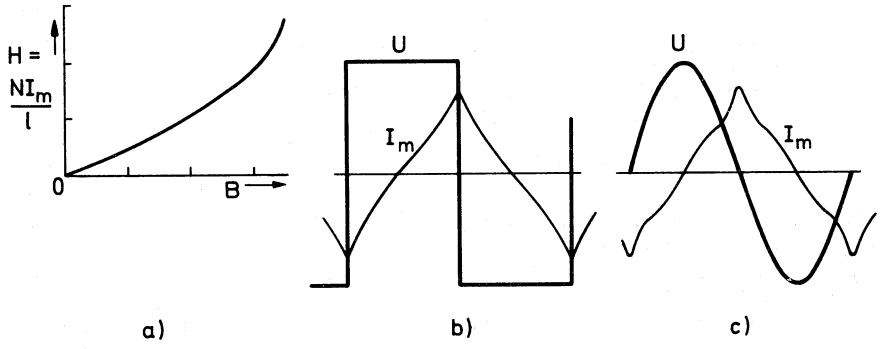

FIG. 5.15. a) Typical H(B) curve, b) the effect of the approaching saturation on the magnetizing current due to a square voltage pulse, c) the same for a sinusoidal voltage wave.

Under normal running conditions, the peak flux density in a ferrite core would generally be limited to a much lower value than 320 mT. This is because various over-voltage and transient conditions can result in momentary rises in flux density which greatly exceed the nominal operating value; this is particularly true of SMPS transformers. The design must ensure that under the worst transient conditions the maximum recommended flux density is not exceeded in any part of the core or the resulting current peak may damage the semiconductors in the circuit.

At operating frequencies above about 10 kHz the transformer design is often constrained by the permitted temperature rise rather than saturation; this limits the permissible total loss of the transformer. For example, referring to Fig. 5.14, if the ambient temperature is specified as 60°C and the core temperature is to be limited to 100°C so that the permitted temperature rise is 40°C, then for the EC41 core the total transformer loss must be limited to about 2.6W.

It will be shown later in this Section that the optimum division of the total power loss between core and winding depends on the relation between the core loss and the flux density. It will be assumed for the purpose of the present discussion that the core and winding losses are equal, so that in the above example the maximum core loss is 1.3W. If the relation between the core loss and the flux density is known, the maximum flux density can be readily obtained.

Core loss data for a ferrite material is generally given in terms of the core loss (volume) density, P_m, expressed as a function of $\hat{B}_e$ and f. Given the permitted core loss, P_c, and the effective volume of the core, V_e, the value of $P_m = P_c/V_e$ and from this the flux density may be obtained. The required number of turns may now be calculated from Eqns. 5.30 or 5.31.

When considering standard cores, graphs such as Fig. 5.22 on p.139 give the data directly. Pursuing the above example with reference to this Figure and assuming an operating frequency of 25 kHz, it can be seen that for a core loss of 1.3W in the EC41 core, the corresponding peak-to-peak flux is about 40 μWebers or

$$\hat{\phi} = \hat{B}A = \sqrt{2}U/\omega N = 20 \times 10^{-6} \quad \text{Wb} \qquad (5.32)$$

The required number of turns may now be calculated. In this Equation, B and A are not sub-scripted; this is to indicate that, in a non-uniform core, they should both relate to the same cross-section. Referring to Table 5.3 (p.146), it is seen that, for the EC41 core, the minimum cross-section of the centre pole is 100.3 mm^2, so the flux density in the centre pole must be limited to $20 \times 10^{-6}/100.3 \times 10^{-6}$ = 199 mT.

Concluding this introductory discussion on the flux density limitation it is seen that there are two possible constraints, the permissible steady state temperature rise and the transient voltage limitation. Both must be checked and the lesser flux density must be used to calculate the required number of turns. Clearly the transformer will make the most efficient use of material if it can be arranged that the two separate flux density limitations coincide.

5.3.2.3. Winding and Core Loss Balance

Earlier in this discussion, mention was made of the division of loss between core and winding. In traditional power transformer design it was usually assumed that an equality of losses was optimum but in practice economic or other considerations often disturbed this balance. In the type of transformer being considered here there is usually no reason why an optimum division should not be the aim.

The winding loss, P_w, is given by

$$P_w = I_1^2 R_s = U^2 R_s/(R_b')^2 \quad \text{W}$$

where R_s = total winding resistance, R_b' = load resistance } both referred to the primary
U = applied voltage
I_1 = primary current

The core loss, P_c, is given by

$$P_c = P_m V_e \propto \hat{B}_e^n = k_1(U/N_1)^n \quad \text{(from Eqn. 5.31 for example)}$$

where N_1 = number of primary turns
n = Steinmetz exponent

Therefore, the total transformer loss equals

$$P_w + P_c = (U/R_b')^2 R_s + k_1 (U/N_1)^n \quad W \tag{5.33}$$

From Eqn. 4.3, the primary resistance is proportional to N_1^2 and since, in a well-designed transformer, the primary resistance approximately equals the secondary resistance referred to the primary, $R_s \propto N_1^2$

$$\therefore \quad P_w + P_c = k_2 (UN_1/R_b')^2 + k_1 (U/N_1)^n \quad W$$

where k_2 = another constant of proportionality.

Differentiating w.r.t. N and equating to zero, the condition for minimum total power loss is found to be

$$k_1 \left(\frac{U}{N_1}\right)^n = \frac{2k_2}{n} \left(\frac{UN_1}{R_b'}\right)^2$$

$$\text{i.e.} \qquad P_c = \frac{2}{n} P_w \tag{5.34}$$

It will be seen in the next Section that for ferrites n lies between 2 and 3; only when n = 2 does the equal division of total loss between core and winding result in minimum total loss according to this analysis. However, the assumption that the total winding resistance referred to the primary side is proportional to N^2 may be invalidated if, as is sometimes the case in ferrite power transformers, the a.c. resistances of the two windings are greater than the d.c. resistances by significantly different factors.

5.3.3. MAGNETIZATION AND CORE LOSS IN POWER FERRITES

5.3.3.1. Forms of Magnetization

Although ferrite-cored power transformers have for many years been used to handle a variety of waveforms, notably the line scan waveform in a television receiver, it was usual until recently to express the magnetization and power loss performance in terms of a symmetrical sinusoidal flux density variation. This was convenient for specification and for measurement, and in practice gave results that were sufficiently relevant to a wide range of applications, at least for the purposes of material comparison. Of course, for the design of transformers intended to carry such a waveform this data enabled an accurate estimation of core performance to be made. The magnetization would trace a normal B(H) loop such as PP in Fig. 5.16. Clearly the non-linearity of the loop will prevent the B and H functions from both being sinusoidal and it is usual for the purpose of material characterization to specify that the B function is sinusoidal as this can often lead to a somewhat simpler measuring arrangement.

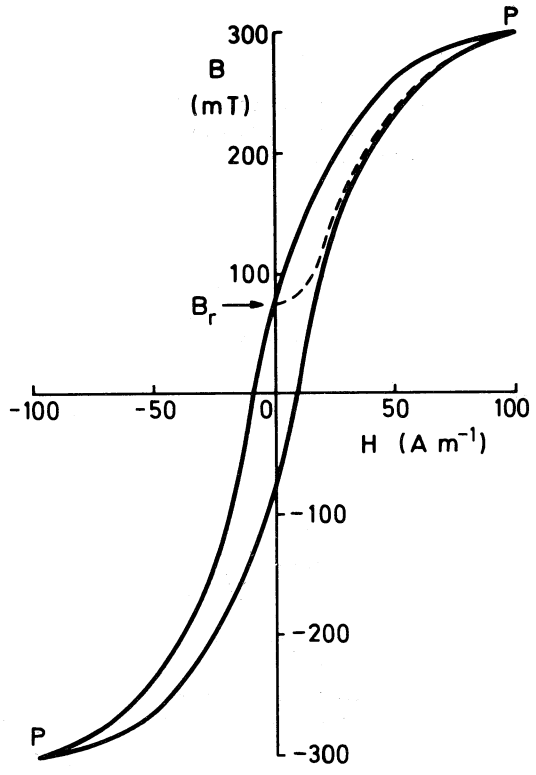

FIG. 5.16. Typical B(H) loop measured at a temperature of 100°C, showing a minor loop from remanence. (Material as for Fig. 5.18)

The next form of excitation to be considered is the symmetrical square wave of applied voltage. This form assumed importance with the development of Switched Mode Power Supplies; most of the early SMPS circuits had switched push-pull voltage inputs alternately exciting balanced halves of the primary winding so that the applied voltage in effect had the waveform shown by the thicker line in Fig.5.17a) on p.132. In this Figure the effects of hysteresis and saturation are omitted for simplicity, so the thinner line represents the variation of the magnetizing current and the flux density. As far as the core material is concerned the difference between the sinusoidal and the square wave excitation is that the magnetization follows a sine wave in the former and a triangular wave in the latter. This makes very little difference to the magnetization performance; referring back to Fig. 5.16, both trace a loop such as PP and result in the same hysteresis loss. It has been shown in Section 3.5.2. that the eddy current core loss for the sine wave is about 23% greater than for the triangular wave.

As the variety of SMPS circuits developed, new types such as the forward converter emerged and in such circuits the excitation is in the form of substantially unidirectional drive pulses. In practice, in most types of SMPS circuit, either push-pull or unidirectional, the actual waveform is complicated by the automatic control circuits which adjust the pulse duration to maintain the required regulation of the output. However, for the present purposes it is sufficient to consider the core performance with the relatively simple waveforms; the performance in a practical circuit can be readily derived from such data[14].

Returning to the consideration of unidirectional pulse excitation, an idealized voltage waveform is shown in Fig. 5.17b). If the circuit were to have zero resistance, the current would rise linearly during the first pulse ($dI/dt \propto E$) and, when the voltage drops to zero, the current would remain at the value attained at the end of the pulse. During the next drive pulse the current would again rise.

In practice, of course, the circuit has finite resistance and at the end of each drive pulse the current falls exponentially to zero, inducing a reverse emf as shown by the broken curve in Fig. 5.17c). This form of excitation is inefficient in a power supply circuit because all the stored magnetic energy is lost after the end of each cycle; it is dissipated in the circuit resistance. A more efficient circuit would recover most of the stored energy, leaving the drive circuit to supply only the energy loss in the core, (for the present argument the resistive loss in the winding can be ignored). Such a circuit would also be an advantage in the measurement of pulse magnetization of a ferrite sample because much less power would be required.

A suitable energy-recovery circuit is one in which the core has a secondary winding which, via a diode, returns the magnetic energy to the supply, as shown in Fig. 5.17d). As soon as the drive pulse ends, the diode conducts and connects the secondary winding to the supply rail which, being at constant voltage, constrains the magnetization to decrease in a linear manner. If the drive winding and the recovery winding have equal numbers of turns, the excitation is as shown in Fig. 5.17e). In the measurement of pulse properties of a ferrite sample, this arrangement has a further advantage over the circuit having exponential recovery in that the rate of change of magnetization has constant magnitude and therefore eddy current loss may be more easily calculated and deducted from the total loss to obtain the hysteresis contribution.

If the ferrite core is subjected to a series of unidirectional pulses the flux density will, in the steady state, trace a minor loop from remanence B_r to some point such as P in Fig. 5.16, the broken curve showing the increasing path of the minor loop. Clearly the available flux density excursion is much less under these conditions and the core material is under-utilized. However, at the higher frequencies of operation, the smaller available flux density excursion is often acceptable and this mode of operation is becoming increasingly popular. It is therefore of importance to extend the data on core magnetization properties to include unidirectional pulse magnetization so that the available flux density excursions and the corresponding hysteresis losses may be established.

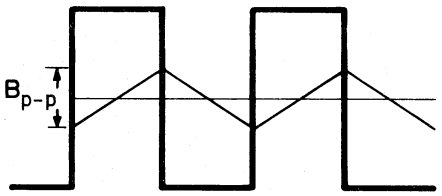

a) symmetrical square wave

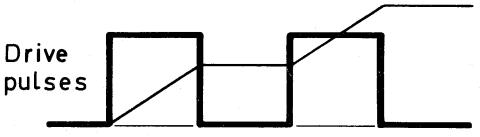

b) unidirectional square wave with zero circuit resistance

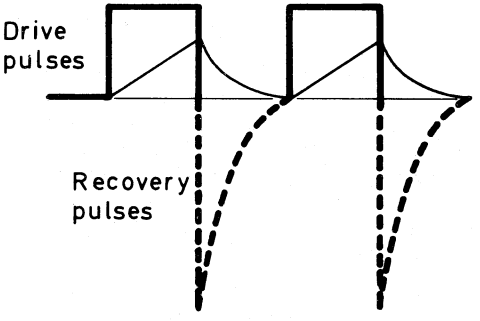

c) as for b) but with finite circuit resistance

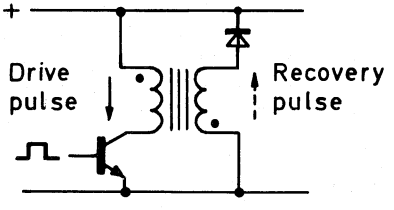

d) a test circuit used to obtain ...

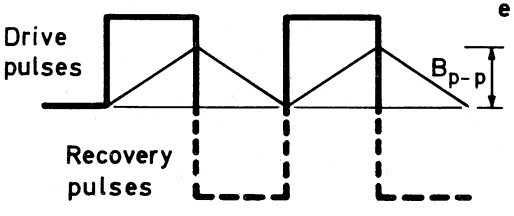

e) ... a unidirectional drive and equal (constant) rates of rise and fall of flux density

FIG. 5.17. Voltage and flux density (or magnetizing current) relations assuming a linear B(H) curve.

5.3.3.2. Magnetization Curves

The curves considered in this Section are normal magnetization curves, i.e. the loci of the tips of a series of hysteresis loops of varying amplitude.

Fig. 5.18 shows such curves for a typical MnZn ferrite intended for power applications*. The upper curves are for symmetrical magnetization while the lower curves relate to unidirectional pulse excitation from remanence as described in the previous Section. It should be noted that the flux density is given in terms of the peak-to-peak excursion. This has been done to avoid ambiguity when dealing with both types of magnetization. In order to reduce the curves for symmetrical mgnetization to the usual scale, the B_{p-p} value must be divided by 2. The field strength is given in terms of the usual zero-to-peak values of H.

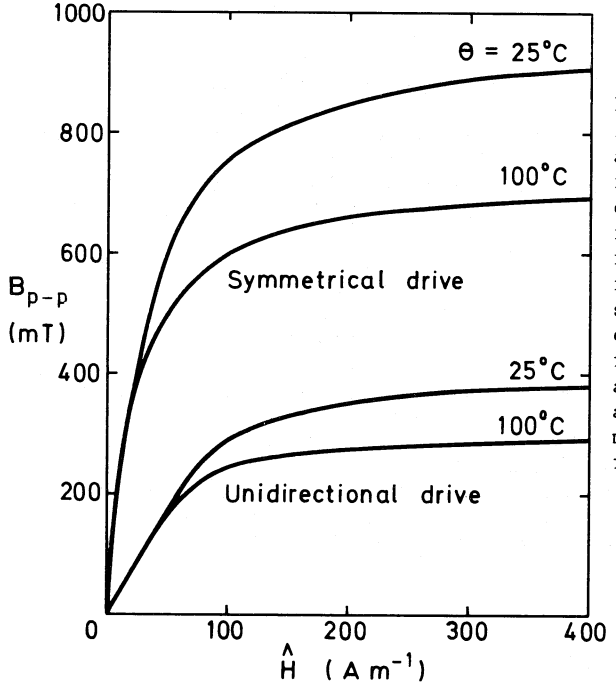

FIG. 5.18. Magnetization curves for a typical MnZn power ferrite*, in terms of the peak-to-peak flux density excursion plotted as a function of peak field strength. The upper curves are for symmetrical magnetization and the lower curves are for unidirectional magnetization from remanence.

* The material data presented in this and later Sections of this Chapter are representative of commercially available MnZn ferrite intended for power applications; they are typical, not limit, data. Specifically, they were obtained by measurements on Philips Ferroxcube Grade 3C8.

Due to the use of B_{p-p} the induction formulae quoted earlier are modified as follows:

For symmetrical sine waves

$$\left.\begin{aligned} B_{p-p} &= \sqrt{2}U/\pi fAN \\ \text{or} \qquad N &= \sqrt{2}U/\pi fAB_{p-p} \end{aligned}\right\} \quad T \tag{5.35}$$

For symmetrical or unidirectional square waves

$$\left.\begin{aligned} B_{p-p} &= Ut_d/AN \\ \text{or} \qquad N &= Ut_d/AB_{p-p} \end{aligned}\right\} \quad T \tag{5.36}$$

It is seen that the available flux density excursion for unidirectional pulses is about 40% of that for symmetrical magnetization. This unidirectional excursion may be increased if the remanence can be decreased and, in principle, this could be done by decreasing the width of the B(H) loop, i.e. by decreasing the hysteresis loss. In practice, the hysteresis loss in power ferrites has been made as low as economically possible by established technology although further improvements are predicted as the technology improves. Another method which has the effect of decreasing the remanence is to introduce an air gap and thus shear the B(H) loop. Although this increases the available flux excursion it would increase the magnetizing current and the inductance would be decreased in accordance with Eqn. 4.6.

When considering specific cores rather than ferrite materials, the magnetization curves are presented more conveniently in terms of flux and ampere-turns. As previously noted, the use of flux as a parameter removes the ambiguity concerning the cross-sectional area of a non-uniform core. Also, it is perhaps more expressive to plot NI vertically as this shows the increase in the magnetizing current as a function of the amplitude of the flux excursion. Fig. 5.19 shows two sets of curves for a standard range of ferrite power transformer cores, namely the EC core range which is described in more detail in Section 5.3.5. One set is for symmetrical magnetization and the other is for unidirectional magnetization. Again it should be noted that the flux is expressed in the peak-to-peak value. This leads to the following versions of Eqns. 5.35 and 5.36:

For symmetrical sine waves

$$\phi_{p-p} = \sqrt{2}U/\pi fN \qquad \text{Wb} \tag{5.37}$$

For symmetrical or unidirectional square waves

$$\phi_{p-p} = Ut_d/N \qquad \text{Wb} \tag{5.38}$$

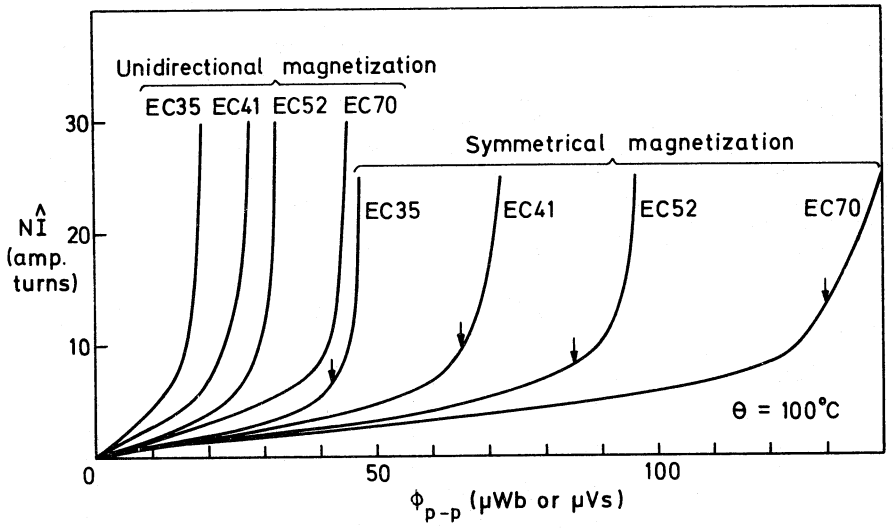

FIG. 5.19. Magnetization curves, relating to both symmetrical and unidirectional magnetization for the EC range of transformer cores. The arrows indicate the recommended maximum operating flux, equivalent to a maximum $\hat{B}$ of 320 mT in the (minimum) centre limb. (Material as for Fig. 5.18 on p.133).

5.3.3.3. Core losses

In normal operation, a typical ferrite power transformer core will have a power loss of several watts; most of this will be hysteresis loss but there will be some residual loss and eddy current core loss in addition. The hysteresis and residual loss, expressed as a power loss (volume) density, i.e. power per unit volume, are each independent of the size and shape of the core and in the present context may be lumped together under the name of hysteresis loss. However, the power loss (volume) density due to eddy currents in the bulk of the core depends on the dimensions of the core cross-section. So when preparing power loss density data relating to ferrite materials, i.e. where the values must be independent of core shape, it is necessary to exclude the eddy current loss from the results. When estimating the total loss of a specific core, the eddy current loss must be calculated separately and added to the hysteresis loss as indicated later in this Section. Alternatively, the total loss for a specific core may be measured directly and quoted as a core parameter.

Considering first the hysteresis loss in the material, Fig. 5.20 shows hysteresis loss (volume) density, P_h, as a function of peak-to-peak flux density with typical operating freqencies as a parameter. The grade of ferrite is the same as that quoted in the previous Section (see footnote on p.133). The crossed points are for symmetrical sine or square waves and the circled points are for unidirectional pulse drive. The pulse durations of 20, 10 and 5 μs correspond to frequencies of 25, 50 and 100 kHz respectively. These results, based on unpublished work by Annis[15], show a surprising conformity between the losses for the two forms of excitation when they are expressed in terms of a common peak-to-peak flux density parameter. The slopes of the lines yield a Steinmetz exponent which is a little over 2.5; it may be taken as 2.5 without significant error.

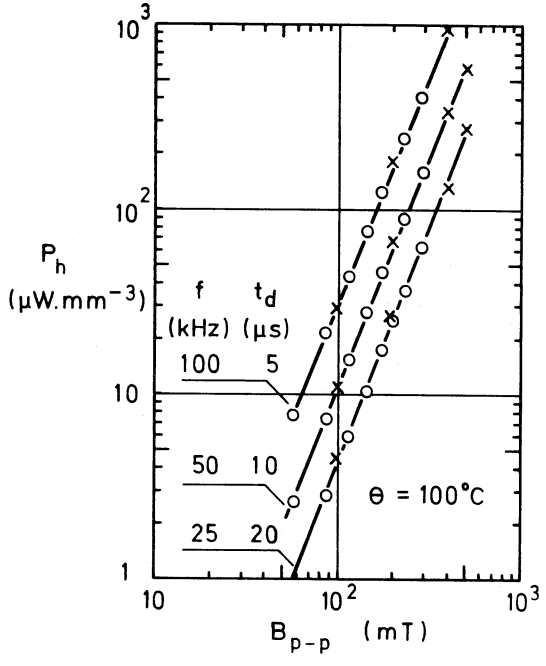

FIG. 5.20. Hysteresis loss density as a function of the peak-to-peak flux density with frequency and pulse duration as parameters.

Data points:
X were measured with a symmetrical sine wave flux density.
O were measured with a 1:1 unidirectional square wave (as in Fig.5.17e)).

(Material as for Fig.5.18 on p.133).

If the hysteresis loss density is plotted as a function of frequency, it is found that this loss is proportional to f^m where m varies from about 1.1 at 10 kHz to 1.5 at 100 kHz. A value of m = 1.3 gives an acceptably accurate representation over the range 10 to 100 kHz.

Thus the whole set of hysteresis loss results for this typical power ferrite, combining both symmetrical drive and unidirectional pulse drive from remanence, may be expressed by the simple empirical formula:

$$P_h = k_h f^{1.3} B_{p-p}^{2.5} \quad \mu W.mm^{-3} \qquad (5.39)$$

where $k_h = 0.748 \times 10^{-6}$
B_{p-p} is in mT
f is in kHz for frequencies between 10 and 100 kHz, and, for a 1:1 continuous square wave, equals $1/2t_d$

Annis, having found this conformity in the loss characteristics for both symmetrical drive and unidirectional pulse drive from remanence, investigated, for this particular power ferrite, the intermediate cases. He applied a constant symmetrical sine wave drive (constant B_{p-p}) and a variable d.c. bias simultaneously and he measured the power loss as the bias was varied from zero (symmetrical magnetization) until the L.H. excursion of the sine wave field strength coincided with zero H (magnetization unidirectional from remanence). It was found that the hysteresis loss remained constant within ± 5% over the entire bias range. So it can be concluded that the loss curves presented in Fig. 5.20, for this ferrite and cores made from it, may be used for the whole range of magnetization from symmetrical to unidirectional-from-remanence, sine wave or pulse. These measurements have not been repeated on other MnZn power ferrites but as such ferrites have similar compositions it is probable that this result is generally applicable. There is some experimental evidence that Eqn. 5.39 represents the typical performance of a variety of commercially available MnZn power ferrites.

It was seen in Chapter 3 that the residual loss in a ferrite has a minimum at the cross-over temperature of the anisotropy. A similar minimum is found for the high-amplitude loss. Fig. 5.21 shows a typical result for the MnZn power ferrite. The composition of such ferrites is arranged to place this minimum towards the upper region of the operating temperature range so that the advantage of the lower loss is obtained near the normal operating temperature.

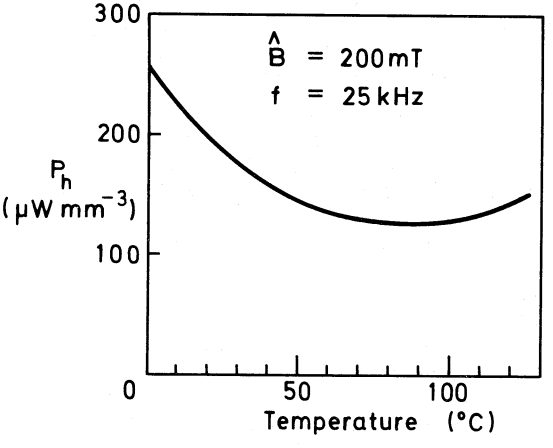

FIG. 5.21. Hysteresis loss density as a function of temperature. (Material as for Fig. 5.18 on p.133).

Data measured by C. Barrow, Mullard Ltd.

If the loss data of Fig. 5.20 were to be used to predict the hysteresis loss of a practical core of uniform cross-section, then P_h could be multiplied by V_e for the particular core to obtain the core loss in watts. If the cross-section of the core is very non-uniform then the core would need to be considered in separate volumes, V, each of approximately uniform cross-sectional area, A. For each volume, the flux density would be calculated from ϕ and A and separate values of P_h determined from Fig. 5.20. The total hysteresis loss would then be $\Sigma P_h V$.

To obtain the total core loss, the eddy current core loss must be added. Again, for a non-uniform core each part needs to be considered separately. The eddy current core loss (volume) density for a cylinder of diameter D is given by

$$P_F = (\pi \hat{B} f D)^2/16\rho \qquad W.m^{-3} \qquad (5.40)$$

where ρ is the bulk resistivity of the ferrite, (see also Section 3.5.2).

For a square core, D may be put equal to the diameter of the circle having the same area, A. Putting $A = \pi D^2/4$ the above equation becomes

$$P_F = \pi \hat{B}^2 f^2 A/4\rho$$

This equation may be used to give the approximate eddy current core loss density in a non-uniform core if the effective values of B and A (i.e. $\hat{B}_e$ and A_e) are used. Then

$$P_F \approx \pi \hat{B}_e^2 f^2 A_e/4\rho \qquad (5.41)$$

For consistency with the hysteresis data, $\hat{B}_e$ may be replaced by $\frac{1}{2}B_{p-p}$. Since this loss is generally only a small proportion of the total loss the error in using A_e is not very significant. A greater uncertainty is in the estimation of ρ at the operating temperature as this is not usually controlled in production; for the typical ferrite considered in this Section it would lie between about 0.30 and 1.0 Ωm at 100°C.

In practice the total core loss, in watts, is relatively easy to measure directly on a given core and its maximum value is usually specified by the manufacturer for a symmetrical sinusoidal drive of given amplitude, $\hat{B}_e$, and frequency, and at a given temperature. In addition, the total loss is often expressed graphically as a function of $\hat{B}_e$ and f. By analogy with the results quoted earlier for the hysteresis loss density of the ferrite material, the hysteresis component of the total loss of a core made of such a material, expressed as a function of ϕ_{p-p}, will apply to both symmetrical and unidirectional excitation, either sinusoidal or pulse. As the eddy current component of the loss is usually small there is no great error in expressing the total loss in the same manner.

Fig. 5.22 shows a typical set of total loss curves for the standard range of EC cores mentioned earlier and described in more detail in Section 5.3.5. The curves occur as linked pairs, one pair for each core size; the solid line of each pair is for f = 25 kHz and the broken curve is for f = 50 kHz. Eqns. 5.37 and 5.38 apply. Using this data the total power loss corresponding to a given total flux excursion, or vice versa, can readily be obtained for these standard cores.

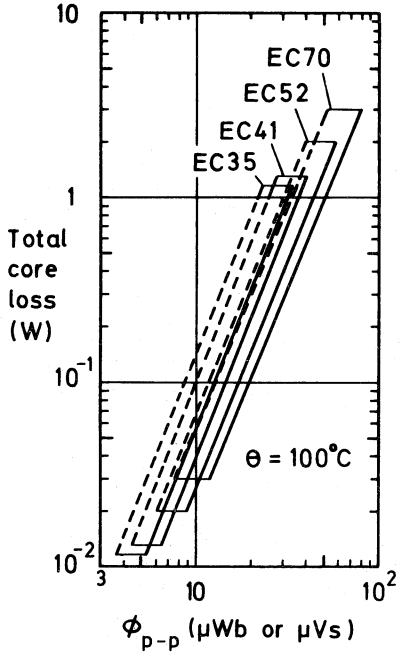

FIG. 5.22. Total core loss as a function of peak-to-peak flux for the EC range of cores. The curves apply for both sine waves or 1:1 square waves, either being symmetrical or unidirectional. The solid curves are for f = 25 kHz or t_d = 20 μs and the broken curves are for f = 50 kHz or t_d = 10 μs (the pairs of curves are joined to aid clarity).

(Material as for Fig. 5.18 on p.133)

5.3.4. WINDING LOSSES

For low frequency transformers, the resistance of the windings may be readily calculated from the required number of turns, the winding area and the mean turn length, see Eqn. 4.3. Generally the mean turn length for the transformer core as a whole is used for each winding, the resulting errors approximately cancelling. The windings generally fill the available winding space.

At higher frequencies, eddy current effects in the copper become significant and as a result the a.c. resistance of the windings may become much larger than the d.c. values.

In the present context only a brief outline of this subject is possible; reference should be made to the literature[16,17,18] for more detailed treatment.

The transverse field in the winding space of a transformer may be assumed to be parallel to the interface between the windings and its value at any point may be calculated without great difficulty. The combination of this transverse field and the field due to the current in an individual conductor causes the current density to increase towards the surface of the conductor that faces the nearest interface. This is the proximity effect. Provided the frequency is not so high that the electromagnetic penetration depth Δ greatly exceeds the copper thickness, the power loss, P_{pe}, due to proximity effect in a cylindrical conductor is easily evaluated[19]:

$$P_{pe} = \pi\omega^2 \bar{\hat{B}}^2 \ell d^4/128\ \rho_c \qquad (5.42)$$

where $\bar{\hat{B}}$ = peak flux density averaged over the length, ℓ, of the conductor diameter, d.

For a winding of N turns, having a mean turn length ℓ_w, the conductor length $\ell = N\ell_w$. The power loss, P_{pe}, may be expressed as an increase in the winding resistance by a factor F_R relative to R_{dc}, i.e.

$$R_{ac} = F_R R_{dc} \qquad (5.43)$$

The factor F_R depends on the winding geometry and a parameter involving the electromagnetic penetration depth Δ, and the determination of this factor is the primary objective of the winding design procedure.

Fig. 5.23 shows how the m.m.f. (= NI) varies between the innermost and outermost layers. For the purpose of the calculation it is necessary to consider so-called portions of windings; these portions are defined as those layers lying between a maximum m.m.f. and zero. The number of layers in a portion is designated p. In transformers having individual windings, as shown in Fig. 5.23a), p equals the number of layers in one complete winding and is therefore an integer. However, if one (or more) winding is divided in an interleaved structure as shown in Fig. 5.23b) then p may not be an integer; it could be an integer plus ½, (in S/2 it must be an integer but in the portion that is half of P it would contain an odd ½ if the total number of layers in P were odd).

In principle F_R is determined for eacn portion but where two portions are identical in the relevant parameters, e.g. as the two halves of S or P in Fig. 5.23b), then F_R need only be found for one portion and can be applied to both portions.

For each portion the following parameters are needed:

Number of turns per layer	N_ℓ
Effective conductor height	h
Layer copper factor	F_ℓ
Penetration depth	Δ

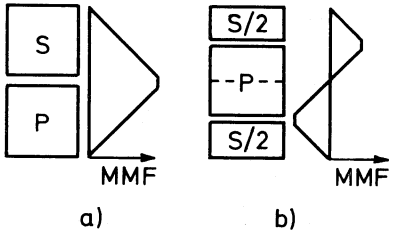

FIG. 5.23. MMF diagrams for two simple transformer winding arrangements.

Fig. 5.24 shows a generalized geometry of a layer of conductors; if the conductors are round then h = b = 0.886d, where d is the copper diameter. The layer copper factor is defined by

$$F_{\ell} = N_{\ell} b / b_w \qquad (5.44)$$

This approaches unity for closely packed conductors. The penetration depth Δ is given by

$$\Delta = k f^{-\frac{1}{2}} \quad \text{mm} \qquad (5.45)$$

where f is in Hz and, for copper conductors at 20° or 100°C, k = 65.5 or 75 respectively.

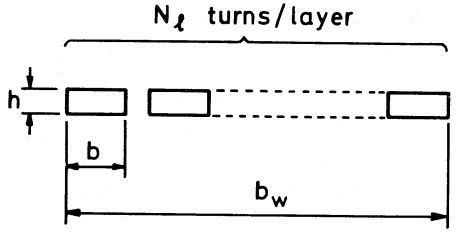

FIG. 5.24. Cross-section of a generalized winding layer.

It is now necessary to calculate the parameter $h\sqrt{F_{\ell}}/\Delta$ and read the value of F_R from the curve corresponding to the appropriate number of layers, p, per winding portion shown in Fig. 5.25.

If the value of $h\sqrt{F_{\ell}}/\Delta$ exceeds about 2.5 then the operating point will be above the knee of the curves and the smallest a.c. resistance will be obtained by using the largest conductor thickness that can be accommodated. However, for lower values of the parameter it can be shown that provided p > 1, the optimum round conductor section is the one that yields $F_R \approx 1.5$. This result is the same as that derived on a different basis, in Section 4.5.2, (Eqn. 4.19) and Section 5.3.6.2, p.151, (Eqn. 5.58).

Reference 17 gives a simple method of obtaining the values of d and p for $F_R = 1.5$. However, a few trial calculations will rapidly converge to a near-optimum winding design.

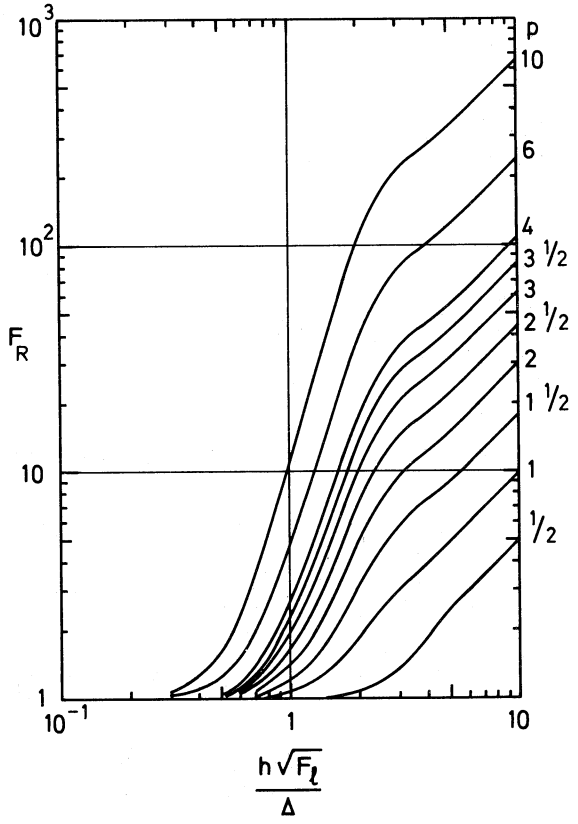

FIG. 5.25. F_R as a function of $h\sqrt{f}\,\ell/\Delta$ with number of layers, p, per winding portion as a parameter

It should be noted that in general the use of the optimum F_R may result in only a partial occupation of the available winding area and so R_{dc} (and therefore R_{ac}) are no longer proportional to N^2. This results in a primary resistance that, in general, is not equal to the value of the secondary resistance referred to the primary. This somewhat invalidates the application of Eqn. 5.34 to a transformer in which eddy current copper loss is significant. Further, it is no longer a valid simplification to use the mean value of ℓ_w for all winding portions; a specific value of ℓ_w should in principle be calculated for each portion.

In many SMPS designs, the secondary windings consist of a few turns intended to carry heavy currents, perhaps hundreds of amperes, at frequencies between 20 and 100 kHz. In such windings the eddy currents may cause a very large increase in resistance and result in high winding losses. Windings consisting of copper or aluminium strips[18] can be beneficial. If strip windings do not yield a sufficiently low a.c. resistance then the windings can be made of (rather expensive) heavy braid consisting of insulated copper strands.

5.3.5. PRACTICAL CORE SHAPES

In the design or choice of a ferrite core shape for high frequency, high power, applications the following attributes are desirable

a) adequate flux-carrying capability,
b) low external magnetic fields,
c) minimization of the winding resistance,
d) minimization of the leakage inductance,
e) maximum natural heat transfer to the surrounding air,
f) adequate space for the necessary isolation of the windings from each other and from the core,
g) winding, assembly and termination to be simple,
h) lowest overall cost or volume consistent with the power handling rating.

Before considering the optimization of the shape with respect to some or all of these attributes it is appropriate to consider some core shapes that are traditional or that have their origins in other applications.

The most obvious traditional shape is the pair of rectangular section E cores and of the many available ranges the DIN[20] range is very popular for power transformers. The dimensions, and other relevant parameters, for a selection of cores from this range are set out in Table 5.2.

Core type	Approx half-core dimensions* mm	ℓ_e mm	A_e mm^2	V_e mm^3	C_1 mm^{-1}	Minimum cross-sectional area mm^2
E20/5	20 x 10 x 5	45	33	1490	1.37	23.5
E30/7	30 x 15 x 7	67	60	4000	1.12	45.6
E42/15	42 x 21 x 15	98	183	17930	0.535	172
E42/20	42 x 21 x 20	98	236	23100	0.42	227
E55/21	55 x 28 x 21	123	352	43300	0.35	341
E65/27	65 x 33 x 27	148	538	79600	0.275	517
U15/6	15 x 11 x 6	48	30	1440	1.6	30
U20/7	20 x 16 x 7	68	56	3800	1.2	52.2
U25/13	25 x 20 x 13	86	100	8600	0.86	100
U30/16	30 x 25 x 16	111	157	17400	0.71	157

* back length x outside leg length x thickness

TABLE 5.2. Dimensions of ferrite E cores[20] and U cores suitable for power transformers

The E cores are characterized by a relatively large ratio of core cross-section to winding cross-section. While this may provide adequate flux-carrying capacity it can lead to a lack of space for insulation and inadequate allowances for creepage. The rectangular centre limb causes the windings to bow outwards and occupy more space, and also to have a higher resistance than an equivalent winding on a cylindrical limb of the same cross-sectional area. On the credit side, the shape is simple to press and this maximizes the ferrite performance and minimizes the cost. Also the uniform cross-section may simplify the transformer design.

Another traditional shape is the rectangular section U core; the dimensional parameters of a selection of these cores are also listed in Table 5.2. Their characteristics are similar to those of the E cores described in the previous paragraph, but it is generally assumed that the external magnetic field will be greater. For the smaller power units, the larger RM cores, e.g. RM10 and RM14 (see Table 5.1), are often used to good effect.

Much attention has been given, in recent years, to modified core shapes that would, to some extent, specifically enhance the desirable characteristics set out at the beginning of this Section. On the grounds of low external magnetic field, the basic E core shape is preferred. In order to minimize the winding resistance (and, therefore, the winding loss in proportion) and also the leakage inductance, a cylindrical centre limb is an obvious choice and is widely adopted. However, it should be noted that whereas the rectangular section E core is pressed perpendicularly to the plane of the E, the round centre limb core almost inevitably needs to be formed by pressing in an axial direction. This can lead to difficulties with non-uniform press-density and degradation of magnetic performance.

The cross-sectional area of the centre limb is somewhat arbitrary; the larger it is the fewer turns will be required for a given voltage. However, many modern SMPS units are required to deliver a low voltage, high current output. A typical voltage at the terminals of the transformer secondary is 7.5V to give 5V d.c. at the load. One approach is to assume this voltage and by trial or experience decide on a small integral number of turns appropriate to the core size and rating. From the maximum permissible flux density, the cross-sectional area and diameter of the centre limb may be calculated[21]. This approach is intended to avoid a transformer design calculation yielding a small non-integer number of turns which, when rounded-up to the next higher integer would result in significant under-utilization of the core (also the primary number of turns would need to be increased in proportion).

The range of EC cores, already frequently quoted in this Chapter, was based on this concept. Fig. 5.26 shows the general shape of the EC core; in the same photograph there are examples of rectangular section E and U cores representing cores from Table 5.2.

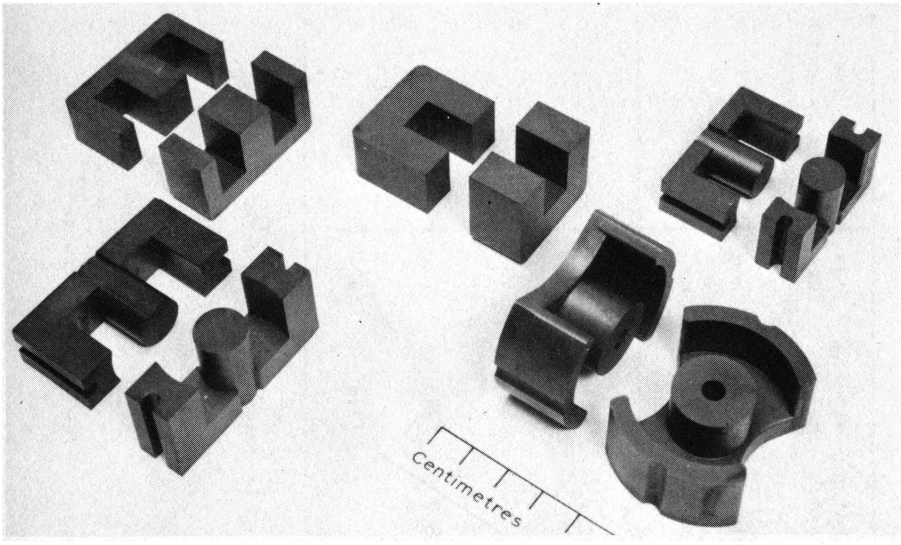

FIG. 5.26. Typical ferrite cores for power transformers

E core. U core. Small EC core.
Larger EC core. PM core.

The "stack height" dimension of the back and outside legs of the EC cores was made equal to the centre leg diameter for ease of tooling and pressing. The remaining dimensions were chosen to satisfy the following practical considerations. The window breadth must allow for the coil former and for adequate creepage distance along the inter-winding insulation. Since the leakage inductance and the a.c. winding resistance depend inversely on the winding breadth this is another reason for making the winding area broad and shallow. In practice a minimum aspect ratio of 3 was used. Finally, the surface area of the transformer must be large enough to dissipate the power loss. This relates to the nominal power rating of the transformer assembly and the assumed surface temperature rise, e.g. 40°C. For these reasons it was considered desirable to make the total cross-sectional area of the back and legs of the EC cores greater than the area of the centre core. In addition to increasing the cooling area this assists the heat transfer, by conduction, from the centre limb and also makes the limbs more robust.

The EC core range is now accepted as an IEC standard[22] and is subject to assessed-quality release. Table 5.3 lists the dimensional parameters of this range of cores and the associated coil formers.

Other geometries have also been proposed. They are essentially variations on the basic round centre-limb E-core design, the proportions being adjusted to give optimum performance under specific conditions, e.g. a particular frequency range or use in forward converters. The interest in optimizing the geometry of ferrite power transformer cores reflects their current importance in power unit design.

Core type	Approx. half-core dimensions* mm	Effective parameters ℓ_e mm	A_e mm^2	V_e mm^3	C_1 mm^{-1}	Centre Pole area, A_{cp} min mm^2	Winding breadth b_w min mm	Winding height h_w min mm	Mean turn length ℓ_w nom mm	Cooling area of fully wound core (approx) A_c mm^2
EC35	35x17x9.5	77.4	84.3	6530	0.918	66.5	21.4	4.6	50	4350
EC41	41x19.5x11.5	89.3	121	10800	0.735	100.3	24.4	5.55	60	5900
EC52	52x24x13.5	105	180	18800	0.581	133.8	28.2	7.5	73	9100
EC70	70x34.5x16.5	144	279	40100	0.514	201.1	41.3	11.4	95	17000

* back length x outside leg length x thickness

TABLE 5.3. Dimensions of ferrite power transformer cores in the EC range[22]

5.3.6. THE EFFECT OF INCREASING FREQUENCY

In the past, the frequency of operation of ferrite power transformers has been constrained at the lower limit by the need to exceed the highest audible frequency since, via magnetostriction, there is a small but significant acoustic radiation. The upper frequency limit was imposed by the performance of the semiconductors and capacitors used in the power supply circuits. These constraints resulted in a frequency of about 25 kHz being favoured.

Developments, particularly in the field of power semiconductors, are now rapidly increasing the possible frequency of operation so it becomes appropriate to consider the effect on transformer design of increasing the frequency. Any analysis of this problem cannot start from the overall design formulae usually quoted because they involve empirical assumptions, such as the relation between core and winding loss, that will not remain valid as the frequency is increased. Instead it is preferable to analyse the effect of frequency by considering the core loss and winding loss separately. This analytical approach may in fact reflect a trend in transformer design since, as the frequency increases, it becomes increasingly appropriate to treat the winding separately from the core to the extent of allowing a different operating temperature in each, and in practice attempting to decouple thermally the winding from the core.

5.3.6.1. Core loss

Considering first the core loss, it has been seen that for a typical MnZn ferrite intended for power applications the hysteresis loss density can be represented by a formula such as Eqn. 5.39. For the convenience of the present discussion the flux density will be expressed in terms of its peak value so that

$$P_h = K_h \hat{B}^n f^m \qquad \mu W.mm^{-3} \qquad (5.46)$$

At frequencies between 10 and about 100 kHz, n = 2.5 and m has an average value of 1.3 for the quoted material. Over this range of frequency, this average value of m yields, for the same material, $K_h = 4.232 \times 10^{-6}$ when $\hat{B}$ and f are in the same units as for Eqn. 5.39. At higher frequencies n does not significantly change but m rises to about 1.65 by 200 kHz (the average value of m and the value of K_h in Eqn. 5.46 depend on the frequency range chosen). In most of the following discussion the frequency range will be restricted to less than 100 kHz so that m may be considered constant at about 1.3; the implications for higher frequencies will be commented upon as appropriate.

The eddy current core loss, from Eqn. 5.40, can be expressed by

$$P_F = K_F f^2 \hat{B}^2 D^2 / \rho \qquad \mu W.mm^{-3} \qquad (5.47)$$

where K_F is a constant and D is the minimum dimension of the core cross-section.

For medium-sized cores operating at a frequency of about 50 kHz and a temperature of 100°C, P_F is only a few percent of P_h. The ratio is given by

$$P_F/P_h \propto \hat{B}^{2-n} f^{2-m} D^2$$

Putting $n = 2.5$ and $m = 1.3$

$$P_F/P_h \propto f^{0.7} D^2/\hat{B}^{\frac{1}{2}} \qquad (5.48)$$

Experimental results on the material being considered show that $f^{0.7}$ holds up to about 200 kHz. However, $\hat{B}$ will not remain constant as the frequency increases. If it is postulated that the core temperature rise shall remain constant, then P_c/A_{ck} = const, where A_{ck} is the core surface cooling area. Then if $P_F \ll P_h$ (and now using $\hat{B}_e$ and the effective volume Ve):

$$P_c/A_{ck} = P_h V_e/A_{ck} = K_h f^{1.3} \hat{B}_e^{2.5} V_e/A_{ck} \qquad (5.49)$$

$$= \text{const. for a given temperature rise}$$

$$\therefore \quad \hat{B}_e \propto f^{-0.52} (A_{ck}/V_e)^{0.4}$$

Substituting for $\hat{B}$ in Eqn. 5.48

$$P_F/P_h \propto f D^2 (V_e/A_{ck})^{0.2} \text{ approx.} \qquad (5.50)$$

$$\propto f L^{2.2} \text{ if the core shape is constant,}$$

where L is a linear dimension of the core.

Since $P_F/P_h \propto 1/\rho$ it follows that, for constant core size, the core resistivity must be increased in proportion to the frequency to keep the ratio of eddy current loss to hysteresis loss constant. In principle the core resistivity can be increased by compositional or process changes. Under these circumstances the eddy current core loss may be left out of the further analysis and the total loss of a core may be expressed as

$$P_h V_e = K_h f^m \hat{B}_e^n V_e \qquad \mu W$$

where V_e is in mm^3

Again, postulating that the core temperature rise shall remain constant, $P_h V_e/A_{ck}$ = const., so

$$K_h f^m \hat{B}_e^n V_e/A_{ck} = K_h f^m \hat{B}_e^n L = \text{const.} \qquad (5.51)$$

where L is a linear dimension

From Eqn. 5.31

$$\hat{B}_e \propto U/NA_e f \propto U/NL^2 f \qquad (5.52)$$

so $$K_h f^m (U/Nf)^n L^{1-2n} = \text{const.}$$

or $$N^n L^{2n-1} \propto K_h U^n f^{m-n}$$

$$\therefore \quad N L^{2-1/n} \propto K_h^{1/n} U f^{(m/n)-1} \qquad (5.53)$$

Again using the typical values, m = 1.3 and n = 2.5, found experimentally to apply over the frequency range 10 to 100 kHz:

$$N L^{1.6} \propto K_h^{0.4} U/f^{0.48}$$

$$\propto K_h^{0.4} U/\sqrt{f} \quad \text{approx.} \qquad (5.54)$$

By definition it is advantageous to reduce the hysteresis constant K_h but this has been an objective of material development for many years so for the present purposes it is practical to assume that K_h is constant. Then

$$N^2 L^{3.2} \approx N^2 V_e \propto U^2/f \quad \text{approx.} \qquad (5.55)$$

This expresses the proportionality between the number of turns, the core volume, the transmitted power $(P_o \propto U^2)$ and the frequency assuming that the core temperature rise stays constant. By substituting the related changes back into Eqn. 5.52 the corresponding change of flux density may be deduced. The results may be conveniently summarized as follows.

At constant temperature rise, doubling the frequency can result in the following related changes:

	Power	Core Volume	Turns	Flux Density
a)	const	const	$N/\sqrt{2}$	$B/\sqrt{2}$
b)	const	$V_e/2$	const	$B/2^{1/3}$
or c)	$2P_o$	const	const	$B/\sqrt{2}$

This analysis shows that for a ferrite core having typical hysteresis loss behaviour and a resistivity such that the eddy current loss may be considered negligible over the frequency range considered, an increase in frequency will give a transformer having a better performance with various possible trade-offs between core volume, number of turns and transmitted power. A lower value of hysteresis constant would, of course, give an added advantage.

The rise of m with frequency will eventually invalidate the numerical proportionalities indicated by this analysis but is unlikely to affect the qualitative results at frequencies up to 200 kHz. On a simple hysteresis model it would be expected that m would equal unity, i.e. hysteresis loss per cycle would be constant. The fact that the $P_h(f)$ relation curves upwards as f increases, the index m rising from 1.1 at about 10 kHz to 1.65 at 200 kHz, is probably due to the same mechanism that causes the residual loss of ferrites to rise with frequency, i.e. the onset of ferromagnetic resonance. By analogy with the behaviour of $(\tan\delta_r)/\mu$ (see Fig. 3.17), the onset of this resonance and probably

therefore the rise in m could be moved to a higher frequency by lowering the permeability. Unfortunately, the lowering of the permeability would increase the magnetizing current for a given flux excursion (which may not be important at the higher frequencies) but it would also increase the hysteresis constant since this is coupled to the permeability by a common magnetization process. So it would appear that the hysteresis loss would behave as $(\tan\delta_r)/\mu$; there would be a composition that would give a minimum loss at a given frequency. There is some experimental evidence that this is so.

At the higher frequencies being considered here, core saturation ceases to be a direct limitation to the transformer design and it is tempting to hope that a lowering of B_{sat} might allow a lower core loss to be achieved. However, it is well-known that the ferromagnetic resonance frequency is proportional to B_{sat}, see Section 3.5.3.2, so decreasing the latter will increase m and this will increase the loss at the higher frequencies. So although B_{sat} is not so critical as it is at the lower frequencies it cannot be traded for a decrease in loss.

5.3.6.2. Winding Loss

Turning now to the effect of design frequency on the winding parameters, some aspects of the design procedure were considered in Section 5.3.4. However, for analytical purposes it is preferable to start from first principles. Combining Eqns. 4.3 and 5.42, the total power loss in a winding is

$$P_w = P_{dc} + P_{pe} = \frac{\hat{I}^2}{2} \times \frac{4\rho_c N \ell_w}{\pi s d^2} + \frac{\pi\omega^2\bar{\hat{B}}^2 \ell_w s N d^4}{128\,\rho_c} \qquad (5.56)$$

where the number of parallel strands, s, has been introduced so that the result applies generally to bunched conductors where d is the strand diameter; for solid conductor s = 1.

Differentiating with respect to d yields the optimum diameter, d_{opt}, for minimum total winding loss

$$d_{opt}^6 = \frac{128\,\hat{I}^2\rho_c^2}{\pi^2\omega^2 s^2 \bar{\hat{B}}^2} \qquad (5.57)$$

This result can be compared to Eqn. 4.20 which is an equivalent expression[23] but formulated in terms of inductance and proximity effect factor instead of $\bar{\hat{B}}/I$.

If d_{opt} is substituted into the terms of Eqn. 5.56:

$$P_{dc} = 2\ell_w N \left\{ \frac{\omega^2\bar{\hat{B}}^2\rho_c\hat{I}^4}{128\,\pi\,s} \right\}^{1/3}$$

$$P_{pe} = \ell_w N \left\{ \frac{\omega^2\bar{\hat{B}}^2\rho_c\hat{I}^4}{128\,\pi\,s} \right\}^{1/3}$$

So when $d = d_{opt}$

$$P_{pe} = \tfrac{1}{2}P_{dc}$$

or $$R_{ac} = 1.5\, R_{dc} \quad \text{as before} \tag{5.58}$$

Assuming that the practical constraints allow the conductor to be optimised

$$P_w = 1.5\, P_{dc} = 6\ell_w N \left\{ \frac{\omega^2 \bar{\hat{B}}^2 \rho}{128\, \pi\, s\, \hat{I}^2} \right\}^{1/3} I^2 \tag{5.59}$$

$\bar{\hat{B}}$ = the average value of the peak flux density over the space occupied by the winding and it is related to the amp.turns in that winding as follows

$$\bar{\hat{B}} = \mu_o N \hat{I}/\ell$$

where ℓ is the effective length of the path of the magnetic field through the winding and back through the core. For an ungapped core this length is approximately equal to the winding breadth, b_w,

$$\therefore \quad \bar{\hat{B}}/\hat{I} \propto N/b_w \tag{5.60}$$

$$\therefore \quad P_w \propto \frac{I^2 \ell_w N^{5/3} f^{2/3}}{s^{1/3}\, b_w^{2/3}}$$

If A_{cw} is the surface cooling area of the winding, assumed isolated form the core, then

$$\frac{P_w}{A_{cw}} \propto \frac{I^2 \ell_w N^{5/3} f^{2/3}}{A_{cw}\, s^{1/3}\, b_w^{2/3}} = \text{const. for a given temperature rise} \tag{5.61}$$

In fact N and f are related by the induction equation (Eqn. 5.52) applied to the core and in addition, if a given core temperature rise is assumed, then Eqn. 5.51 applies. This yields $N \propto \sqrt{f}$ (approx) if the typical values of n and m are assumed. Putting this into Eqn. 5.61 results in P_w/A_{cw} being virtually independent of f. Since P_w/A_{cw} is, to a first approximation, proportional to the winding temperature rise this result indicates that for a constant power and core size (and shape) the temperature rise of an optimised winding is approximately independent of frequency. This conclusion is only valid for a winding consisting of several fully wound layers.

Too much should not be read into this result because it involves a number of unstated but fairly complicated geometric parameters. It is sufficient to note that as the operating frequency is increased the winding loss need not rise significantly provided the winding can be optimised at the operating frequency.

The remarks made at the end of Section 5.3.4. still apply. Very large currents require very large conductor cross-sections. If large solid conductors are used the optimization expressed in Eqns. 5.57 and 5.58 breaks down. The alternative is to use stranded conductor i.e. $s > 1$.

If s becomes large this leads to the use of bunched conductor or insulated braid, a well-known but expensive way of reducing or practically eliminating eddy current loss in the winding. However if s can be held down to a small number then, for example, bi, tri- or quadrifilar windings can be used and this need not be an expensive solution. The use of copper or aluminium strip is also to be recommended for high current, high frequency windings.

5.3.6.3. Conclusions

Bringing the results of this Section together it can be said that as the design frequency rises the core performance improves even if the core material does not, although in principle the core resistivity should increase in proportion to frequency if the eddy current core loss is to be held much smaller than the hysteresis loss. This is true up to frequencies of several hundred kilohertz. The winding performance will not deteriorate significantly as the frequency rises provided the winding can be optimised. Thermal decoupling of the core and winding may be a good design aim. The core material characteristics impose the lower maximum temperature limit; the winding may generally operate safely at significantly higher temperatures than this.

Finally, any power loss leads to temperature rise so any steps that can be taken to reduce loss, even if it is a minor loss, will enable more output to be obtained from a given size of core. So there is an incentive to reduce core loss by one or more of the conceptional methods discussed earlier in this Section, e.g. by reducing K_h, m or n in Eqn. 5.46 or by increasing ρ in Eqn. 5.47. However, whether the ferrite materials can be improved or not, increased operating frequency results in improved transformer performance. The only limits at present are imposed by other circuit elements and perhaps, the need to restrict the level of electromagnetic interference.

CHAPTER 5. REFERENCES

1. Lee, R. Electronic Transformers and Circuits. John Wiley & Sons, Inc. New York, 2nd Ed, (1955).
2. Grossner, N.R. Transformers for Electronic Circuits. McGraw-Hill Book Company, (1967).
3. Snelling, E.C. Soft Ferrites, Properties and Applications. Butterworths, London, (1969).
4. Snelling, E.C. ibid, pp.354-357.
5. Snelling, E.C. ibid, pp.350-354.
6. Knowles, J.E. The effect of surface grinding upon the permeability of manganese-zinc ferrites. J.Phys.D (G-B), (1970), 3, pp.1346-1351.
7. Maurice, D. and Minns, R.H. Very-wide band radio frequency transformers. Wireless Engr., (1947), 24, p.168 (Pt.1) and p.209 (Pt.2).
8. Snelling, E.C. Soft Ferrites, Properties and Applications, p.262. Butterworths, London, (1969).
9. Snelling, E.C. ibid, p.28.

10. Ruthroff, C.L. Some broadband transformers. Proc. IRE., (1959), 47, pp.1337-1342.
11. Hilbers, A.H. High-frequency wideband power transformers. Electron. Appl. Bull., (1970), 30, No.2, pp.64-73, and (1973), 32, No.1, pp.46-48.
12. Snelling, E.C. Soft Ferrites, Properties and Applications. pp.298-305. Butterworths, London, (1969).
13. Jansson, L.E. Power handling capability of ferrite transformers and chokes for switched-mode power supplies. Mullard Tech. Note, London, (1975), No.31, p.4.
14. Jansson, L.E. ibid.
15. Annis, A.D. Unpublished report.
16. Dowell, P.L. Effects of eddy currents in transformer windings. Proc. Instn. Elect. Engrs. (1966), 113, pp.1387-1394.
17. Snelling, E.C. Soft Ferrites, Properties and Applications, pp.322-326. Butterworths, London, (1969).
18. Jongsma, J. Minimum loss transformer windings for ultrasonic frequencies, Electron. Appl. Bull., (1978), 35, No.3, pp.146-163, and 35, No.4, pp.211-226.
19. Snelling, E.C. Soft Ferrites, Properties and Applications. pp.345, Butterworths, London, (1969).
20. German Standard DIN 41295. E-cores of soft magnetic ferrite. Deutschen Normenausschuß (DNA), July, (1974).
21. Barrow, C. Cores for switched mode power supply transformers. Mullard Tech. Note, London, (1974), No.3.
22. International Electrotechnical Commission. Publication 647, Dimensions of Magnetic Oxide Cores Intended for use in Power Supplies (EC-cores). Geneva, (1979).
23. Snelling, E.C. Ferrites for power applications. Paper No.6 in Colloquium on Trends in forced commutation components. Instn Elect. Engrs., (1978), Digest No.1978/3.

CHAPTER 6
Future Trends

In this concluding Chapter a brief attempt will be made to look to the future, mainly for those ferrites that are used in inductors and transformers but widening the scope a little to embrace soft ferrites more generally.

At present about 90% of soft ferrite production by weight is of the MnZn range of compositions. This proportion is currently falling a little, not due to an increase in NiZn ferrite, but because MgZn and LiZn ferrites are being introduced as materials for some types of deflection yokes for television picture tubes, where the very high resistivity of these materials permits simpler winding techniques.

Ruthner[1] estimates that the world production of soft ferrite has been increasing at a rate of 8% per annum and predicts that this rate will continue. He gives the following figures:

Year	World production (tonnes)
1975	70 000
1980	100 000
1985	140 000

In the light of known technological changes in the electronics industry it is difficult to be confident that this extrapolation is reliable, but the ferrite industry is evidently maintaining its position at present. The total position is, of course, the sum of a number of contributory factors, some of which are leading to increased demand in certain sectors while others cause decline in less favoured sectors. A number of these aspects will now be considered, starting with the ferrite material and its production processes and leading on through the major application sectors. Most of the discussion will be concerned with MnZn ferrite and its products.

Considering developments in soft ferrite materials and their magnetic properties, it is evident that the rate of progress has diminished in recent years. Röss[2] states that no really outstanding development in ferrite materials has taken place since 1970. Some of the earlier developments aimed at making 'super' ferrites, in which prolonged annealing produced uniaxial anisotropy and consequent very low losses, were not commercially successful. The products were too

expensive and were susceptible to large degradation of performance if subjected to mechanical, magnetic or thermal shock. The use of titanium substitution[3] and very pure raw materials was more successful in improving the magnetic properties and, although the product is somewhat more expensive, developments of this type are likely to continue.

While recent developments in the ferrite material itself have not been very remarkable, the finished product, the core, has in fact improved significantly. This has been achieved mainly by better production technology and process control. For example, in the manufacture of small cores for inductors and transformers, the use of box kilns with precisely controlled and repeatable temperature/gas cycles has reduced production spreads. Not only has this meant a reduction in the tolerances on the magnetic properties but also smaller tolerances on the as-fired physical dimensions, ± 1.6% now being typical for an inductor core dimension. For larger cores, the omission of the pre-sintering or calcining stage together with better control of the temperature and atmosphere in the tunnel kiln has led to improved production efficiency. At the same time, the ability to use cheaper raw materials has been developed and the rationalization of production has led to improved economy of scale. These trends towards better finished products and more efficient production will continue[4].

Acting against the economy of scale has been a trend towards the proliferation of core shapes and sizes. This has been motivated by the rapid advance in electronic circuit development and the desire of the circuit designer to optimize the core shape for specific applications. This has been particularly marked in the case of cores for Switched Mode Power Supplies. Novel core shapes may give technical advantages but usually mean increased production costs due to more types sharing the same market size. A moderating influence, apart from the cost of proliferation, has been attempts at international standardization. The principal agent in this field has been the International Electrotechnical Commission (IEC) acting through its Technical Committee No. 51. Some standard IEC ranges of ferrite cores have already been referred to in Chapters 4 and 5 and other ranges are under active consideration. IEC TC51 has also provided, through its Publications, guidelines on measurements and specifications. It is currently involved[5] in the international move towards the introduction of products of "Assessed Quality" whereby conformance to a specification based on acceptable quality levels is certified by the manufacturer thereby obviating the need for inspection and testing by the purchaser. This leads to better quality and more uniformity in the product, and interchangeability between suppliers.

Moving now from the general to the particular, the prospects for some of the more important application sectors will be discussed.

Cores for inductors. In the examples of inductor design given in Section 4.8, the quoted inductor core performance represents about the best that is currently available on a commercial scale. After the rapid development of improved ferrite material properties and

core geometries in the 1960's, the manufacturers have concentrated on consolidating these developments in response to market pressures. These pressures arise from factors such as competing technologies, the increasing use of digital systems and the need to reduce labour-intensive operations. They have led to a demand to reduce inductor cost and size, and to simplify the assembly and mounting.

It was shown in Section 4.6 that, for a constant Q-factor performance, a reduction of core loss leads to a size reduction. Although further core loss reduction is no doubt possible, this would probably only be achieved at increased cost and at the expense of increased variability. The alternative means of size reduction is, of course, to arrange matters so that reduced performance requirements are acceptable and this appears to be a significant trend. The peak of inductor performance was achieved in the application to channel filters in Frequency Division Multiplex telephony systems, but as these analogue systems are being progressively superseded by digital transmission, the demands on inductor performance in general has relaxed. Another influence has been the development of competing technologies designed to replace the inductor as a circuit element by alternatives that are compatible with microelectronic circuits. Such developments include gyrators[6], switched-capacitor circuits[7] and active and digital filtering, all of which provide the means of implementing frequency selectivity within the technology of silicon integrated circuits. Parallel developments are the surface[8] and bulk wave filters[9] which achieve selectivity through the use of acoustic waves in piezoelectric materials such as quartz or lithium niobate.

These developments are displacing the inductor from applications where large numbers of identical frequency selective circuits are required, e.g. in telephony systems and television receivers. However, the inductor still provides flexibility; it can be quickly and cheaply designed and made, and it provides low noise circuits that are free of aliassing problems that are characteristic of digital and switched techniques. So the ferrite inductor will tend to become less of a specialized high-performance mass-produced component; its applications will become more diversified over a wider range of less-demanding functions in electronic systems. Modern winding and assembly techniques will help to keep it competitive in these applications. The total demand for ferrite inductor cores is currently increasing at a modest rate; within this total, the ratio of RM cores to pot cores shows a very significant increase.

Cores for low power, wide-band transformers. The pressure to implement as many circuit functions as possible in the form of silicon integrated circuits, referred to above, applies also to the low power transformers. Many of the transformer functions can now be achieved or obviated by suitable transistor circuits but so far wide-band isolation of circuits has generally been more conveniently achieved by wound transformers. The great proliferation of digital systems has generated a demand for a wide variety of signal and pulse transformers and the production of cores for these applications is increasing. In the long term, the use of opto-electronic couplers[10] may replace the

isolation function of the wound transformer in low power mass-demand applications but for the foreseeable future they are unlikely to be generally competitive.

As in the case of the inductor, the wound transformer will continue to offer the advantages of flexibility, ease of design and rapid implementation.

Cores for power applications. As discussed in some detail in Section 5.3, the principal application of ferrites in the power field is in Switched Mode Power Supplies. The relatively low power transformers used to drive the switching semiconductors present no problems as far as the ferrite core is concerned; the use of automatic winding and assembly has been the main development. For the output choke, used to remove switching ripple from the d.c. at the output, the ferrite core suffers the disadvantage of low saturation magnetization and although ferrite cores are very widely used, the powder iron core is becoming a contender for this application.

The main SMPS power transformer almost invariably uses a ferrite core. The demand for ferrite cores for this class of application is rapidly increasing. In Section 5.3.5 some standard ranges of ferrite power transformers were described. As new circuit configurations evolve and switching frequencies increase to 100 kHz and beyond, new core shapes are designed to optimise the transformer performance. Examples are the PM range[11], the PQ range[12] and more recently the ETD range[13]. The latter has been proposed as an IEC standard.

In most ferrite-cored SMPS transformers rated at less than about 300W, the design has been saturation limited up to frequencies approaching 100 kHz. The object of the more recent core shape designs has been to make the power loss and saturation limitations more nearly coincide over the relevant frequency range.

At present the 3C8 grade of MnZn ferrite quoted as an example in Section 5.3 is typical of the power ferrite used for SMPS transformer cores. The saturation limitation might have been regarded as a disincentive to further reduce the core losses. However, any reduction of loss reduces the operating temperature and increases the transformer efficiency. Recently several lower loss or higher frequency power ferrites have been announced, e.g. N47 in Germany[14], H7C4 in Japan, and a tin-titanium-cobalt substituted MnZn ferrite under development in The Netherlands[15]. Generally these materials will be more expensive and a real saving in overall transformer cost will have to be demonstrated before they come into common use.

There is, for this SMPS application, an important competitor on the horizon. The last ten years has seen the development of a range of amorphous metal alloys[16]. These are continuously cast at high speed in the form of thin tapes, 50-75 μm thick, quenched from the melt at the rate of a million Celsius degrees per second. At this rate of cooling no crystalline structure can form so the alloy has a glassy structure. Tapes can now be made in widths up to 200 mm but narrower tapes are more applicable to SMPS cores.

The absence of grain boundaries results in low hysteresis loss and the thinness of the tape minimizes the eddy current loss. Some grades, such as METGLAS^{R*} alloy 2605S-3 are specifically formulated for applications such as cores for SMPS transformers. The saturation flux density is typically 1.5T and the power loss (volume) density of the best materials, as wound into toroids and annealed, is lower than that for 3C8 ferrite over a major part of the operating range, see Fig. 6.1. At B = 200mT it is significantly better over the whole frequency range shown and at B = 50mT it is better up to about 60 kHz. It should be noted, however, that the horizontal line at P = 150 $\mu W.mm^{-3}$ represents an approximate heating limit so in practice the higher flux densities are not generally accessible without enhanced cooling. On the other hand designs using amorphous alloy cores will not be saturation limited.

There are a number of factors that have to be taken into account in making an overall comparison. Amorphous alloys have a density about 1.5 times that of ferrite. As wound into toroids and annealed they are stress sensitive and must be protected by enclosure in an annular case; this reduces their effective flux density and permeability when these properties are averaged over the cross-section of the encasement. Toroidal cores are not so convenient to wind and assemble and although cut versions (C-cores) are becoming available, the cutting operation appears to degrade the properties, particularly the losses, which according to some advance publication data become inferior to 3C8 ferrite over the whole of the operating range. The great advantage of the ferrite core is that its shape can be easily adapted to meet optimization and assembly requirements. Finally and perhaps most importantly, the cost of amorphous alloy cores is at present much higher than that of the equivalent ferrite cores.

From the above outline of the relative merits of the competing core materials it may be concluded that where minimum transformer volume is paramount and cost is a secondary consideration, the amorphous alloy toroid core can give advantage but at present the ferrite core shows substantial overall advantage in terms of convenience, cost and, in many cases, performance. The future of this competition is not clear. The cost of the amorphous alloy core will certainly fall as production quantities rise, but as noted above there is considerable room for loss reduction in power ferrite materials. The amorphous alloys will always have the advantage of potentially higher saturation flux densities, but ferrite cores will for the foreseeable future remain more convenient to use.

---

* METGLAS is Allied Corporation's registered trademark for amorphous alloys of metals.

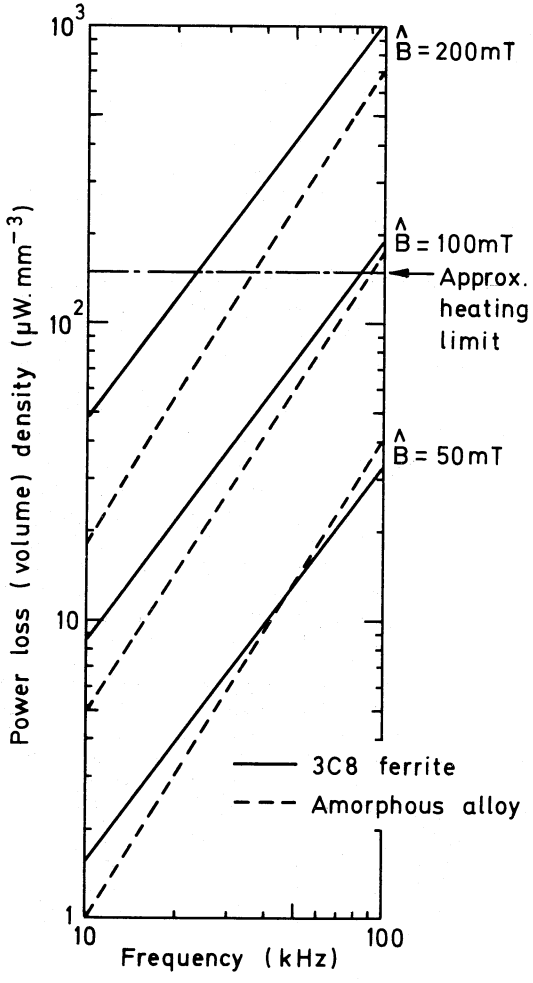

FIG. 6.1. Power loss comparison for a 3C8 MnZn ferrite E core and a low loss amorphous alloy core toroidally wound and annealed.

Miscellaneous applications. Perhaps the largest production of soft ferrites by weight is that of deflection yoke rings[17] for picture tubes in television receivers. The magnetic properties have hitherto been of little importance since the magnetic circuit is operated with a very large effective gap, i.e. the aperture through which the neck of the picture tube is inserted. However, in recent years there has been a strong incentive to simplify the setting up and adjustment of the wound deflection assembly and this has led to a very close control of the profile dimensions, particularly those of the inner flair in which the deflection field is generated. This can be done by greatly improved pressing and firing techniques or by profile grinding. As mentioned at the beginning of this Chapter, a current trend is the introduction of very high resistivity ferrites to simplify the applications of the windings by allowing the enamelled wire to be applied directly onto the ferrite. A future consideration may be the power loss in the ferrite; although this is small, the need to conserve the power supplied from the line output transformer may make such a saving worthwhile.

There is at present a massive expansion in the use of cathode ray tubes for Visual Display Units and this has created a large demand for deflection yokes specially designed for this application. These are often of the castellated design, that is, the inner diameter or bore is fluted with typically eight slots for the windings (giving eight inward facing poles).

There has been much speculation about the product life of the cathode ray tube as a display device. Much research and development has been devoted to alternative techniques that may ultimately provide a flat display. Such displays would be very unlikely to require ferrite deflection yokes. However, the generally-held opinion is that the investment in conventional cathode ray picture tube production is so large, and so great is the economy of scale that has been achieved, that the conventional picture tube with its ferrite deflection system will remain the dominant method of display for many years.

There are of course many other significant applications of soft ferrites such as recording heads, antenna rods, proximity sensors, interference suppression cores, etc. but space does not permit a discussion of these items.

This concludes the brief review of the future outlook for soft ferrite materials and their principal applications. Although the ferrite industry has become mature and the great advances that rewarded past research and development efforts have slowed, it is clear that soft ferrites continue to play an essential role in the electronics scene and there is ample scope for further innovation and development.

CHAPTER 6 REFERENCES

1. Ruthner, M.J. The importance of hydrochloric acid regeneration processes for the industrial production of ferric oxides and ferrite powders, Ferrites (Proceedings of IFC3). pp.64-67. Ed. Watanabe, H., Iida, S. and Sugimoto, M. Centre for Academic Publications, Japan, (1981).
2. Röss, E. Soft magnetic ferrites and applications in telecommunications and power converters. IEEE Trans. Magn., (1982), MAG-18, No.6, pp.1529-1534.
3. Stijntjes, Th.G.W., et al. Effects of various substitutions in Mn-Zn-Fe ferrites. Ferrites (Proceedings of Intnl. Conf. Kyoto, 1970). pp.194-198. Ed. Hoshino, Y., Iida, S. and Sugimoto, M. University Park Press, Tokyo, (1971).
4. Street, B.G. Ferrite component manufacture. Powder Metall. (GB), (1982), 25, No.3, pp.173-176.
5. International Electrotechnical Commission. Publication 723-1, Inductor and Transformer Cores for Telecommunication, Part 1: Generic Specification. Geneva, (1982).
6. Voorman, J.O., Brüls, W.H.A. and Barth P.J. Integration of analog filters in a bipolar process. IEEE J. Solid-State Circuits, (1982), SC-17, No.4, pp.713-722.
7. McCharles, R.H. and Hodges, D.A. Charge circuits for analog LSI. IEEE Trans. Circuits and Systems, (1978), CAS-25, pp.490-497.
8. Murray, R.J. and White, P.D. Surface acoustic wave devices. Wireless World, (1981), 87, Pt.1, March, pp.38-41, Pt.2, April, pp.79-82.
9. Mason, W.P. Use of piezo-electric crystals and mechanical resonators in filters and oscillators in Physical Acoustics, Principles and Methods. (Edited by W.P. Mason), 1, pp.335-416. Academic Press (1964).
10. Dance, B. Using optocoupler devices. New Electron., (1983), 16, No.1, pp.36-39.
11. Röss, E. Soft magnetic materials and applications in telecommunications and power converters. IEEE Trans. Magn., (1982), MAG-18, No.6, pp.1529-1534.
12. TDK. PQ cores for switching power supplies. TDK Data Book. TDK Electronics Co. Ltd., (May 1979).
13. Bracke, L.P.M. Optimizing the configuration of ferrite-cored transformers for advanced switched-mode magnetics. Proc. Powercon 9, Power Concepts, Inc., Ventura, California (1982).
14. Zenger, M. Ferrites and core forms for power electronics at frequencies up to 1 MHz. Siemens Components (Engl. Ed.)(Germany), (1982), XVII, No.4, pp.113-117.
15. Buthker, C., Roelofsma, J.J. and Stijntjes, Th.G.W. Low loss power material with improved temperature behaviour. Amer. Ceram. Soc., Fall Mtg. (1982), Paper No.58-BE-82F.
16 Smith, C.H. Magnetic shielding to multi-gigawatt magnetic switches; ten years of amorphous magnetic applications. IEEE Trans. Magn., (1982) MAG-18, No.6, pp.1376-1382.
17. Barten, P.G.J. and Kaashoek, J. 30AX self-aligning 110° in-line CTV display. IEEE Trans. Consum. Electron., (1978), CE-24, No.3, pp.481-488.

Index

Note: Underlined figures refer to the first page of the Section dealing with the subject.

Ferrites for Inductors and Transformers

E. C. Snelling
and
A. D. Giles

Ferrites for Inductors and Transformers
E. C. Snelling *and* **A. D. Giles**